OSLO METROPOLITAN UNIVERSITY
STORBYUNIVERSITETET

Department of Civil Engineering and Energy Technology
Institutt for Bygg- og energiteknikk
Energi og miljø i bygg
Postal address: Postboks 4 St. Olavs plass, 0130 Oslo
Visitor address: Pilestredet 35, Oslo

Telephone 67 23 50 00
www.oslomet.no

Thesis/candidate no.
5

Accesibility
Open

THESIS FOR THE DEGREE OF MASTER

Title	Date
A new framework for long-term vibration-based SHM	2021-06-09
	No. pages/no. appendices: 81/7
Author	Supervisor
Lone Næss, Frida Kristin Ulla	Emrah Erduran

Executed in cooperation wih	Contact

Abstract
This thesis presents a methodology for vibration-based damage identification in a long-term structural health monitoring scheme. The frequency with which damage is detected is proposed as a new parameter. In order to evaluate the proposed framework a railway bridge is modeled in a FE-software in which accelerograms are collected for varying damage scenarios. These are contaminated with noise to simulate operational conditions, before SSI-Cov is applied to extract modal properties. Three modal property derivatives are investigated as features for for damage identification, namely modal curvature, modal flexibility and modal strain energy. It is found that modal strain energy is the best fit for the framework; damage is detected and located at low levels of severity at moderate noise levels. Moreover, the performance of the proposed framework is found to exceed traditional approaches for vibration-based SHM regardless of which feature for damage identification is applied, providing a more consistent and reliable approach.

Keywords
Long-term Structural Health Monitoring
Operational Modal Analysis
Vibration-based Damage Detection

Preface

This thesis is written as the concluding work for the degree of Master of Science in Structural Engineering and Building Technology at Oslo Metropolitan University. Composed through the spring of 2021 it was considered the most enjoyable time of our studies. This is largely thanks to our supervisor Emrah Erduran and his commitment, encouragement and indispensable academic input. We would also like to thank Ole Jacob Velle who gave us an invaluable introduction to programming.

Oslo, June 9, 2021.

Frida Kristin Ulla

Lone Næss

Summary

The civil infrastructure throughout the world is inevitably growing older. Along with technological and social development, operational demands are also increased. Therefore, monitoring structures to ensure structural integrity or to uncover damage is necessary. Current inspection and maintenance of structures is for the most part conducted manually by experienced engineers. This is resource-heavy and leaves structures unchecked for long intervals of time. Techniques of structural health monitoring (SHM) have emerged as a promising alternative; these provide a frequent, continuous and objective means of assessing the condition of structures. Vibration-based techniques are particularly attractive, being cost-efficient, physically interpretative and global in nature.

Utilizing techniques of modal analysis, vibration-based SHM relies on the extraction of dynamic features from measured vibration data. These dynamic features are determined by a structures inherent physical properties, such ass stiffness and mass, and are thus indicative of a systems health. The comparison of dynamic features at two discrete points in time, where the structure is undamaged at the first point in time and its state unknown and sought after at the second, is the traditional approach of vibration-based monitoring. Changes in dynamic features can thus be detected and are used to indicate the presence of damage. Due to the presence of noise in vibration data, as well as mathematical biases, this traditional approach remains insufficient being inaccurate in prediction of damage.

In order to overcome these present-day shortcomings, a framework for long-term SHM that rely on frequent and continuous vibration measurements and their subsequent statistical analysis is presented. Applicable to any dynamic feature used for vibration-based damage detection, the derived modal properties of modal curvature, modal strain energy and modal flexibility are investigated herein. A railway bridge is simulated in a finite element (FE) software for this purpose. Vibration data in the form of accelerograms are collected from discrete, simulated accelerometers and polluted with normally distributed noise signals in order to emulate real-life operational conditions. Different levels of noise is applied and different levels of damage is introduced to several locations in the FE model in order to assess the efficacy of the proposed framework.

The results of the analyses lead to the conclusion that both where the damage is located as well as the noise and damage level is found to have an effect on the ability of the proposed framework to detect and localize damage. Where damage occurs affect the resulting change in dynamic features differently: Damage occurring by the abutment of the bridge is found more difficult to detect. Increasing levels of noise is found to delay detection of damage: High levels of damage is detected regardless of noise level whereas detection of low levels of damage is limited to noise levels of 10 % or less.

The three modal features investigated in the framework perform differently. Whereas modal

flexibility demonstrates high sensitivity to damage, being able to detect low levels of damage even at high levels of noise, localizing the damage is not feasible. Modal curvature on the other hand display a higher sensitivity to noise although localization is significantly better. Modal strain energy performs best out of the three dynamic features investigated, exhibiting consistent damage detection and localization.

Overall, the proposed framework provides a more reliable and consistent procedure for detecting and continuously tracking the development of damage, compared to the traditional discrete approach.

Sammendrag

Bygningsmasse og infrastruktur knyttet til transport vil over tid kunne utvikle strukturelle svakheter. Dette stiller krav til regelmessige og helst ikke destruktive inspeksjoner for å bekrefte strukturell integritet eller avdekke skader. Per i dag utføres inspeksjoner manuelt av erfarne ingeniører med kompetanse i bygnings- og konstruksjonsteknikk. Dette er ressurskrevende og tilstandskontroller utføres ved diskrete tidspunkter der tidsintervallene mellom hver inspeksjon kan bli lange. Senere har nye teknologier kommet på banen, omfattet av samlebegrepet tilståndsovervåking (structural health monitoring – SHM). Utviklingen av denne teknologien er lovende da den muliggør tilnærmet kontinuerlig overvåking og objektiv vurdering av strukturintegritet. Overvåking basert på vibrasjonsresponser er særlig attraktive grunnet kostnadseffektivitet, fortolkningsvennlighet av resultater og i tillegg deres globale egenskap.

Vibrasjonsbasert SHM utnytter modale analyseteknikker for å bestemme en strukturs dynamiske egenskaper. Disse er gitt av strukturens utforming samt iboende, fysiske egenskaper som stivhet og masse. Tradisjonell bruk av denne metoden innbærer å sammenlikne de dynamiske egenskapene til strukturen ved ulike tidspunkt. Endringer i disse mellom to tidspunkter vil indikere struktursvikt og fordrer dermed at strukturen er uskadet ved det første tidspunktet. Metodikken slik den benyttes i dag fremviser imidlertid svakheter knyttet til støy i målesignaler samt bias i de matematiske modellene som benyttes. Dette bevirker en utilstrekkelig nøyaktighet for gode predisksjoner av skade.

Dette arbeidet beskriver en fremgangsmåte som kan forbedre nøyaktigheten i vibrasjonsbasert SHM. Den baserer seg på frekvente observasjoner og påfølgende statistisk analyse av målte responser. De dynamiske egenskapene modal krumning, tøyningsenergi og fleksibilitet vil benyttes, men prosedyren vil også være anvendbar for andre dynamiske parametre. En "finite element" modellert jernbanebru utgjør testobjektet for fremgangsmåten. For å vurdere teknikkens slagkraft produseres ulike vibrasjonsdatasett, akselerogrammer, generert fra simulerte, diskrete måleinstrumenter på brua. De ulike settene reflekterer ulike grader av og lokasjoner for skade i strukturen. Deretter påføres de ulike nivåer av normalfordelt støy for å emulere reelle signaler. Disse "reelle" datasettene er deretter gjenstand for analyse for prediksjon av skade i brua.

Resultatet av undersøkelsene viser at både lokasjon og nivå av simulert skade samt støynivå influerer på modellen(e)s evne til å forutsi både tilstedeværelse av og lokasjon på skade. Stedet der skaden opptrer påvirker bruas dynamiske respons ulikt. Eksempelvis viser det seg vanskeligere å predikere og stedfeste skade nær bruas landkar. Økende grad av støynivå i målingene gjør at skader oppdages senere og ved en høyere grad av skade. Større skade oppdages konsekvent, uavhengig av støynivå. Dersom amplituden av støynivået er mindre enn 10 % av råsignalet detekteres også lavere nivåer av skade.

De tre modale egenskapene (krumning, tøyningsenergi og fleksibilitet) benyttet som predikatorer for skade har ulik slagkraft for forutsigelse av skade. Den modale fleksibiliteten utviser høy følsomhet for strukturskade også ved mindre skader og høyt påført støynivå. Den modale krumningen har høyere følsomhet for skadens plassering men påvirkes i større grad av nivået på støy i signalene. Tøyningsenergien viser seg å være den beste predikatoren med konsistent god forutsigelse av både lokasjon og nivå på skade.

I sum viser resultatene at den foreslåtte fremgangsmåten gir en sikrere og mer konsistent metode for å oppdage og kontinuerlig følge utviklingen av en strukturs integritet, sammenliknet med tradisjonelle diskrete metoder.

Contents

Preface i

Summary ii

Sammendrag iv

List of Figures viii

Nomenclature xii

1 Introduction 1
- 1.1 Introduction to VBM, VBDD and OMA . . . 2
  - 1.1.1 Feature Extraction by OMA . . . 3
  - 1.1.2 Damage Sensitive Features . . . 3
- 1.2 Motivation . . . 5
- 1.3 Problem Statement . . . 6
- 1.4 Objective . . . 6
- 1.5 Scope and Limitations . . . 7

2 Methodology 9
- 2.1 Methodological Approach . . . 9
- 2.2 Data Collection and Data Analysis Methods . . . 10
- 2.3 Reflection and Quality Check . . . 11
  - 2.3.1 Validity . . . 11
  - 2.3.2 Reliability . . . 12
  - 2.3.3 Objectivity . . . 12
  - 2.3.4 Generalizability . . . 13
  - 2.3.5 Source Criticism . . . 13

3 Theoretical Background 14
- 3.1 Structural Dynamics . . . 14
- 3.2 Stochastic Subspace Identification . . . 16
- 3.3 Modal Shape Curvature . . . 19
- 3.4 Modal Strain Energy . . . 20
- 3.5 Modal Flexibility . . . 20

4 Analysis Procedure and Application 22
- 4.1 Numerical Model . . . 24
- 4.2 Operational Modal Analysis . . . 25
- 4.3 Damage Detection Strategies . . . 27

4.3.1 Proposed Framework . . . 27
4.3.2 Traditional Approach . . . 28

5 Results and Discussion **30**
5.1 CSiBridge . . . 30
5.2 Operational Modal Analysis . . . 34
5.3 Damage Detection Strategies . . . 38
5.3.1 Development of Damage . . . 38
5.3.2 Effect of Modes . . . 41
5.3.3 Effect of Noise . . . 53
5.3.4 Effect of Damage Location . . . 62
5.3.5 Effect of Threshold Values . . . 67
5.3.6 Comparison of Damage Indicators . . . 68

6 Conclusions **73**
6.1 Recommendations for Further Work . . . 74

Bibliography **75**

Appendices **81**

List of Figures

4.1 The railway bridge as modeled in CSiBridge. 22
4.2 Flow chart demonstrating the different combinations of damage locations, damage levels and noise levels which accelerograms will be created for. 23
4.3 Cross section of the bridge deck [mm]. 24
4.4 Plan view of the railway bridge [m]. Joints from which accelerograms are collected are marked with green dots and the elements in which damage is introduced are marked with red. 25
4.5 Timeline illustrating how the severity of damage increases with time for a given location of damage and noise level. 26

5.1 accelerograms from all ten sensors with the bridge in its undamaged and damaged states. The damage is introduced at mid-span. 31
5.2 Mode shapes from CSi Bridge with varying level of damage by the abutment. 32
5.3 Mode shapes from CSi Bridge with varying level of damage at quarter-span. 32
5.4 Mode shapes from CSi Bridge with varying level of damage at mid-span. 33
5.5 Mode shapes from CSi Bridge with varying level of damage by the column. 33
5.6 Mode shape of mode 4 between 0 and 30 m from CSi Bridge with varying level of damage at quarter-span. 34
5.7 Stabilization diagram produced from the signal of the bridge in its undamaged state, influenced by 0.5 % noise. 35
5.8 Mode shapes from SSI-Cov with varying level of damage by the abutment. 36
5.9 Plots of extracted mode shapes for all four modes. Each subfigure contains 17 500 plots; 500 for each of the seven damage levels times five levels of noise. Damage located at quarter-span. 37
5.10 Mode shape 1 from SSI-Cov with all damage levels in abutment for varying noise levels. 38
5.11 Mode shape 1 from SSI-Cov with no damage and 500 variations of each noise level. . . 39
5.12 Development of damage by frequency of exceedance from Sensor 3 by modal curvature with two modes with increasing damage at mid-span, 5 % noise and 5 % threshold. . . 39
5.13 Development of damage indicator from Sensor 3 by modal curvature with two modes with increasing damage at mid-span and 5 % noise. 40
5.14 Probability of detection using modal curvature for two modes, increasing damage occurring at mid-span, noise level and threshold value 5 %. 41
5.15 Probability of detection for modal curvature at different damage locations and with different combinations of modes. 42
5.16 Frequency of exceedance using modal curvature with varying number of modes for damage by the abutment, 5 % noise and 5 % threshold. 42
5.17 Mode 3 with varying damage by the abutment without noise. 43

5.18 Scatter plot for modal curvature as damage indicator from three modes for Sensor 10 and damage by abutment with varying noise levels. 44
5.19 Bar chart for the modal curvature damage indicator at Sensor 10 with varying levels of noise and damage by abutment, using a combination of three modes. 44
5.20 Probability of detection for modal strain energy at different damage locations and with different combinations of modes. 45
5.21 Frequency of exceedance using modal strain energy with varying number of modes for damage by the abutment, 5 % noise and 5 % threshold. 45
5.22 Probability of detection for modal flexibility at different damage locations and with different combinations of modes. 46
5.23 Frequency of exceedance using modal flexibility with varying number of modes for damage by the abutment, 5 % noise and 5 % threshold. 47
5.24 Frequency of exceedance using modal curvature with one mode for all damage locations, 5 % noise and 5 % threshold. 47
5.25 Frequency of exceedance using modal curvature with three modes for all damage locations, 5 % noise and 5 % threshold. 48
5.26 Frequency of exceedance using modal curvature with four modes for all damage locations, 5 % noise and 5 % threshold. 48
5.27 Frequency of exceedance from modal strain energy varying numbers and combinations of modes caused by damage by abutment with 5 % noise and 5 % threshold. 49
5.28 Frequency of exceedance from modal strain energy varying numbers and combinations of modes caused by damage at quarter-span with 5 % noise and 5 % threshold. 49
5.29 Frequency of exceedance using modal curvature with varying number of modes for damage by the abutment, 20 % noise and 5 % threshold. 50
5.30 Frequency of exceedance using modal strain energy with varying number of modes for damage by the abutment, 20 % noise and 5 % threshold. 50
5.31 Frequency of exceedance using modal flexibility with varying number of modes for damage by the abutment, 20 % noise and 5 % threshold. 51
5.32 Frequency of exceedance using modal strain energy with varying number of modes for damage at quarter-span, 5 % noise and 5 % threshold. 51
5.33 Frequency of exceedance using modal strain energy with one mode and varying damage locations, 5 % noise and 5 % threshold. 52
5.34 Frequency of exceedance using modal flexibility with one mode and varying damage locations, 5 % noise and 5 % threshold. 53
5.35 Probability of detection with modal curvature using two modes for different levels of noise and damage by the abutment as well as at mid-span. 54
5.36 Frequency of exceeding the 5 % threshold value using modal curvature with varying noise levels and increasing damage at quarter-span using two modes. 54
5.37 Probability of detection with modal curvature for different levels of noise and damage by the column as well as at quarter-span. 55
5.38 Probability of detection with modal strain energy for different levels of noise and damage by the abutment as well as at mid-span. 55
5.39 Probability of detection with modal flexibility for different levels of noise and damage by the column as well as at quarter-span. 56
5.40 Frequency of exceeding the 5 % threshold value using modal strain energy with varying noise levels, with increasing damage at quarter-span by looking at two modes. 56
5.41 Frequency of exceeding the 5 % threshold value using modal flexibility with varying noise levels, with increasing damage at quarter-span by looking at two modes. 57

5.42 Scatter plot of damage indicator from modal strain energy, from Sensor 2 and damage at quarter-span for varying noise levels with corresponding threshold values. 58
5.43 Scatter plot of damage indicator from modal strain energy, from Sensor 3 and damage at quarter-span for varying noise levels with corresponding threshold values. 58
5.44 Scatter plot of damage indicator from modal curvature, from Sensor 2 and damage at quarter-span for varying noise levels with corresponding threshold values. 59
5.45 Scatter plot of damage indicator from modal curvature, from Sensor 3 and damage at quarter-span for varying noise levels with corresponding threshold values. 59
5.46 Scatter plot of damage indicator from modal flexibility, from Sensor 2 and damage at quarter-span for varying noise levels with corresponding threshold values. 60
5.47 Scatter plot of damage indicator from modal flexibility, from Sensor 3 and damage at quarter-span for varying noise levels with corresponding threshold values. 60
5.48 Frequency of exceedance by modal curvature from two modes. Varying damage locations with the closest sensor of each location respectively. 1 % noise and 5 % threshold. 61
5.49 Frequency of exceedance by modal curvature from two modes. Varying damage locations with the closest sensor of each location respectively. 20 % noise and 5 % threshold. 61
5.50 Probability of detection for modal curvature with different levels of damage and at different damage locations. A combination of two modes is utilized and the noise and threshold is at 5 %. 62
5.51 Frequency of exceedance using modal curvature with two modes for all damage locations, 5 % noise and 5 % threshold. 63
5.52 Probability of detection for modal strain energy with different levels of damage and at different damage locations. A combination of two modes is utilized and the noise and threshold is at 5 %. 64
5.53 Frequency of exceedance using modal strain energy with two modes for all damage locations, 5 % noise and 5 % threshold. 64
5.54 Probability of detection for modal flexibility with different levels of damage and at different damage locations. A combination of two modes is utilized and the noise and threshold is at 5 %. 65
5.55 Frequency of exceedance using modal flexibility with two modes for all damage locations, 5 % noise and 5 % threshold. 66
5.56 Frequency of exceedance by modal flexibility from two modes. Varying damage locations with the closest sensor of each location respectively. 5 % noise and 5 % threshold. 66
5.57 Development of damage by frequency of exceedance from Sensor 3 by modal curvature with two modes with increasing damage at mid-span, 5 % noise and 2 % threshold. . . 67
5.58 Development of damage by frequency of exceedance from Sensor 3 by modal curvature with two modes with increasing damage at mid-span, 5 % noise and 10 % threshold. . 68
5.59 Frequency of exceedance for modal curvature, modal strain energy and modal flexibility with damage occurring by the column. The first mode and a noise level of 5 % is utilized. 68
5.60 Frequency of exceedance for modal curvature, modal strain energy and modal flexibility with damage occurring by the column. The first mode and a noise level of 10 % is utilized. 69
5.61 Frequency of exceedance for modal curvature, modal strain energy and modal flexibility with damage occurring by the column. The first mode and a noise level of 20 % is utilized. 70

5.62 Frequency of exceedance for modal curvature, modal strain energy and modal flexibility with damage occurring at mid-span. The first mode and a noise level of 5 % is utilized. 70
5.63 Frequency of exceedance for modal curvature, modal strain energy and modal flexibility with damage occurring at quarter-span. The first mode and a noise level of 5 % is utilized. 71
5.64 Frequency of exceedance for modal curvature, modal strain energy and modal flexibility with damage occurring at quarter-span. The first mode and a noise level of 10 % is utilized. 71

Nomenclature

[A]	State matrix
[C]	Damping matrix
[C]	Discrete output matrix
[F]	Flexibility matrix
[G]	Cross-correlation matrix
[K]	Stiffness matrix
[M]	Mass matrix
$[R_k]$	Discrete correlation matrix
α	Mass proportional coefficient
β	Stiffness proportional coefficient
Δt	Time lag
$\dot{q}$	Time variation of velocities
$\hat{\lambda}_r$	Discrete-time system pole
$\varkappa$	Curvature
λ_r	Continuous-time system pole
ω	Natural circular frequency
ω_D	Natural circular frequency with damping
ϕ	Continuous-time eigenvector
ϕ''	Modal curvature
τ_i	Controllability matrix
ϑ_i	Observability matrix
ζ	Damping ratio
$\{\ddot{u}\}$	Acceleration vector
$\{\dot{u}\}$	Velocity vector
$\{\phi\}$	Mode shape vector

$\{\psi\}$	Discrete-time eigenvector
$\{u\}$	Displacement vector
E	Expected value operator
EI	Flexural stiffness
f_s	Sampling frequency
H_i	Block-Hankel matrix
I_F	Modal flexibility damage indicator
I_S	Modal strain energy damage indicator
M	Bending moment
q	Time variation of displacements
t	Time
v_k	Measurement noise vector
w_k	Process noise vector
y_k	Discrete-time output vector
z_k	Discrete-time state vector
I_C	Modal curvature damage indicator

Chapter 1

Introduction

As the civil infrastructure of the world is aging, along with increasing operational demands, the ambition and necessity of monitoring and assessing the performance and health of such structural systems increases. Current maintenance and inspection of civil structures is for the most part performed manually and periodically by experienced engineers. For longer periods of time structures thus remain unchecked and the outcome of a manual inspection is subjective and reliant on the skill of the inspecting engineer. Through recent years techniques of structural health monitoring (SHM) have emerged as an alternative strategy, providing a continuous and objective means of assessing the health of structural systems. Among the different techniques available, vibration-based monitoring (VBM) approaches have gained popularity through their non-invasiveness, cost efficiency and ability to observe the global response of a structure, requiring no prior knowledge about damage location.

The vibratory response of structures is dictated by their inherent mechanical properties of mass, stiffness and damping. Several types of damage will affect the structural properties and thus the dynamic response of a system, such as cracking which results in a local loss of stiffness in a structure. Traditional applications of VBM employ the fundamental idea that detected changes in one or more dynamic features of the system, between two discrete points in time, indicate the presence of damage. At one of these points the system is undamaged, while the damage situation at the second point in time is unknown and sought for. Several dynamic features for vibration-based damage detection (VBDD) exist. Early applications were focused on the basic modal properties of natural frequencies and mode shapes. Since then, methods applying derivatives of these basic properties have been developed in order to increase sensitivity to damage. Modal curvature, modal strain energy and modal flexibility can be mentioned herein.

The development of tools for determining modal properties from measured vibration response-time histories has also fuelled the interest for VBM in civil engineering. Early on, artificially exciting structures with a known input force was necessary to determine modal properties of a system from the registered output of this excitement. This procedure is called experimental modal analysis (EMA). Artificially exciting civil structures is however both economically and practically challenging due to their size and the required halt of operation. The introduction of operational modal analysis (OMA) has eliminated these issues. As its name suggests, OMA is performed using output data collected from a system during its operation, when subjected to natural, ambient, unknown loads.

Currently the reliability and consistency in conclusive damage detection by means of VBM and OMA is insufficient. The global quality of modal properties makes them insensitive to low levels of damage, which is typically a local phenomenon. Moreover, inevitable noise present in measured

responses, related to both operational conditions as well as equipment, may cause detected alteration in dynamic features that falsely indicate damage. The calculation of the dynamic features used in damage detection can also produce mathematical biases. In order to overcome these obstacles a new, long-term monitoring framework is proposed, based on any of the three mentioned damage-sensitive features. Rather than comparing features at two discrete points in time, the proposed framework relies on the statistical analysis of extracted features from frequent observations over a significant period of time.

1.1 Introduction to VBM, VBDD and OMA

VBM encompasses the use of vibration measurements sampled over time to continuously or periodically monitor structural system health. VBDD can be considered a subset to VBM, which concerns approaches to identify damage in a structure. In this context, these terms will be used interchangeably. In the scheme of VBDD damage can be defined as changes in material and/or geometrical properties that will adversely affect a structure. The goal of VBDD is to capture these changes, in order to evaluate the health of a structural system. Depending on the ability of VBDD methods to identify damage, they can be categorized into four levels as first proposed by [1]:

1. Existence - is there damage in the system?
2. Location - where is the damage?
3. Type - what kind of damage is present?
4. Extent - what is the severity of the damage?

Furthermore, VBDD techniques can be classified as either response-based or model-based [2, 3, 4]. By direct or indirect interpretation of measured dynamic responses, the former approach relies on the comparison of modal parameters between intact and damaged system states. Model-based approaches incorporate numerical models, usually with the aid of finite element analysis. By assuming some predetermined response that can be simulated by a model, intact and damaged model states are compared and can be used to identify the location and severity of damage. Model-based approaches thus allow for a higher level of damage identification than response-based ones.

This thesis is focused on response-based methods. These are generally limited to level 1 damage identification, however level 2 is in some cases achievable [5]. For many practical applications this is sufficient, although valid damage identification at all 4 levels is undeniably sought after. However, several challenges already exist at level 1. These include how to select damage sensitive features, excluding false alarms in early damage detection, eliminating noisy effects stemming from operational and environmental conditions and lastly quantifying the probability of detection [6].

Inherent to response-based VBDD are the measurements of vibration responses of the system to be investigated. In such a sensor system, which measures the responses of the system, is required. Although the application of hybrid and integrated sensing systems have been shown to increase accuracy and reliability in measurements, accelerometers are commonly used in vibration-based approaches [7, 8, 9, 10]. The resolution of the sensing system, including the number and location of sensors, must be considered in order to extract relevant measurements [11, 12].

Once the measurement data has been obtained it must be analyzed and manipulated in order for the desired damage sensitive features to be extracted. Included in this process is normalization,

cleansing, feature extraction and information condensation [13]. Normalization is applied to separate changes in sensor readings caused by damage from those caused by operational and environmental conditions. Cleansing is the process of rejecting faulty measurements and selecting the data from which desired damage sensitive features are extracted. Should a sensor be loosely mounted for instance, its readings may be rejected. Information condensation becomes necessary as measurement data accumulates over time. Retaining only the measurements necessary to evaluate the system health and disposing of overshooting data will increase the efficiency of VBM.

1.1.1 Feature Extraction by OMA

The popularization of VBDD in civil engineering is largely contributed to the OMA technique, which is used to extract the modal parameters (the features) of a system subjected to unknown, operational loading. Traditionally, modal parameter extraction was done with methods of EMA. In EMA a system is perturbated with known, artificial sources of excitation. Applying this to civil structures is however challenging: The size of these structures makes it expensive and practically difficult. Neither can they be tested in a controlled environment and ambient loads such as temperature and wind will affect measurements. Civil structures are also usually unique, making the modal analysis of one structure non-applicable to others.

To overcome these obstacles methods of OMA were proposed. Rather than artificially exciting a structure with a known input to measure a dynamic response, already existing operational loads are utilized instead. This poses a challenge as the operational loads are not quantifiable. Solving this is done by modelling the input stochastically, as a random process with zero mean and limited variance. Herein lies the assumption that the input has equally distributed energy over a wide frequency range: Accordingly, the structure is not excited at any particular frequency. This is useful as any significant responses measured can be associated with the natural frequencies of a structure.

The dynamic behavior of a structure can be physically decomposed and mathematically described by frequency and position. The natural frequency of a system can be described as the frequency with which a system will oscillate when distributed with an initial displacement and when no external forces are applied. If an external force oscillates a system in or close to one of its natural frequencies, a phenomenon called resonance in which the amplitude of the oscillations can be significantly increased occurs. Therefore OMA can utilize the assumption that any protruding responses measured, induced by an input with a white noise distribution, can be associated with the natural frequencies of a system.

Mode shapes describe the spatial deformation patterns that a system will assume when oscillating in its natural frequencies. Estimating these two modal parameters by means of OMA can be done in a multitude of ways [14, 15, 16, 17, 18, 19, 20, 21]. Generally OMA includes both normalization and cleansing of measurements, as well as system identification which involves the estimation of mathematical models from the measured data. Methods of system identification are often categorized according to which domain they are implemented in; usually time or frequency. Notably existing OMA techniques apply assumptions of linearity and time-invariance. This is an idealization of the true behaviour of civil structures, which to some extent will be both nonlinear and time-dependent.

1.1.2 Damage Sensitive Features

The most commonly used features in VBDD are the basic modal properties of natural frequencies and mode shapes. Using natural frequencies as a damage sensitive feature is practical as only one measurement is required for determining this global structural property, providing there is motion

in the corresponding mode at the chosen point [22]. Spatial information on structural changes is however not available at lower frequencies. At higher frequencies the modes are associated with local responses. These are however difficult to measure as it is practically challenging to excite these frequencies [23].

Using frequency shifts as a feature for damage detection is based on the assumption that abnormal loss of stiffness in a structure will result in shifts in its natural frequencies. So will however temperature differences, as well as changes in boundary conditions and mass distributions [2, 24, 25]. As an example, marine growth which can add significant mass to a structure, was found to corrupt the data measured from offshore oil platforms [22]. The frequencies associated with lower modes, which are usually the ones measured, are particularly affected by these changes as well. Frequency shifts therefore has low sensitivity to damage, and a high precision of measurements or severe damage is required for application to civil engineering structures [23].

Mode shapes, as opposed to natural frequencies, are spatially distributed quantities which contain local information. This makes them more sensitive to local damage. A high number of sensors may be required for obtaining sufficient characterization of the mode shapes and adequate resolution for determining damage location. Mode shapes are less prone to the effects of temperature changes, as compared to natural frequencies [26]. Nonetheless, several similar issues with using both of these features exist. Not all modes are useful for locating damage [27]. As the lower frequency modes are global in nature they perform poorly in identifying the location of small-scale damage. Higher modes are associated with local responses and therefore provide better indications, but as mentioned these are difficult to measure [28].

Several other damage sensitive features have been proposed to overcome the issues with natural frequencies and mode shapes, particularly relating to their insensitivity to damage. In 1991 Pandey, et al. showed that the absolute change in modal shape curvature can be an efficient indicator of loss of stiffness [29]. They estimated modal curvatures from mode shapes by central difference approximation. According to beam theory, the curvature of an element cross-section is inversely proportional to the bending stiffness at that point. Correspondingly a loss of stiffness will increase the magnitude of the curvature. In the study, which was performed on analytically modelled beams, it was found that changes in modal curvature were localized in the region of damage, compared to the changes in the mode shapes. Moreover, the changes in curvature increased with an increasing size of damage.

Early applications of the approach seemed to verify modal curvature as a sensitive damage indicator, however for higher modes the differences in curvature sometimes falsely indicated damage [29, 30]. Furthermore experiments have indicated that modal curvature cannot by itself locate small damages [31]. It has also been found that the numerically calculated curvatures resulted in unacceptable errors by amplifying the noise in the measurements [32, 33, 34, 35].

Modal strain energy, another damage sensitive feature, can in beam- and plate-type structures be directly related to modal curvature. Modal strain energy is therefore often derived from modal curvature [3, 36, 37]. The variation of the modal strain energy stored in a structural sub-element was proposed as a damage feature by Stubbs, et al. [38]. Applications of this and similar methods have proven successful, with the ability to handle noise contaminated data and the errors introduced by the central difference approximation [39, 40, 41].

Another damage identification feature is that of modal flexibility. From estimated mode shapes, which must be mass-normalized, a flexibility matrix can be identified [33]. The information of many modes are combined in the flexibility matrix, into a single damage feature which gives this method increased sensitivity. The modal contribution to the flexibility matrix decreases as the frequency increases, rendering only the lower modes necessary [42, 37, 43]. To detect damage, flexibility matrices are typically constructed from the modes of a damaged as well as an intact structure or a FEA representation. These are then compared to detect changes [44].

Using the comparison of flexibility changes was proposed by Atkan, et al. [45]. They found that modal flexibility is a reliable tool for condition assessment of bridges. Pandey and Biswas performed several numerical and experimental procedures to verify a damage detection and localization method based on changes in modal flexibility [46, 47]. The results showed that estimates of both condition and location could be obtained using only the first two modes of the structure. By computing modal flexibility and examining cross-sectional deflection profiles, Toksoy and Atkan found that damage could be indicated even when a baseline data set is not available [48]. They emphasize however, that a structure must be accurately characterized in order to achieve effective and reliable monitoring.

Several other methods have been proposed, in which modal flexibility constitutes a foundation. These include the unity check method, the stiffness error matrix method, effects of residual flexibility and changes in measured stiffness matrices. These can be explored in more detail in the following references [49, 50, 51, 52, 53, 54, 55, 56].

1.2 Motivation

The motivation for applying vibration-based monitoring to civil infrastructure is multifaceted. The ultimate goal however is to ensure reliability and safety in the operation of the infrastructure, as the consequence of not doing so can result in catastrophic consequences. A grave example of this is the Ponte Morandi bridge in Italy, which on August 14^{th} 2018 collapsed claiming the lives of 43 people.

The collapse of Ponte Morandi was succeeded by its demolition, the thorough investigation of the event and eventually the inauguration of a new bridge. The investigative procedure is undoubtedly valuable. Uncovering the nature of the collapse contribute to the knowledge of good bridge design and in such the avoidance of recurrence of such catastrophic events. Had the bridge been equipped with a monitoring system however, damage may possibly have been detected before the eventual failure. This could have allowed for repairs or closure of the bridge if necessary, sparing not only costs and resources, but also the 43 lives. Vibration-based monitoring can in such provide an excellent tool for decreasing the life cycle cost of a structure, as well as environmental and societal impacts.

Vibration-based monitoring provides a cost efficient tool for SHM. Most current structural maintenance is based on what can be considered time-based philosophies. Periodical inspections are performed by experienced and competent professionals. The concept of VBM on the other hand, represents a condition-based maintenance philosophy. A sensing system monitors the structural system response and notify if damage is detected. Dependent on the efficiency of such a system, clear benefits are associated with such a philosophy. In Norway, roughly 17 000 bridges are in operation on the road network. Replacing physical inspections with a sensing system is not only economically and practically beneficial. It also seems necessary, as the sheer quantity of civil infrastructure makes sufficient time-based maintenance practically challenging.

Ponte Morandi had been operating for 50 years before it collapsed. Several bridge constructions throughout the world are more than twice that age. The inevitable deterioration these have been subjected to, along with ever-increasing demands in traffic, is a strong incentive for their condition monitoring. Furthermore the designs of many of these bridges, including structural and material properties, are unknown. Using vibration-based monitoring, valuable information on these inherent features, the dynamic response and the state of these structures can be obtained.

Vibration-based monitoring is also useful for modern constructions, as these too eventually will deteriorate. Moreover global warming leads to a harsher environment with more extreme weather, affecting old and new structures alike. The increased environmental focus in the building industry also pushes for less use of materials and more slender civil structures. Slender structures have low natural frequencies. This makes them subject to dynamic phenomena such as flutter, dynamic buckling and parametric excitation. Monitoring these structures as to detect and avoid failure, as well as possibly predicting future behavior, is therefore highly relevant.

Current applications of VBM rely on the extraction and comparison of dynamic features from two discrete observations in time. The success rate of such applications remain insufficient as insensitivity to low levels of damage and sensitivity to noise and mathematical biases is demonstrated. The clear, physical interpretation of vibration-based features for damage detection, as well as the cost- and resource-effectiveness of VBM and the development of OMA nonetheless renders it an attractive tool for SHM. A motivation for developing a framework that include these features while mitigating the mentioned shortcomings therefore exists.

1.3 Problem Statement

The main purpose of this work is to demonstrate and assess a proposed framework for long-term monitoring of civil structures, using vibration-based features for damage detection. Several parameters may have an influence on the success rate of vibration-based damage detection. The following questions are therefore formulated and assessed:

- How does noise present in vibration data affect the efficacy of the methods?
- How does the location of damage affect the efficacy of the methods?
- How does utilizing different combinations of modes affect the efficacy of the methods?
- Which of the damage indicators provide the most successful damage detection approach?
- How do threshold values for chance of false damage detection affect the performance of the proposed framework?
- How does the proposed framework perform in comparison to traditional approaches?

1.4 Objective

This thesis aims to develop and evaluate a framework for vibration-based long-term structural health monitoring. Herein, the efficacy of different methods for damage detection and localization based on operational modal analysis techniques are to be investigated. The methods that will be considered are based on different damage indicators, namely modal shape curvature, modal flexibility and modal

strain energy. The proposed framework takes basis on these damage indicators and the frequency of how often damage is detected in various locations along a bridge.

In order to do this a railway bridge is simulated in a FEA software. From different points over the span of the bridge acceleration time histories, or accelerograms, which constitute the vibratory response of the bridge to a dynamic, operational load are collected. An OMA technique, namely covariance-driven stochastic subspace identification, is applied to extract the modal parameters of the bridge from these responses. Once the modal parameters have been extracted, the three different algorithms for damage detection and localization are implemented.

Different damage scenarios will be introduced to the numerical model. This is one link in the evaluation of the efficacy of these three different damage detection and localization algorithms: Whether their ability to do this is affected by the extent and severity of the damage. Acceleration time histories are necessarily collected both on the intact and the damaged models. In such the vibratory response of the undamaged model will function as a basis for comparison. Comparing undamaged and damaged system states through their related modal parameters and damage indicators is a recurring approach in VBDD.

In real life several factors, such as temperature, moisture, non-linear behaviour and noise in recorded data will affect the sensor readings and consequently the values of the different damage indicators, even if no damage occurs. The effect of these uncertainties are however not present in the controlled environment of a numerical model. To account for the influence of these uncertainties, the accelerograms will be polluted with randomly distributed noise.

In order to study the sensitivity of the damage indicators and the possibility of false indications of damage, several hundred noisy variations of the readings from the bridge in its different intact and damaged states will be produced. The level of noise will also be varied. By considering these readings as consecutive vibration measurements through time, and computing the frequency with which damage is indicated throughout time, the efficacy of the damage indicators can be evaluated statistically in a continuous, long-term monitoring scheme.

A thorough description on the complete procedure can be found in Chapter 4. The collective goal of the work is to provide an assessment of whether modal curvature, modal strain energy and modal flexibility can be used as an effective tool in long-term SHM of civil structures when the detection of damage is presented as the frequency of which a threshold value is exceeded.

1.5 Scope and Limitations

The purpose of this thesis is to evaluate the efficacy of three different vibration-based features for damage detection, with the application of OMA techniques, in a long-term monitoring scheme using a new, proposed framework. OMA was developed to facilitate the opportunity of determining the modal characteristics of real structures in operation. Herein, the evaluation of the different damage detection and localization methods is limited to a numerical model. To simulate a situation as closely representing an actual bridge as possible, noise is added to account for the uncertainties that would be present in real-life signals. Nonetheless, it is emphasized that the obtained results might deviate from what can be expected with measurements from a real, operative bridge.

Four different locations of damage are simulated herein, however, neither occur at the same

time. Therefore, the efficacy of the damage indicators and the frequency parameter of the proposed framework are only evaluated for single damage locations and not multiple. This limits the generalizeability of the work as multiple damages may occur in real structures, however, it is realistic to assume that the same framework is applicable for more complex scenarios.

Damage is in this thesis modelled as a reduction in the bending stiffness in one element of the structure. This reduction in stiffness is important as it alters the modal properties of the structure. However, some types of damage may not occur at discrete locations or lead to reduced bending stiffness. Nevertheless, it is assumed that this is a realistic emulation of many types of damage that may occur on a real structure. Furthermore, the methods discussed herein may be applicable and efficient in detection of other types of damage, though this has not been checked herein.

Mode shapes should be mass normalized when applying the modal flexibility as a damage indicator. This is not possible for mode shapes obtained through operational modal analysis as the input forces are unknown. This is a constraint to the modal flexibility method and limits its applicability to real-life structures.

The application of VBDD requires multiple steps. Several of these are not considered, as measurements are extracted from a numerical model rather than a real one. This includes the processes of normalization and cleansing of sensor data. Neglecting these steps will presumably not affect the results. Properly conducting them in a situation with real-life measurements is however important, but not always straightforward. The statistical evaluation of the efficacy of the damage indicators will therefore be idealized.

Chapter 2

Methodology

The following chapter elaborates on the research design and approaches applied in this study. The pros and cons of qualitative and quantitative methodological approaches are discussed, as they are both utilized herein. The software and methods used are further described as well as procedures to ensure that the research can be replicated. Furthermore, important values that a researcher should evaluate when conducting scientific research are described with emphasis on how well this is maintained in this work.

2.1 Methodological Approach

Methodological approaches to research are generally categorized as either quantitative, qualitative or as a combination of the two. Several methods, falling within these categories, may be applied depending on the goal of the study. Several definitions on the terms for an approach to be either qualitative or quantitative exists. In the following an attempt is made to give a general description on the two.

Quantitative research is the process of collecting and analyzing numerical data. The quantitative data may be collected from experiments and is usually statistically analyzed to directly present the findings, or to describe patterns and relationships. This process is a large part of this thesis: Collecting data in the form of accelerograms and to evaluate whether this data can describe patterns in the health and behaviour of civil structures. Quantitative research is primarily concerned with demonstrating cause-effect relationships and is often used when the purpose is to substantiate or reject a hypotheses. A hypothesis is often necessary because standardized data is needed for statistical analyses, which can not be collected without a clear idea about the subject of interest and their attributes. Although evaluating whether different damage indicators are affected by damage and biases, a hypotheses is not formulated. It is deemed unnecessary as procedures similar to the one applied in this work already exists in literature: Which data that needs to be collected to evaluate the efficacy of different damage indicators is therefore known. By excluding a hypothesis the risk of biased interpretation of results is mitigated. Deductive reasoning is often possible as well as strived for in quantitative research. The basic rule of deduction is that knowledge should only be rearranged, and nothing which is not known to be true may be added to its content. Hence, valid deductive inferences will lead to valid conclusions [57, 58, 59, 60]. The foundation of VBDD rests on the assumption that changes in physical properties of structures will render an alteration in their dynamical behavior. Evaluation of the efficacy of the damage indicators relies heavily on this deductive inference.

Qualitative research approaches, on the other hand, are generally naturalistic and interpretive, meaning that the subject to be studied is in its natural settings and attempts are made to make sense of the phenomena. The purpose of evaluating the framework of this research is to uncover whether it can be used in reliable and efficient damage detection of real-life civil structures. It is however applied to a numerical model rather than to a real structure. In such the approach can not be considered qualitative. However, measures will be taken in order to simulate and accurately represent the conditions that would be present with real-life applications. Qualitative approaches also include the process of collecting nonnumerical data and analyzing it, where for instance grounded theory or thematic analysis is often used. This approach is relevant if numerical data alone is not adequate to understand phenomena. For this reason, a comprehensive literature study is conducted: This will aid the authors in accurate interpretation of results. Furthermore, the purpose is generally to generate theory and explanations rather than testing a hypotheses. In such the present work can be considered qualitative: Rather than testing a hypothesis, generating explanations and understanding of the way the different damage indicators work is sought after. Inductive reasoning is often used in qualitative research, so that conclusions are made based on an extension of knowledge beyond what can actually be known [57, 59, 60, 61, 62]. The conclusions of this thesis can hopefully be inferred to real-life structures, but this is notably an inductive inference.

Deep and detailed understanding of the subject of interest can be obtained with qualitative research, however, this may be at the expense of generalizability [59]. Furthermore, qualitative research is often not possible nor desirable to approach entirely objectively because qualitative data may be understood and interpreted differently depending on the eye who sees it. With quantitative research, large data sets can be analyzed objectively which can lead to more generalizable conclusions. On the other hand, all aspects of complex or sensitive issues may not be covered with these approaches. Quantitative and qualitative methods are often compatibly combined, which can even be said to be necessary if one is to gain comprehensive knowledge on a field [57]. Hence, a combination of the two is used herein to ensure the integrity of the thesis.

2.2 Data Collection and Data Analysis Methods

Qualitative data is collected from online sources by a literature search and review. It is carried out to provide information relating to the general background and context of the research, as well as the development of the applied framework and evaluation of results. The focus of the literature search has been on academically authoritative texts like academic books, journals and research reports. The sources used are listed in the reference list. This is expected to lead to reasonable decisions and conclusions throughout the whole work.

Furthermore, different software are used for data collection and as a tool for data analyses, in which well established methods from the literature are applied. The programs and methods are presented in the following where a discussion of their respective credibility also is given.

The software CSiBridge 22 produced by Computers and Structures, Inc. as well as the software MATLAB 9.9 produced by MathWorks is used. CSiBridge is a three dimensional bridge modeling, analysis and design software which utilizes the finite element method in its calculations. This method is commonly applied in software dedicated to modeling and analysis of structural systems and it is generally accepted that finite element based software produce satisfying results applicable in the design of civil structures. MATLAB is a mathematical program developed for iterative analyses and design processes. It uses a script language based on C and allows for the analysis of data

through a multitude of algorithms. Several toolboxes with collections of functions are available, all professionally developed, tested and fully documented. The integrity of results obtained with both programs thus depend on the ability of the user to provide the correct input information, rather than the inherent abilities of the software.

Herein, a bridge is modeled in CSiBridge before acceleration data and modal parameters are derived from the program. A script to generate noise disturbances of the acceleration data is produced in MATLAB to simulate a realistic, operative bridge model. MATLAB is also used as a tool to analyze the acceleration data with the damage identification methods of interest. These damage identification methods utilize damage indicators which can be derived from the modal parameters and their change over time. The damage identification methods used for the analyses herein are based on the damage indicators modal shape curvature, modal flexibility and modal strain energy. The development and research on these parameters is extensive. Although the efficacy of their application remain insufficient with regards to damage sensitivity, their further development and investigation is attractive due to these parameters' clear physical interpretation and the sound theoretical approach of their mathematical construction.

In order to increase the efficiency of the different damage indicators mentioned, as compared to the findings presented in existing research on the area, the data will herein rather be evaluated statistically. Current research evaluates the efficacy of the indicators based on discrete data. By accumulating discrete data over a period of time it is the goal of this research to evaluate the statistical properties of the accumulated data and to assess whether this can provide more efficient and reliable damage detection as compared to existing procedures. The frequency of detection of damage is thus calculated to present the trend over time.

2.3 Reflection and Quality Check

An evaluation of the credibility of the work is presented in the following. The key terms that are evaluated are the validity, reliability, objectivity and generalizability of the work, of which general definitions are presented as well. Furthermore, many different literary sources are used during the study and so the credibility of these will have an influence on the credibility of this work as a composition. This will also be discussed.

2.3.1 Validity

Validity refers in the process of research particularly to the obtained results. The validity of the results are dependent on the quality of the different measures employed in deriving the results. Validity refers to whether research really measures what it claims to be measuring [63, 64]. Different criteria have been proposed on how to evaluate the validity of research. Those found relevant for this research are internal validity, construct validity and criterion validity.

Internal validity can be defined as the extent to which results are representative for the observed phenomenon. With high internal validity all alternative explanations for the findings can be eliminated and the research project is free from theoretical or methodological error. Consequently, the internal validity is threatened when other plausible rival explanations can not be eliminated [65, 66]. All results from the analyses performed in this report are dependent on accelerogram measurements which are obtained from CSiBridge. After polluting these data with noise it is the purpose to detect whether damage occurs in the modelled bridge, through different algorithms.

As previously explained the theoretical computation of true structural behaviour through FEA is generally accepted. The controlled environment of this software as well as the theoretical soundness of the proposed algorithms will make the results highly representative of the observed phenomenon. The internal validity is thus considered satisfactory.

Construct validity, on the other hand, is kept high when the measurements from an instrument support predictions that are made from theory. The accelerograms produced by CSiBridge are in line with theoretical expectation, and the construct validity is thus good. The criterion validity may be high if the measurements produced by an instrument is close to those made by another instrument which is known to be valid [63, 67]. The measurements produced in CSiBridge accurately represents expected behavior based on actual vibration measurements on true structures. This si particularly true for when noise has been added to the measurements, although the general trend of the accelerogram both with and without noise is representative of reality. The criterion validity is therefore considered high.

2.3.2 Reliability

Reliability has to do with the quality, or consistency, of the measurements. Reliable measurements will produce the same results when performed repeatedly. Errors often occur in research that includes measurements which can effectively degrade the reliability of the research. These errors can be random or systematic. Random errors in general do not affect the average results. This is opposite to systematic errors, which can therefore be considered biases in measurement. It has been argued that reliability can not be computed because one would have to know the truth, which on a general term can not be known. However, the reliability may be estimated as the correlation between two observations of the same measure [59].

The collection of acceleration data that constitute the basis for this study is generated with software. Therefore, the output is the same every time the simulation is run. This is also checked and approved. This indicates high repeatability and accordingly high reliability. However, a white noise signal is applied to the acceleration time histories which consists of different random values for each time. This is done intentionally to investigate whether the damage identification methods repeatedly give the same results, and to ensure a generalizable outcome and evaluate the reliability of the damage detection algorithms.

2.3.3 Objectivity

Something is said to be objective when it does justice to the object of study. Therefore, an objective researcher must attempt to let the object speak as well as avoiding distortions. It is greatly debated whether it is possible for a researcher to ever be purely objective because all have interests and knowledge from previous experiences that affect their work. It is often said that objectivity is easier to maintain with a quantitative research approach than with a qualitative one. This is because quantitative methods generally relies on numbers and the mathematical analysis of these. In qualitative research, on the other hand, the researcher stands more freely to evaluate the data [68, 69].

Both quantitative and qualitative research approaches are used here, in which the quantitative methods are used for data collection and calculations, while theoretical knowledge is used to evaluate and draw conclusions from the results. A thorough literature study was conducted at the initiation of this project so that choices could be made based on well established theory rather than the subjective minds of the researchers. The purpose of this report is to evaluate the efficacy of different damage

detection indicators applied in VBDD. With varying the parameters of noise level, damage location and damage level it is possible to compare the efficacy of the different strategies. This allows for comparison and a better objective fundament. Moreover the production of the results are highly dependent on quantitative approaches through the mathematical manipulation of the accelerograms. The production of the results is therefore considered highly objective, whereas the evaluation of the results through the authors interpretation will be influenced by subjectivity.

2.3.4 Generalizability

Generalizability can be defined as the degree to which the findings are relevant in other contexts. With low generalizability, the results would be unique and unlikely to occur again in another settings than the one from which they were obtained [70, 71].

With the test object being a numerically modelled bridge, considerations are done to establish a model that replicates responses similar to what would be obtained from a real bridge. Vibration measurements on real bridges exposed to operational loading will usually deviate due to operational or environmental factors such as temperature differences and humidity. Furthermore errors may be present in the sensors that measure the vibratory responses. These factors are in the context of OMA referred to as noise. To account for these uncertainties and hopefully generalize the results to real-life applications, an attempt is made to include the effects of noise through the addition of a normally distributed noise signal to the accelerograms.

Another issue regarding the generalizability is that this fictitious bridge is analyzed both in an undamaged and a damaged state. This is convenient for the purpose of the study, as different damage scenarios can be investigated without any expensive full scale experiments. However, real structures have often not been monitored in an undamaged state, which is a common issue in structural health monitoring. The work here can therefore not be directly generalized to real structures which have not been monitored at an early age. Nevertheless, the introduction of statistical analyses when evaluating the trends of the damage indicators may be applicable either way.

2.3.5 Source Criticism

The sources that are used in the production of this thesis are generally collected online. In theory, anyone can publish their work online. Therefore, one must be critical when considering the integrity of the sources. For instance, the level of objectivity in the sources can be discussed as the incentives of their authors can not be known. Moreover, the literature available on some of the topics herein frequently refers to the same, few researchers. This may indicate that there are only a few experts on the field and that more research should be done on these topics.

The theory presented herein is gathered from a spectre of sources, in which the content is compared to one another to ensure reliability. Theory is gathered from recognized online databases like EI EngineeringVillage and ScienceDirect. The literature from these platforms is peer-reviewed to ensure credible research for users. Furthermore, credible search engines like Oria and Google Scholar have been used. Herein, the credibility of the sources referred to is also checked.

Chapter 3

Theoretical Background

This chapter provides the theoretical background of the proposed framework. The classical formulations on dynamic systems, which can be solved to acquire the continuous time vibration response as well as the modal characteristics of a system, is included in this. Vibration-based damage detection is attractive due to its clear physical interpretation, and by including the formulations of classical structural dynamics it is the purpose of the authors to provide the reader with an understanding of the dynamic features used in damage detection.

For the purpose of this work the information needed to solve the classical formulations is not available and the technique OMA is applied instead to acquire the modal characteristics of a simulated railway bridge. Nonetheless, an introduction to classically formulated structural dynamics is provided. This is to ensure a comprehensive understanding of the modal properties of a structure and their effect on its dynamic response. Moreover the classical formulations are incorporated in several OMA algorithms, including Stochastic Subspace Identification (SSI) which is utilized herein. The definition of the phenomenon of damping is also relevant to the numerical modelling of the railway bridge that is investigated.

A description of the mathematics that go into calculating different damage sensitive features is provided next. This includes the SSI algorithms, as well as modal curvature, modal strain energy and modal flexibility.

3.1 Structural Dynamics

Structural dynamics concerns the mathematics used in the description of the behaviour of structures subjected to dynamic loading. Structural systems in operation are subjected to a range of dynamic forces, such as winds, people, earthquakes and traffic. Understanding the principles of structural dynamics is thus of high relevance to the understanding of OMA and VBDD, as the ambient loads existing in the operational conditions as well as structural response is of a dynamic nature. Describing the reaction of a system to dynamic loading is aided by the idealization of the system into a so-called multiple degree of freedom (MDOF) system. In a MDOF system a structure is discretized into a set of lumped masses, connected by massless columns with pertaining stiffnesses. Highly idealized elements called viscous dampers are implemented to represent the combined contribution of damping to the system. Each of the lumped masses in the system represent a degree of freedom. An n-DOF system will contain n mode shapes, n natural frequencies and n modal damping ratios.

Considering a hypothetical case of an undamped structure, its free vibration response, when

initiated with the appropriate distribution of displacements in its n DOFs, will demonstrate perpetual oscillations in a simple harmonic motion. In this motion a characteristic deflected shape is present. This shape is called a mode shape. The single resonant frequency that this simple harmonic motion and characteristic shape pertains to is called a natural frequency. These modal properties are inherent features of a system. They are completely determined by the system´s structural properties, including masses, stiffnesses and damping [72].

During dynamic loading a structural system is subjected to so-called forced vibration, in which the dynamic behavior of the system is influenced and "contaminated" by the loading. When the loading ceases the remaining movement in the system is referred to as free vibration. During free vibration the behaviour of the system is solely dependent on the inherent properties of that system. In classical structural dynamics, the free vibration response of a structural system is described by the equation of motion:

$$[\mathrm{M}]\{\ddot{\mathrm{u}}(\mathrm{t})\} + [\mathrm{C}]\{\dot{\mathrm{u}}(\mathrm{t})\} + [\mathrm{K}]\{\mathrm{u}(\mathrm{t})\} = 0 \tag{3.1}$$

[M], [C] and [K] are the mass, damping and stiffness matrices. $\{\ddot{\mathrm{u}}(\mathrm{t})\}$, $\{\dot{\mathrm{u}}(\mathrm{t})\}$ and $\{\mathrm{u}(\mathrm{t})\}$ are the acceleration, velocity and displacement vectors. As according to Equation 3.1 the free vibration response of a system can be described with the inherent structural properties mass, damping and stiffness. The general solution to Equation 3.1, when the system is classically damped, is presented in Equation 3.2. A system can also be non-classically damped. Whether classical or non-classical damping should be applied is dependent on the nature of the structure they aim to describe, particularly with respect to the distribution of damping properties throughout it. The main advantage of using classical damping is that the orthogonality of modes is preserved. This allows for more convenient mathematical descriptions, compared to non-classical damping. It is nonetheless remarked that the system response may be underestimated and that non-linear behavior will not be captured with classical damping [73].

$$\{\mathrm{u}(\mathrm{t})\} = \sum_{\mathrm{n}=1}^{\mathrm{n}} \{\phi_{\mathrm{n}}\} \mathrm{e}^{-\zeta_{\mathrm{n}}\omega_{\mathrm{n}}\mathrm{t}} \left[\mathrm{q}_{\mathrm{n}}(0)\cos(\omega_{\mathrm{nD}}\mathrm{t}) + \frac{\dot{\mathrm{q}}_{\mathrm{n}}(0) + \zeta_{\mathrm{n}}\omega_{\mathrm{n}}\mathrm{q}_{\mathrm{n}}(0)}{\omega_{\mathrm{nD}}} \sin(\omega_{\mathrm{nD}}\mathrm{t}) \right] \tag{3.2}$$

The solution, which provides the displacement as a function of time, $\{\mathrm{u}(\mathrm{t})\}$, due to initial displacement $\{\mathrm{u}(0)\}$ and velocity $\{\dot{\mathrm{u}}(0)\}$, contains the following parameters:

- $\{\phi_{\mathrm{n}}\}$: The n^{th} mode shape of the system, assembled into a vector.

- ζ_{n}: The damping ratio of the n^{th} mode.

- ω_{n}: The natural circular frequency of the n^{th} mode.

- q_{n}: The time variation of displacements.

- ω_{nD}: The natural circular frequency with damping of the n^{th} mode, determined by

$$\omega_{\mathrm{nD}} = \omega_{\mathrm{n}}\sqrt{1-\zeta_{\mathrm{n}}^2} \tag{3.3}$$

- $\dot{\mathrm{q}}_{\mathrm{n}}$: The time variation of velocities.

When damping is included the displacement amplitude at any DOF will decrease with every oscillation. The rate of decay depends on the damping ratio ζ_{n} of the n^{th} mode. The damping influences the natural frequency of the system as according to Equation 3.3. Damping is a complex phenomenon. It is a collective term for a variety of factors that contribute to the dissipation of the

energy stored in an oscillatory motion. Describing these contributions mathematically is difficult and some factors are even hard to identify [74]. The mathematical description and calculation of the modal damping ratios therefore rely on assumptions that the damping is viscous and that the response of the system is linear [75].

A common approach to construct the damping matrix of a structure is Rayleigh damping. The damping is expressed as a linear combination of the stiffness and mass matrices as presented in Equation 3.4.

$$\zeta_n = \alpha[M] + \beta[K] \tag{3.4}$$

α and β are called mass and stiffness proportional coefficients with units sec^{-1} and sec respectively. The damping ratio for the n^{th} mode of a system can also be expressed with these scalars and the natural frequency of the n^{th} mode, as expressed in Equation 3.5.

$$\zeta_n = \frac{\alpha}{2}\frac{1}{\omega_n} + \frac{\beta}{2}\omega_n \tag{3.5}$$

Equation 3.5 can also be expressed in matrix form. This allows for α and beta to be determined from specified damping ratios ζ_i and ζ_j of any two modes denoted i and j:

$$\frac{1}{2}\begin{bmatrix} 1/\omega_i & \omega_i \\ 1/\omega_j & \omega_i \end{bmatrix}\begin{Bmatrix} \alpha \\ \beta \end{Bmatrix} = \begin{Bmatrix} \zeta_i \\ \zeta_j \end{Bmatrix} \tag{3.6}$$

ζ_i and ζ_j can be specified from experimental data obtained from experiments of structures similar to the one being analyzed. Based on collective experimental data it is reasonable to assume that the damping ratios of the i^{th} and j^{th} mode are equal [76]. Equation 3.6 can then be rewritten to solve for α and beta as according to Equation 3.7:

$$\alpha = \zeta\frac{2\omega_i\omega_j}{\omega_i + \omega_j} \qquad \beta = \zeta\frac{2}{\omega_i + \omega_j} \tag{3.7}$$

Naturally, a structure in operational conditions will rarely be excited such that an appropriate initial displacement for harmonic motion is observable. Rather, an initial excitement will result in a motion of the structure that is determined by several modes acting in combination. This was mathematically described in Equation 3.2. The frequency of the exciting forces will impact which modes that participate in the resulting free vibration motion of the structure. No matter the size or location of the imparted force, the motion of the structure is completely determined by some combination of its inherent modes.

Another concept in structural dynamics and modal analysis is that of modal participation mass ratio (MPMR). When a structure is excited, some modes may contribute more to the resulting motion, depending on their mode shapes. Generally, the MPMR represents the percentage of the mass of the structure that participate in a mode. In such the MPMR is a measure on the energy contained in each mode and usually the modes with the highest MPMR will have the biggest contribution to a structural dynamic response.

3.2 Stochastic Subspace Identification

Stochastic Subspace Identification (SSI) is a time domain system identification technique. SSI methods are considered to be among the most robust and accurate methods available for estimation

of modal parameters from output-only data [77, 78]. The two most common SSI methods are the covariance-driven stochastic subspace identification (SSI-Cov) and the data-driven stochastic subspace identification (SSI-Data). SSI-Cov was introduced in 1996 by De Moor and Van Overschee [79]. It uses direct estimates of the covariance of the response to identify the system. This method addresses the stochastic realization problem, which is the problem of identifying a stochastic state-space model from output-only data [80]. SSI-Data is somewhat similar but is rather based on projecting the row space of the future outputs into the row space of the past outputs. SSI-Data is relatively slow compared to SSI-Cov as a QR factorization is used instead of utilizing the fast Fourier transform algorithm to compute covariances [81].

For the application of OMA in this project SSI-Cov is therefore utilized. A pre-written algorithm provided by MATLAB will be used [82]. Further follows a brief description of the SSI-Cov implementation this algorithm provides, with equations gathered from the following references [83, 84].

For ambient vibration tests, the input can be considered to be stationary random white noise. A stochastic and discrete state-space model is assumed to represent a n-degree-of-freedom dynamical system exited by white noise as

$$\{z_{k+1}\} = [A]\{z_k\} + \{w_k\} \tag{3.8}$$

$$\{y_k\} = [C]\{z_k\} + \{v_k\} \tag{3.9}$$

where $\{y_k\}$ is the discrete-time output vector modelled by a discrete-time stochastic state-space model and $\{z_k\}$ represents the discrete-time state vector. $\{w_k\}$ and $\{v_k\}$ are noise terms, presenting process and measurement noise as zero-mean white noise vectors. [A] and [C] are the state matrix and discrete output matrix, respectively. The sub-indices correspond to discrete time sample numbering during the time $t = (k - 1)f_s^{-1}$, where f_s is the sampling frequency. The recorded data are so arranged in the matrix [Y],

$$[Y] = \begin{bmatrix} \{y_1\}^T \\ \{y_2\}^T \\ \vdots \\ \{y_N\}^T \end{bmatrix} \tag{3.10}$$

[Y] has dimensions N$x\mathit{l}$, as the data has l channels and N samples. Now, discrete correlation matrices are estimated by employing fast Fourier transform and inverse fast Fourier transform. The discrete correlation matrix, $[R_k]$, at a time lag $\Delta t = kf_s^{-1}$ is defined below.

$$[R_k] = E\left(\{y_{n+k}\}\{y_n\}^T\right) \tag{3.11}$$

In which E denotes the expected value operator. The output data is used to construct a block-Hankel matrix or alternatively a Toeplitz matrix, the former will be used herein. The block-Hankel matrix consists of correlation matrices arranged as sub-matrices, as in Equation 3.12.

$$[H_i] = \begin{bmatrix} [R_1] & [R_2] & \dots & [R_i] \\ [R_2] & [R_3] & \dots & [R_{i+1}] \\ \vdots & \vdots & \ddots & \vdots \\ [R_i] & [R_{i+1}] & \dots & [R_{2i-1}] \end{bmatrix} \tag{3.12}$$

In which 2i - 1 is the maximum number of time lags. The block-Hankel matrix can be decomposed into its observability matrix, $[\vartheta_i]$, and controllability matrix, $[\tau_i]$.

$$[H_i] = [\vartheta_i][\tau_i] \tag{3.13}$$

where,

$$[\vartheta_i] = \begin{bmatrix} [C] \\ [C][A]^2 \\ \vdots \\ [C][A]^{i-1} \end{bmatrix} \qquad [\tau_i] = \begin{bmatrix} [G] & [A][G] & \dots & [A]^{i-1}[G] \end{bmatrix} \tag{3.14}$$

In which [G] is the cross-correlation matrix between the state vector shifted by one sample and the output vector, defined in equation 3.15.

$$[G] = E\left(\{z_{n+1}\}\{y_n\}^T\right) \tag{3.15}$$

The block-Hankel matrix may be pre- and post-multiplied with weighting matrices before a singular value decomposition is preformed. This is done to improve the identification of modes which are poorly excited. For this work no weighting will be involved, which is called the balanced realization (BR) method or, alternatively, unweighted principal components (UPC). So, the weighting matrices are set to identity matrices [80, 83, 85]. Now, a singular value decomposition is performed on the unweighted Hankel matrix to estimate the observability and controlability matrices. The state matrix, [A], is computed as in Equation 3.16.

$$[A] = [\vartheta_{down}]^{+}[\vartheta_{up}] \tag{3.16}$$

In which $[\vartheta_{down}]$ is obtained by removing the first l rows from $[\vartheta_i]$, whereas $[\vartheta_{up}]$ is found by removing the last l rows. + means that the pseudo-inverse is taken of the $[\vartheta_{down}]$ matrix. The first l rows from $[\vartheta_i]$ are extracted to create the output matrix, [C].

$$[C] = [\vartheta_i]_{1:l} \tag{3.17}$$

Next, the estimated state matrix is subjected to an eigenvalue decomposition to yield discrete system poles, $\hat{\lambda}_r$ and system eigenvectors, ψ. The reader is referred to [85] for details. These are converted to continuous system poles and eigenvectors as follows:

$$\lambda_r = \exp\left(\hat{\lambda}_r f_s^{-1}\right) \tag{3.18}$$

$$\{\phi\} = [C]\{\psi\} \tag{3.19}$$

The application of SSI-Cov requires some user-defined parameters. One of these is the model order, which equals the number of eigenvalues present in the model. The accurate prediction and selection of this parameter is however not the primary concern in modal testing applications. The primary concern is rather the physical relevance of the modes that constitute the model [86]. An approach which has become a key tool in modal testing has been developed to handle this: It is based on empirical observations that in a large number of modal identification problems, the physical modes of a structure appear at nearly the same natural frequency when the model order is over-specified, whereas other, spurious modes do not [87]. Spurious modes may occur due to both noise present in the output signals (caused by for example a loose sensor, winds or temperature change) as

well as mathematical biases [14]. In this approach parametric models are identified for a wide range of model orders, most of which larger than the number of modes in the relevant frequency band. The modes of all these models are plotted in a model order vs. eigenfrequency diagram, called a stabilization diagram. In a stabilization diagram the physical modes appear as vertical lines alligned with stable poles. Selecting a proper model order thereby depends on identifying which frequencies and pertaining mode shapes correspond to these vertical lines.

3.3 Modal Shape Curvature

In 1991 Pandey, et al. demonstrated that the absolute change in modal curvature can be used to indicate damage, due to the relationship between curvature and bending stiffness [29]. This can be illustrated by a simple Euler-Bernoulli beam, in which the curvature and the flexural stiffness of a cross section are related by the following expression:

$$\varkappa = \frac{\mathrm{M}}{\mathrm{EI}} \tag{3.20}$$

$\varkappa$ denotes the curvature, M is the bending moment of the cross section and EI is the bending stiffness of the cross section. Damage resulting in a reduction in the bending stiffness at some location will, as according to Equation 3.20, result in an increase in the curvature at that location. Thus it can be inferred that curvature can be used to both detect and locate damage entailing a reduction in bending stiffness.

The modal shape curvature can be estimated from mode shapes. The constituents of the mode shape are estimated, by SSI, in correspondence with available sensor readings. For practical and economical reasons not many sensor readings are always available. In order to increase the resolution of the description of the deformed shape, the available data can be interpolated by means of cubic spline. The curvature, which is the second derivative of displacement, can be estimated using numerical methods. Applying central difference approximation, presented in Equation 3.21, the second derivative of the mode shapes can be estimated as follows:

$$\phi''_{\mathrm{k,i}} = \frac{\phi_{\mathrm{k,i+1}} - 2\phi_{\mathrm{k,i}} + \phi_{\mathrm{k,i-1}}}{\mathrm{h}^2} \tag{3.21}$$

$\phi''_{\mathrm{k,i}}$ denotes the modal shape curvature of the k^{th} mode shape at the i^{th} location, and similarly $\phi_{\mathrm{k,i}}$ denotes the k^{th} mode shape at the i^{th} location. h is the distance between the i^{th} locations.

Detecting damage using modal shape curvature requires the comparison between a reference, undamaged (U) and possibly damaged (D) curvature configuration. The damage indicator $\mathrm{I_C}$ is at each i^{th} location defined as the sum of variation of modal curvature, $\Delta\phi''_{\mathrm{i}}$, over all identified modes according to Equation 3.22 [33].

$$\mathrm{I_C} = \Delta\phi''_{\mathrm{i}} = \sum_{\mathrm{k=1}}^{\mathrm{n_{modes}}} |\phi''_{\mathrm{k,i,D}} - \phi''_{\mathrm{k,i,U}}| \tag{3.22}$$

The modal shape curvature is sensitive to stiffness variations. The method has shown to be effective in detection and localization of damage as the change in curvature typically is higher close to damage [43, 88, 89]. However, its performance in localization of damage is varying in the case of multiple damage locations on a structure [43, 90]. Drawbacks in its use has also been found with the use of noisy signals. The approximation of the second derivative, used to compute the curvature from the mode shapes, amplifies the effect of noise and has also been found to introduce unacceptable

errors [32, 34, 35]. This may obstruct the possibility to localize damage [33]. Furthermore, some of the modes may be more effective than other for damage identification [43].

3.4 Modal Strain Energy

The ratio of the change in the modal strain energy was proposed as a damage feature by Stubbs in 1992 [38]. This damage identification method is based on the same theory as the previously mentioned methods and it is so assumed that damage does not affect the fractional modal strain energy. Meaning that the ratio between the strain energy in the i^{th} element and the total strain energy for the k^{th} mode is constant. This leads to a Equation 3.23, which is a function of the modal curvature as the ratio between the bending stiffness in the damaged and undamaged state.

$$I_S = \beta_i = \frac{\sum_{k=1}^{n_{modes}} (EI)_{i,k}^{D}}{\sum_{k=1}^{n_{modes}} (EI)_{i,k}^{U}} = \frac{\sum_{k=1}^{n} \left[\frac{\int_{x_i-\Delta x/2}^{x_i+\Delta x/2} (\phi''(x))_D^2 \, dx}{\int_0^L (\phi''(x))_D^2 \, dx} \right]}{\sum_{k=1}^{n} \left[\frac{\int_{x_i-\Delta x/2}^{x_i+\Delta x/2} (\phi''(x))_U^2 \, dx}{\int_0^L (\phi''(x))_U^2 \, dx} \right]} \tag{3.23}$$

I_S is the damage indicator and it is assumed that a value higher than 1 means that the structure is damaged at that location.

The modal strain energy method has shown to effectively detect and locate single or multiple damage locations in a structure [90, 88, 39]. This method is also tested to be more robust against noisy signals compared to the curvature and flexibility method, although damage location results are affected by this [90]. The method is typically more efficient when several modes are included [39]. Furthermore, it has successfully been used to quantify damage for normal noise levels when many modes are used [91].

3.5 Modal Flexibility

Damage detection in structures based on changes in the flexibility was first proposed by Pandey and Biswas [46] in 1994. The modal flexibility method may be used to both detect and localize damage, and is most sensitive to changes in the first few modes [42]. The basic theory of this method is that the stiffness of a structure will decrease when damaged occurs, which again leads to a more flexible structure. This method is therefore closely related to the modal shape curvature method as well as the modal strain energy method.

The flexibility matrix is defined as the inverse of the static stiffness matrix. So, the applied static force and the resulting structural displacement are related by the flexibility matrix [42]. The method is therefore sometimes referred to as the matrix force method. The flexibility matrix can be relatively accurately estimated from the first few modes, which is what is normally found. This is because the contribution of each mode is scaled so that the higher, less reliably identified, modes have a reduced contribution [33]. However, a complete and accurate flexibility matrix may only be computed when all mode shapes and natural frequencies are given [92]. Furthermore, the mode shape vectors must be mass normalized. If the mass is uniformly distributed through a structure the mode shapes can be normalized with respect to a diagonal matrix whose terms are proportional to the length of influence of each node [33]. In such a case this allows them to be normalized with respect to the identity matrix as according to the method proposed by Quqa et al. [93].

The measured flexibility matrix is usually compared to the flexibility matrix of the undamaged structure as an indicator to damage. The flexibility matrix, [F], is estimated by the mode shapes as follows

$$[\mathrm{F}] = \sum_{\mathrm{k}=1}^{\mathrm{n_{modes}}} \frac{1}{\omega_{\mathrm{k}}^2} \{\phi\}_{\mathrm{k}} \{\phi\}_{\mathrm{k}}^{\mathrm{T}} \tag{3.24}$$

Here, each mode is scaled by the inverse of the circular pulsation squared, ω_{k}^2, so that the first modes have a higher contribution. $\{\phi\}_{\mathrm{k}}$ denotes the mode shape vector of the k^{th} mode shape. The damage indicator, [ΔF], is the variation in the modal flexibility matrix, as defined below.

$$[\Delta \mathrm{F}] = [\mathrm{F_D}] - [\mathrm{F_U}] \tag{3.25}$$

Where $[\mathrm{F_D}]$ and $[\mathrm{F_U}]$ are the flexibility matrix of the damaged and undamaged structure, respectively. The j^{th} column of [ΔF] corresponds to the variation of the deformed shape due to a unit force applied at location j. The absolute value of the maximum variation of the flexibility, $\mathrm{I_F}$, is computed for each column and is assumed to be a measure of the damage at each measurement location,

$$\mathrm{I_F} = \delta_{\mathrm{j}} = \max|\delta \mathrm{f_{ji}}| \tag{3.26}$$

where $\delta \mathrm{f_{ji}}$ are the elements of [ΔF].

The modal flexibility method has been tested to perform adequately in detection and localization of damage [43, 90]. However, issues often arise with higher noise levels [94].

Chapter 4

Analysis Procedure and Application

This chapter concerns the procedure of the analysis that is performed to evaluate a new, proposed framework for long-term vibration-based methods for SHM.

A two span, single lane, concrete railway bridge is modeled with the software CSiBridge. A simple illustration of the bridge model is presented in Figure 4.1. An analysis with a moving load (a train) is then performed to obtain the vibration response of the bridge. The response is collected in the form of accelerograms from several locations along the spans of the bridge deck. Only the vertical direction is considered, as this is the direction the loading is applied in. This procedure is repeated with several different conditions in the bridge. In one state the bridge will be undamaged. In others, varying degrees of damage is introduced into one of the bridge spans: a 5 %, 10 %, 20 %, 50 % and 80 % reduction in the bending stiffness in the vertical direction of the bridge. This is done to simulate an increasing damage over time. This will be repeated for four different locations in the respective span.

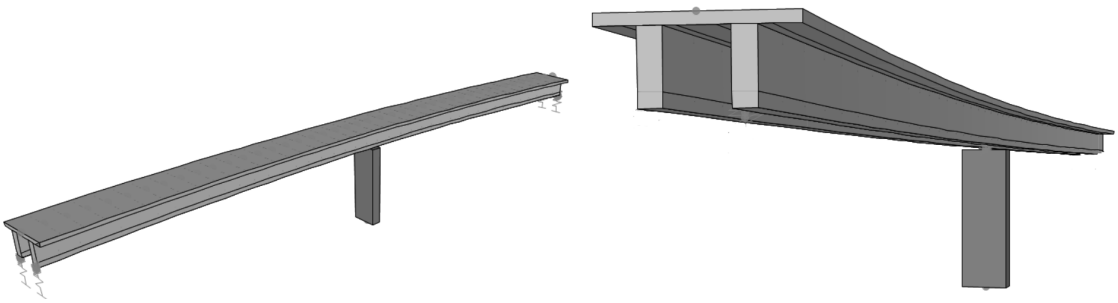

Figure 4.1: The railway bridge as modeled in CSiBridge.

The accelerograms are then used to obtain the modal properties of the bridge in its different intact and damaged states, through OMA. This is done in MATLAB with the system identification approach SSI-Cov. To simulate the ambient conditions that would affect acceleration measurements of a real bridge, a normally distributed random noise signal is added to the acceleration data. 500 different noise signals are applied to each of the accelerograms, in each state of the bridge and for each damage location. In such, each of these 500 now noise corrupted accelerograms are deemed actual sensor readings for consecutive days in a timeline.

As described in Chapter 3, the different damage indicators are calculated by comparing some modal properties of the intact system to those of the system with damage. The properties of

the structure are thus compared between two discrete points in time. Noise in the measurements which are used to derive the modal properties, may however lead to false indication of damage. By introducing a time perspective the purpose is to evaluate if the confidence in the damage indicators can be increased by statistical analysis of the evolution of these discrete data. Different levels of noise are evaluated as well, to investigate the ability of SSI-Cov and the different damage indicators in handling this. Figure 4.2 presents a flow chart that demonstrates the different combinations of damage locations, damage levels and noise levels which accelerograms will be created for.

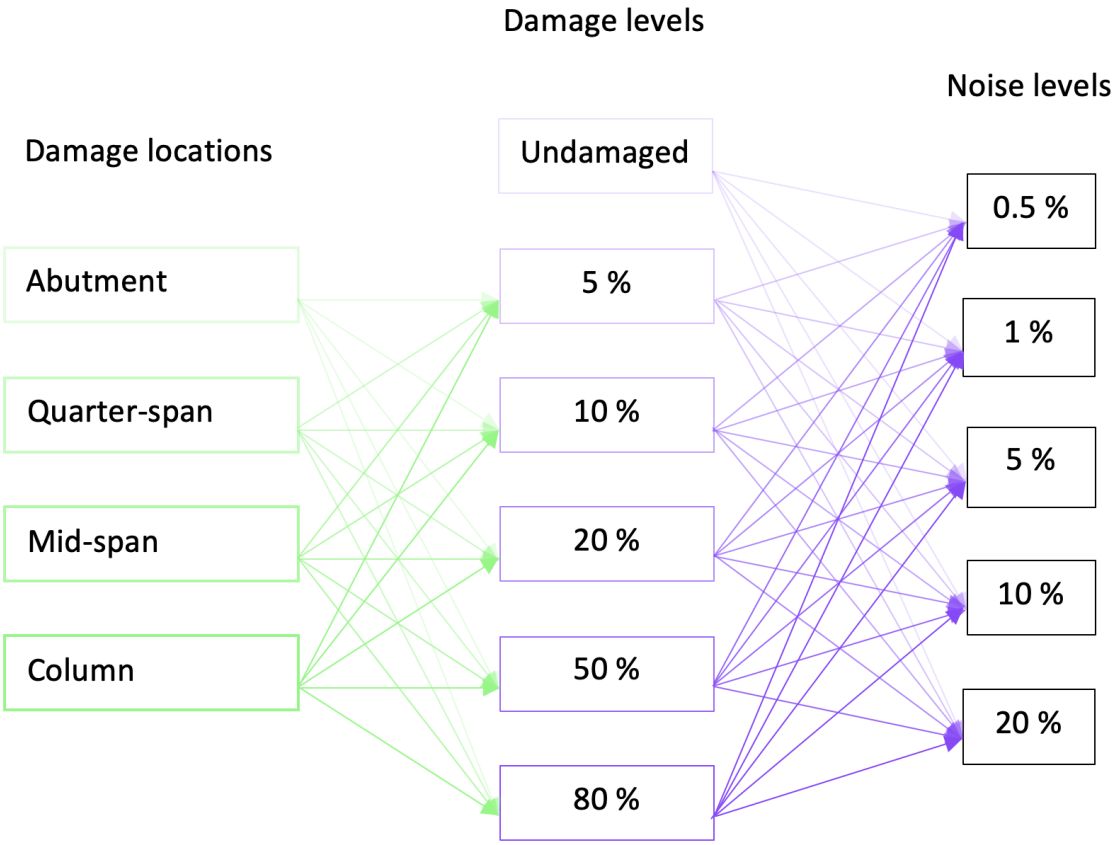

Figure 4.2: Flow chart demonstrating the different combinations of damage locations, damage levels and noise levels which accelerograms will be created for.

CSiBridge is also used to run a modal analysis on the bridge in its different intact and damaged states. The modal analysis determines the modal properties of the structure. By comparing the modal properties from the modal analysis in CSiBridge with the modal properties from SSI, the efficacy of the SSI algorithm and the significance of its results can be further ensured. Notably, this would not be an option in the application of VBDD in real life. Even if a numerical model of a real bridge is available for modal analysis, the results may deviate as perfect numerical representations of real structures are difficult to achieve.

When the modal properties of the structure are determined in its intact and damaged states, for different noise levels and damage locations, the different damage sensitive features are applied to evaluate their efficacy in detecting and localizing the introduced damage. This primarily entails computation of so-called damage indicators, as well as visualization and representation of the data. MATLAB will be used for this purpose.

4.1 Numerical Model

Herein follows a brief description of the numerical railway bridge model that is the test specimen for the evaluation of the different damage detection strategies.

The numerical model is created in the FEM software CSiBridge. The bridge is 84 meters long, divided into two spans by a supporting column at 44 meters. The deck constitutes a prestressed concrete double-tee section, illustrated in Figure 4.3, with a total depth of 2910 mm, which houses a single railway track. The supporting column as well as the deck are modeled with elastic beam-column elements. The column is a rectangular, reinforced concrete section with dimensions 1300 mm x 3600 mm. The bridge is assumed pinned at each of the abutments. Both the top and the bottom of the column are modeled as fixed. The damping in the bridge is defined as viscous proportional, or classical Rayleigh damping. It is specified by period so that the mass proportional coefficient, α, equals 0.19 sec^{-1} and the stiffness proportional coefficient, β, equals 0.00027 sec.

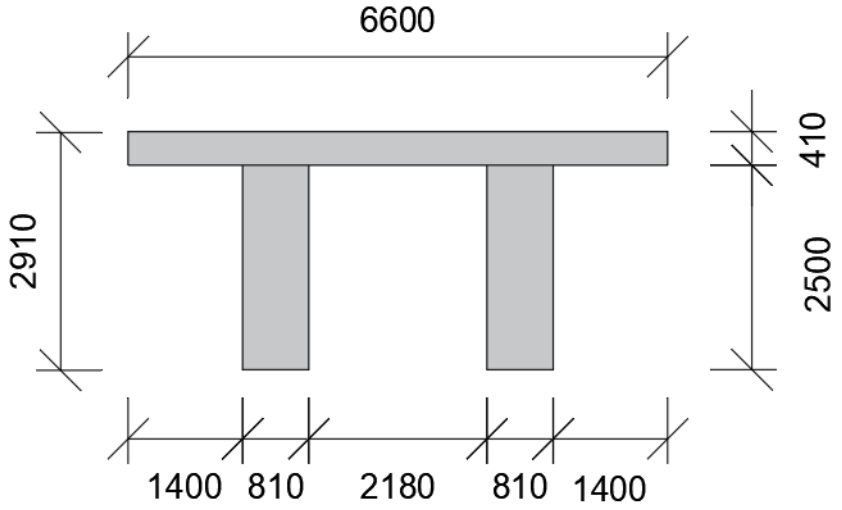

Figure 4.3: Cross section of the bridge deck [mm].

A moving load simulating a train is applied to obtain vibration data from the bridge. This data is collected in the shape of accelerograms in the lateral direction, as this is the direction the dynamical loading is applied in. The sampling frequency of the data is set to 200 Hz. The data is collected from ten different points on the bridge, five in each span. The bridge and the data collection points, which would represent real-world sensors, are illustrated in Figure 4.4. The geometrical locations of the sensors are presented in Table 4.1.

Sensor	1	2	3	4	5	6	7	8	9	10
Joint no.	3	7	12	17	21	26	30	34	38	42
Location [m]	4.0	12.1	22.2	32.3	40.1	48.4	56.4	64.4	72.3	80.2

Table 4.1: Joint numbers and geometrical locations of sensors.

A modal analysis is performed as well, from which mode shapes, natural frequencies and modal participation mass ratios are collected. The natural frequencies and MPMRs are only collected from the bridge in its undamaged state as a reference. As different states of damage are introduced to the

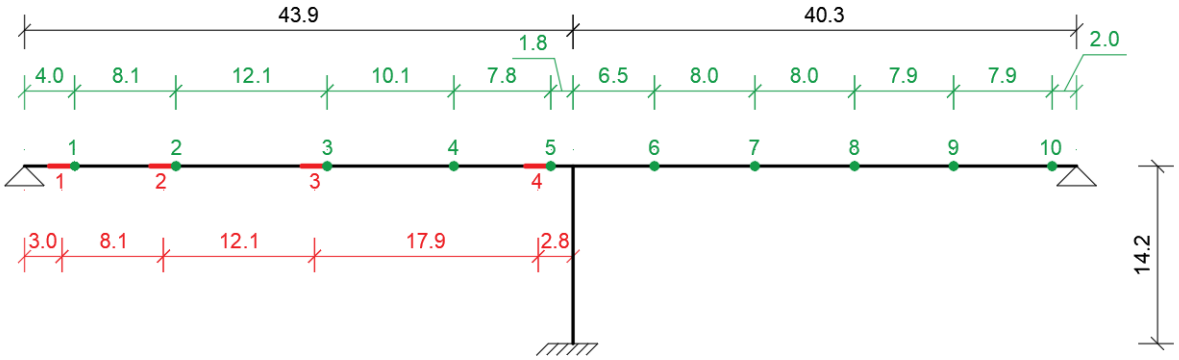

Figure 4.4: Plan view of the railway bridge [m]. Joints from which accelerograms are collected are marked with green dots and the elements in which damage is introduced are marked with red.

model only the mode shapes and the accelerograms from the ten locations are collected. Damage is introduced into four different elements, illustrated in Figure 4.4 and described in Table 4.2. This is done by reducing the vertical moment of inertia of these elements by different degrees: 5 %, 10 %, 20 %, 50 % and 80 %. The purpose is to check whether the efficacy of the damage identification strategies is affected by the severity and location of the damage.

Damage	1. Abutment	2. Quarter span	3. Mid span	4. Column
Joint no.	2 – 3	6 – 7	12 – 13	21 – 22
Location [m]	2.0 – 4.0	10.1 – 12.1	22.2 – 24.2	40.1 – 42.0

Table 4.2: Joint numbers and geometrical locations of damage.

4.2 Operational Modal Analysis

To determine the modal parameters of the structure operational modal analysis is applied to the collected accelerograms. A prewritten SSI-Cov function, provided by a toolbox from the programming platform MATLAB, is used for this purpose [82]. The SSI function requires the variables "order" and "s" to be determined. order refers to the desired maximum model order to be identified, while s refers to the number of block rows in the block-Hankel matrix. The recommended value $s = 2 * \text{order}$ is applied. The desired maximum model order is used in the construction of the so-called stabilization diagram and is set to 80.

Once these parameters have been selected the accelerograms, hereby referred to as signals, are uploaded. All the signals from CSiBridge, from different points on the bridge and for different damage scenarios, are uploaded. The signals include the full response of the bridge during and after the train crossing. The forced vibration response, which occurs when the train crosses, is removed from the signals. The free vibration response is the primary interest, as this part of the response of the bridge is solely contingent on the bridge, not the mass of the bridge and the loading in combination. Notably, this would not make a difference as the accelerograms are collected from CSiBridge and not actual recordings. For real-life applications this is however necessary.

The signals are contaminated with normally distributed noise signals in order to reflect a real-life

situation. This is done in accordance with Equation 4.1.

$$\ddot{u}_{j,k} = \ddot{u}_j^0 + \beta\lambda\ddot{u}_j^0 \tag{4.1}$$

$\ddot{u}_{j,k}$ refers to the k^{th} noisy sample of the acceleration record at the j^{th} sensor. $\ddot{u}_j^0$ refers to the non-noisy accelerogram at sensor j. β is a parameter for varying the level of noise applied to $\ddot{u}_j^0$. λ is a random number from the standard normal distribution. For the signals from the bridge in its intact state, 1000 samples for each noise level are created. 500 of these will be deemed training data for the different damage indicators. For the different signals where damage is introduced, 500 noisy signals are created.

In doing this each signal will emulate sensor readings from consecutive days in a timeline of the bridge. The procedure is repeated for five variations of β: 0.5 %, 1 % and 5 %, 10 % and 20 %. For each damage location and noise level, monitoring data is thus collected for a total of 3500 days. The data will be sorted such that damage increases along with time. This is illustrated in Figure 4.5.

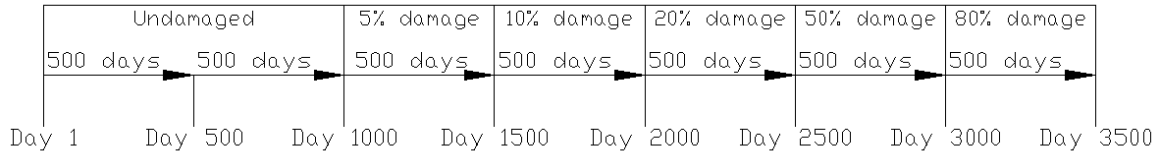

Figure 4.5: Timeline illustrating how the severity of damage increases with time for a given location of damage and noise level.

Before running the SSI-Cov function, a test run is performed from which a stabilization diagram is plotted for a signal with low noise from the bridge in its intact state. It is then inspected and an initial model order is selected. As previously described an over-identification of the model order will produce spurious modes which are not representative of the structural behavior of the system, but rather related to noise and mathematical biases [14]. Under-identification may however result in some physical modes not being captured.

The number of natural frequencies and mode shapes calculated corresponds to the stable points in the stabilization diagram of the selected model order: The stable points presumably correspond to the true structural modes of the structure rather than spurious ones. As a modal analysis has been run in CSiBridge the actual natural frequencies of the bridge in its intact state are available for comparison. The four lowest modes which can be identified as true physical modes of the structure will be extracted. To ensure that the same modes are extracted from all the signals, the natural frequencies pertaining to the different damage levels and locations are inspected from test runs with signals corrupted with a low percentage of noise. As a total of 17 500 iterations for each damage location will be necessary, efforts have been made to automatize the process of extracting just these four modes. This is done accordingly:

- For the first iteration of every damage level, for every damage location, the natural frequencies which were identified from the test runs will be the criteria for extraction. The mode shapes corresponding to these frequencies will be saved. A while loop is constructed which will be initiated if these frequencies cannot be identified. The while loop will then increase the model order, rerun SSI-Cov and again try to extract modes pertaining to the frequency criteria.
- For the remaining iterations, the extraction of the same mode shapes rely on a comparison to

the mode shapes identified from the first iteration. This is done according to Equation 4.2 for all four modes:

$$\min_{\forall j} \left\{ \left| \sum_{k} |\phi_k^{i=1}| - |\phi_{j,k}^{i}| \right| \right\} \tag{4.2}$$

$\phi_k^{i=1}$ is the k^{th} location of the mode shape of the first iteration. $\phi_{j,k}^{i}$ is the k^{th} location of the j^{th} mode shape identified by SSI-Cov in the i^{th} iteration. Using this equation the code will extract the mode shape of the i^{th} iteration which differs the least from the mode shape from the first iteration. This will however not guarantee that the correct mode shape is extracted. Therefore, a limit is introduced. If

$$\min_{\forall j} > \alpha = 0.5$$

a while loop is executed in which the model order is increased and SSI-Cov and the process of extraction by mode shape comparison will be rerun. Selecting this limit value was also aided by some test runs. The value can neither be too small, as variations in the mode shapes will occur due to noise, nor too big as the correct mode shape might not be extracted. Moreover the mode shapes are normalized in order for this to work.

A mode shape is as previously explained the shape with which a system will oscillate in one of its natural frequencies around its equilibrium position. The shape is identical at each side of the equilibrium. The SSI-Cov function returns the calculated mode shape at one of the sides of the equilibrium position. The results are thus identical except with different signs (+/-). This is handled in the script so that all the results of the calculated mode shapes are at the same side of the equilibrium position.

The code to retrieve the four lowest natural frequencies and mode shapes of the structure is provided in Appendix A.

4.3 Damage Detection Strategies

Two different strategies for VBDD will be applied. The first is the proposed new framework which relies on the statistical analysis of several populations of observations. The second is the traditional approach which relies on comparing observations at two discrete points in time. The latter approach is included to contextualize the efficacy of the proposed framework.

4.3.1 Proposed Framework

In evaluating the efficacy of the different features for damage detection the concept of a timeline has been introduced. The idea is that each of the different noisy signals represent daily, consecutive sensor readings from a true bridge in operational conditions. In such, the modal properties of the structure can be calculated from the signals for each day. Notably, any frequency of measurement (rather than daily) should still render the proposed procedure applicable. By comparing the consecutive modal properties with those from the structure in its undamaged state, alterations in the physical properties of the structure can be revealed, possibly indicating damage. This procedure is applied for all the different damage detection features. The values obtained from these comparisons are referred to as damage indicators.

The different damage indicators are calculated for different combinations of modes to evaluate whether including more modes will increase the efficacy of damage detection. Accordingly, damage indicators are created for mode 1 alone, mode 1 and 2 in combination, mode 1, 2 and 3 in combination

and lastly mode 1, 2, 3 and 4 in combination.

The calculation of modal properties by OMA is not an exact science. Noise present in the signals, from a number of sources previously mentioned, is inevitable. This will have an effect on the calculated modal properties, distorting them. The subsequent manipulation of the mode shapes and natural frequencies into modal shape curvature, strain energy and flexibility may further these issues. As a result one can expect false indications of damage, because the damage indicators will predict damage. This is where the concept of time might come in handy. Rather than evaluating each daily observation discretely, a new framework that rather rely on a population of observations is proposed:

$$freq = \frac{\mathrm{n(DI > TH)}}{\mathrm{n_{pop}}} \tag{4.3}$$

In applying Equation 4.3 the population size $\mathrm{n_{pop}}$ must be determined. Herein a size of 100 is selected. The parameter DI refers to the discretely calculated damage indicators. TH is a threshold value which the damage indicators must exceed to account for a given, acceptable false alarm rate. Therefore the *freq* parameter will be referred to as both frequency of detection and frequency of exceedance in the further. At any given day, *freq* will be calculated for the last $\mathrm{n_{pop}}$ observations.

As previously described, 500 "daily readings" affected by noise, are produced for each of the different damage states. For the undamaged case however, 1000 samples are created, as 500 of these will be used as a set of training data. In total, 3500 readings are thus created for each of the damage locations. The noise is also varied such that five variants, differing in the amount of noise applied to the signal, are produced for each of the damage locations. For all of these readings the damage indicators are calculated.

The training data, or training period, consists of 500 days. The three different damage indicators will be computed during this period. The variation of the damage indicators during this period will be used to compute thresholds for false alarms. This is done by sorting these data from low to high and extracting the damage indicator values that a certain number of observations exceeds. For an accepted false alarm rate of 5 % for example, five % of the 500 training data will exceed the selected threshold value. Threshold values are calculated for all noise levels, all damage locations and all sensors.

The subsequent monitoring period, which starts at day 501, thus consists of 3000 daily observations through which damage increases every 500 days. For each damage indicator and observation, damage indicators are calculated and recorded. The frequency with which the damage indicators of these observations exceeds the threshold values is computed for the last 100 observations, starting from day 600. These results will be plotted against the number of days or observations. *freq* is expected to increase with the evolution of damage.

4.3.2 Traditional Approach

The efficacy of damage detection with discrete observations will also be evaluated. This is done by calculating a probability of detection, determined by Equation 4.4:

$$prob = \frac{\mathrm{n(DI > TH)}}{\mathrm{n_{tot}}} \tag{4.4}$$

The number of times the damage indicator exceeds the threshold value is divided by the total

number of observations, n_{tot}, for each damage scenario; 500. By calculating both the frequency of exceeding a threshold, as well as the probability of detection, the relative success of the proposed *freq* damage indicator, compared to existing procedures.

MATLAB scripts for the calculation of the different damage indicators and corresponding frequencies and thresholds is provided in Appendices B – G.

Chapter 5

Results and Discussion

The results of the performed analyses along with their interpretation and evaluation are presented in this chapter. First the results from CSiBridge are outlined, followed by the results of SSI-Cov. These are discussed and compared with the results of the modal analysis performed by CSiBridge. This is done to ensure a solid foundation for the continued application of the different damage detection strategies: The accurate prediction and extraction of modal parameters is paramount to the efficacy of the different damage indicators.

Further, the results of the application of the three different damage indicators in a traditional as well as a proposed long-term framework are provided. These will be discussed with emphasis on their ability to detect and possibly localize damage in the railway bridge.

5.1 CSiBridge

The vibration data is collected in the form of accelerograms. These data constitute the basis for the entire analysis. Therefore, they are plotted and inspected to ensure their integrity. Figure 5.1 presents accelerograms collected from ten sensors for varying degrees of damage introduced at mid-span. These results coincide with the accelerograms collected from the bridge with damage at the other locations.

The coherence and appearance of each of these ten signals, as well as the coherence between the signals obtained from the different damage states, consolidate the integrity and comparability of the signals. The duration of the loading, easily calculated by the speed and length of the train and the bridge, corresponds to the duration of the signal before it begins to dissipate (approximately seven seconds). These seven seconds thus constitute the forced vibration response of the bridge. After seven seconds, the acceleration begins to die down. This is the free vibration response of the bridge, initiated by the train crossing. The fact that the acceleration dies down until movement is stalled proves that damping is included in the model.

Slight differences in the acceleratory response of the bridge in its different damage states can be observed. The free vibration response seems to decrease with increasing damage. This supports the fact that the dynamic response of a system is contingent on its inherent stiffnesses and masses; the introduced reductions of bending stiffness in the bridge yields differences in the accelerograms. Although this change can be observed, it is clearly not possible to identify and localize damage conclusively from the accelerograms. The changes are slight and could in real-life applications be related to noise in the form of changes in temperature, wind or other ambient influences existing in

an operational environment. Noise in the signals pertaining to the abilities of the components of a sensing system may also be present.

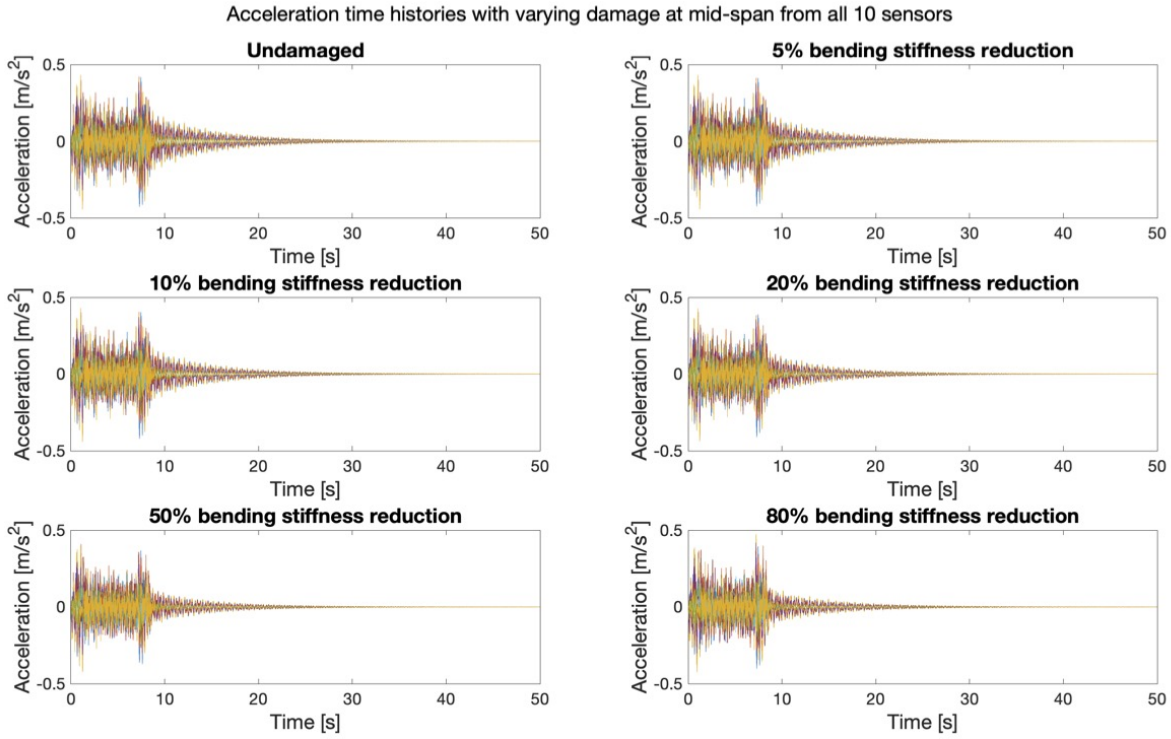

Figure 5.1: accelerograms from all ten sensors with the bridge in its undamaged and damaged states. The damage is introduced at mid-span.

In Table 5.1 the natural frequencies and MPMRs of the twenty identified modes of the structure, calculated by CSiBridge, are presented. These results are collected from the bridge in its undamaged state and are included as they in the further will be used as a basis for comparison to the natural frequencies calculated with SSI-Cov.

Mode	1	2	3	4	5	6	7	8	9	10
Natural freq. [Hz]	2.53	2.69	3.58	4.46	6.79	8.00	10.23	11.58	11.63	15.43
MPMR [$*10^{-2}$]	0.04	3.38	60.84	0.13	5.99	0.07	0.13	0.03	0.88	0.05
Mode	11	12	13	14	15	16	17	18	19	20
Natural freq. [Hz]	18.70	19.14	21.70	22.61	24.27	26.34	29.74	30.16	33.03	33.31
MPMR [$*10^{-2}$]	1.53	1.57	7.24	0.16	4.52	0.04	0.01	0.27	0.70	0.01

Table 5.1: Natural frequencies and modal participation mass ratios (MPMRs) of the first ten modes of the railway bridge in its undamaged state, collected from CSiBridge.

The modes with the largest MPMRs will presumably be most easily identified with SSI-Cov. However, higher frequencies corresponding to higher modes are not easily excited, and these may therefore be more difficult to detect with SSI-Cov. Moreover, the frequency of the loading (train) that crosses the bridge influences which modes are excited. As will be demonstrated in the further, mode 2, 3, 5 and 7 are consistently identified by SSI-Cov. To ensure the integrity of the results of SSI-Cov, the mode shapes of these modes, collected from CSIBridge with varying levels and locations of damage are plotted and presented in Figures 5.2, 5.3, 5.4 and 5.5. From here on out these are renamed mode 1, 2, 3 and 4.

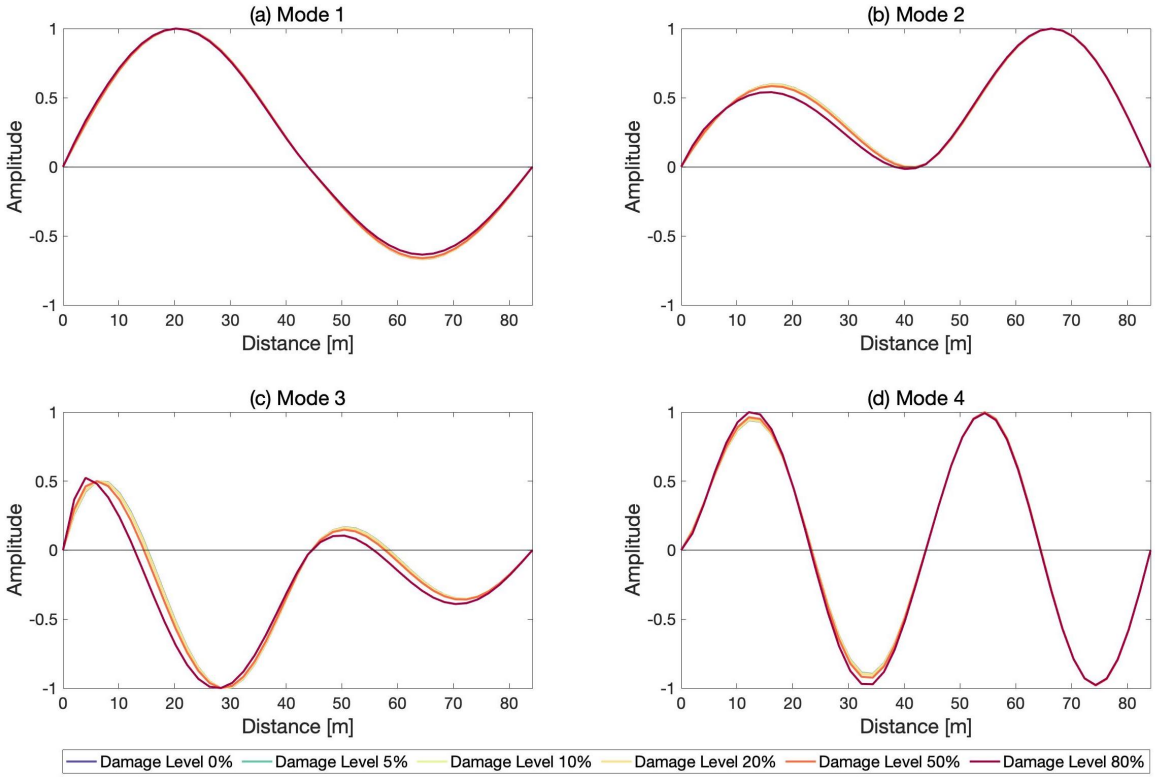

Figure 5.2: Mode shapes from CSi Bridge with varying level of damage by the abutment.

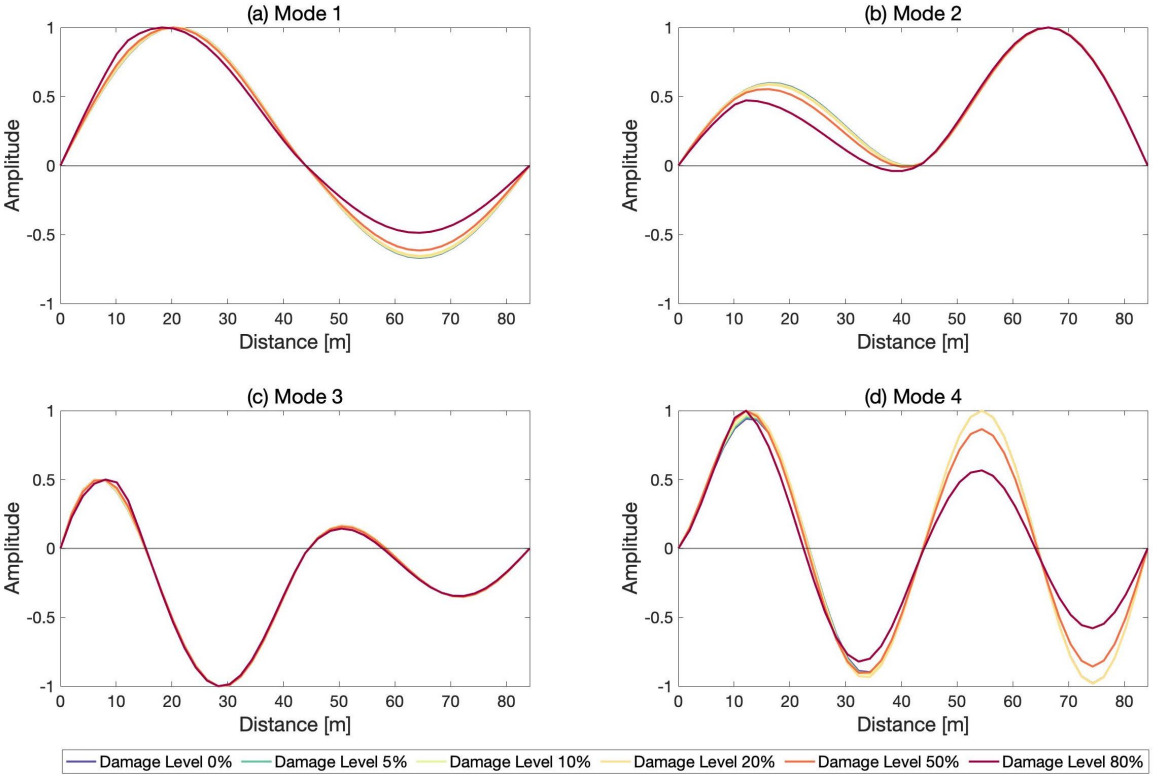

Figure 5.3: Mode shapes from CSi Bridge with varying level of damage at quarter-span.

The mode shapes are clearly affected by the introduced damage. Generally, the amplitude of the mode shapes can be seen to consistently decrease or increase with increasing damage, between

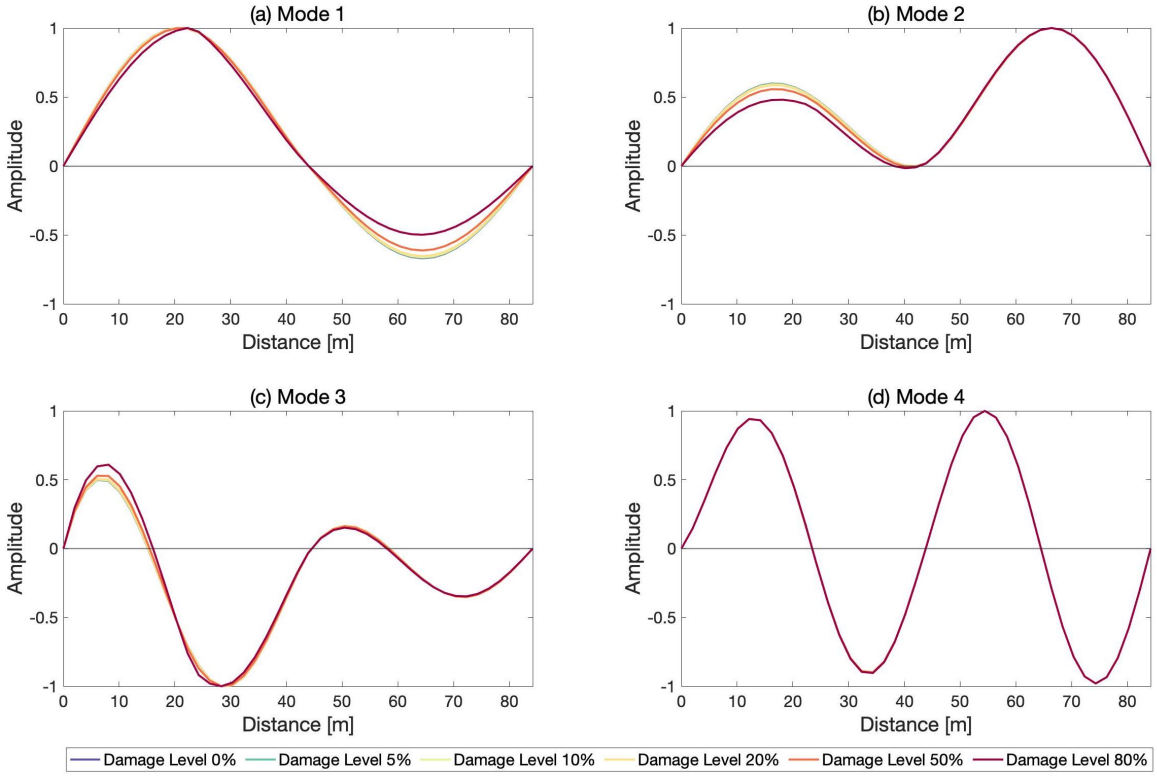

Figure 5.4: Mode shapes from CSi Bridge with varying level of damage at mid-span.

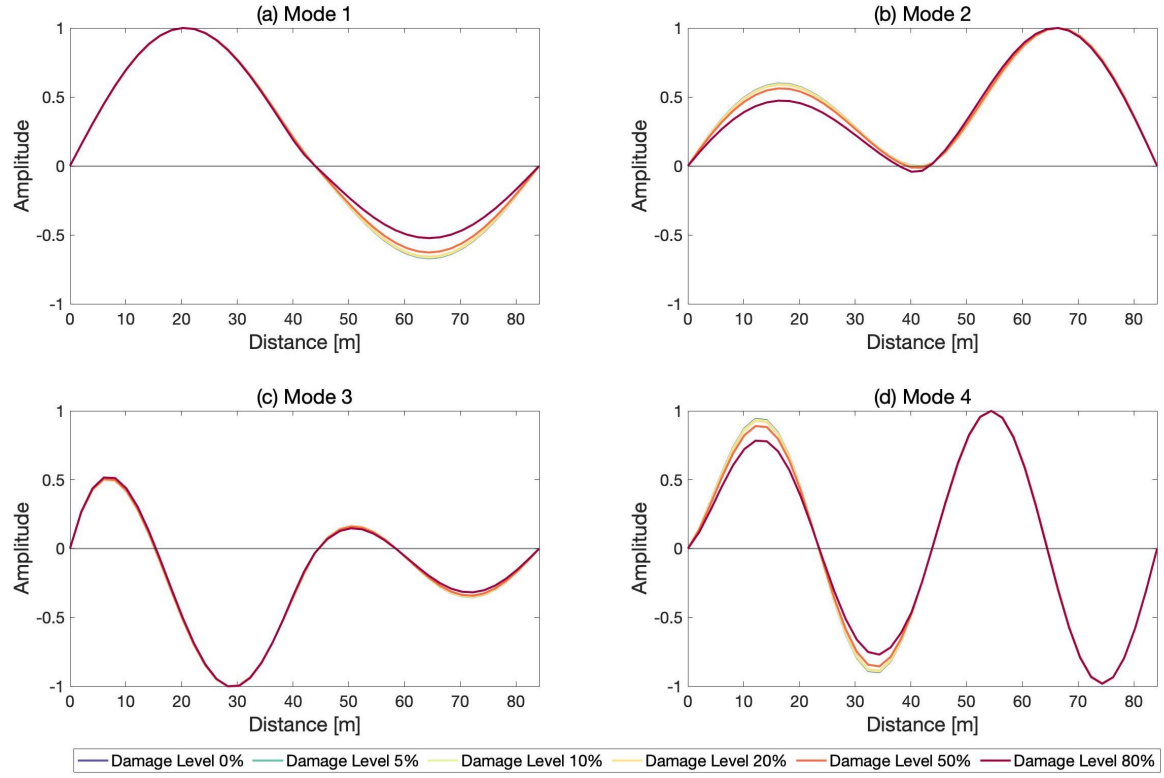

Figure 5.5: Mode shapes from CSi Bridge with varying level of damage by the column.

points where all the mode shapes for the different damage levels intersect. Exceptions to this however exists. This is particularly prominent in mode 4 when damage occurs at quarter-span. Looking at the mode shape between 0 and 30 m, presented in Figure 5.6, it becomes clear that the mode shape

shifts as damage increases. As a result, the amplitude is not increased with increasing damage from approximately 11 meters to 16 meters.

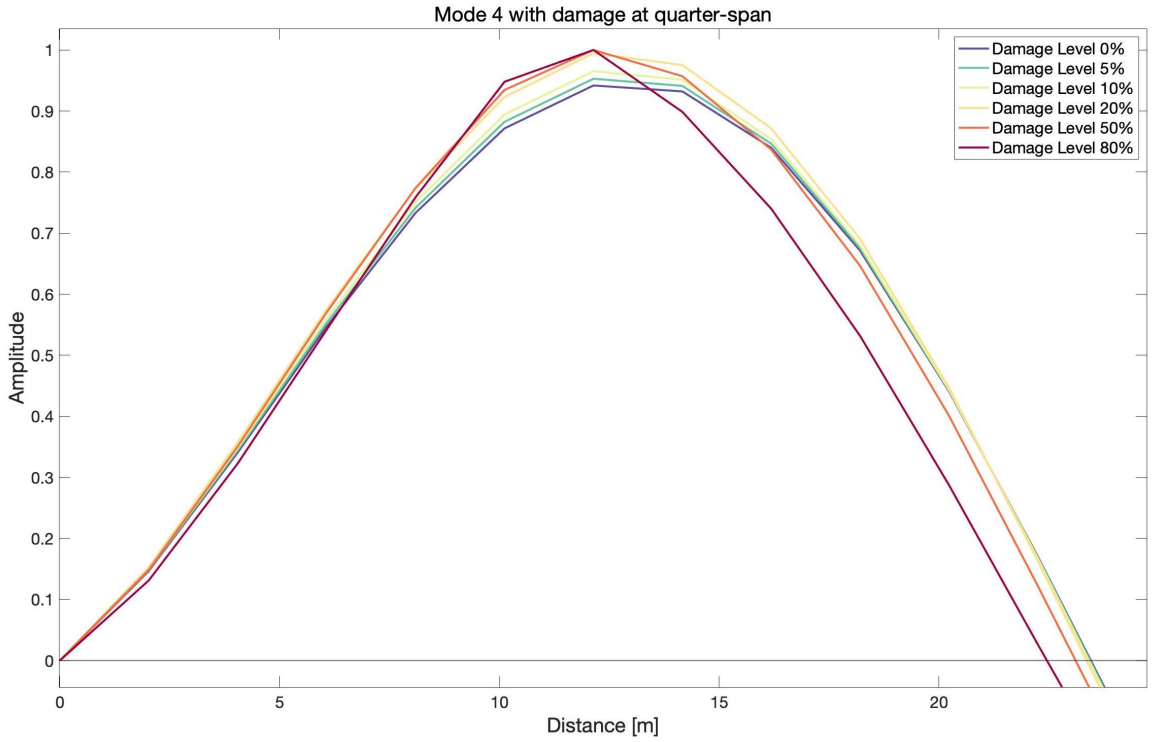

Figure 5.6: Mode shape of mode 4 between 0 and 30 m from CSi Bridge with varying level of damage at quarter-span.

Moreover, the location of the damage has a significant impact on the evolution of the mode shape as damage increases. In Figure 5.2 (a), 5.3 (c), 5.4 (d) and 5.5 (c) the mode shapes remain quite consistent with increasing levels of damage, as compared to the other mode shapes presented. Another observation is that although damage is introduced to the left span only, some mode shapes are impacted in the right span of the bridge as well. This demonstrates the global property of mode shapes: Locally occurring damage affects the global vibratory response of the bridge. Considering the fact the damage indicators, which are all computed using the mode shapes, utilize a comparison of the undamaged properties of the structure to its properties when damage is occurring, this might have an effect on both detection and localization of damage.

5.2 Operational Modal Analysis

Extracting the natural frequencies from the accelerograms using OMA is contingent on the proper model order selection. The selection of a proper model order is aided by inspecting a stabilization diagram. In Figure 5.7 the stabilization diagram calculated from the signal from the undamaged bridge, polluted with 0.5 % noise, is presented. It is plotted for an order of 80, represented along the vertical axis.

A model order of 25 was selected for the extraction of the modal parameters. In doing so SSI-Cov conclusively identifies the same first four modes from all the signals until damage and noise is significantly increased. When the bending stiffness reduction reaches 80 %, the model order is incrementally increased to capture these four modes. The same is applied for significant levels of noise.

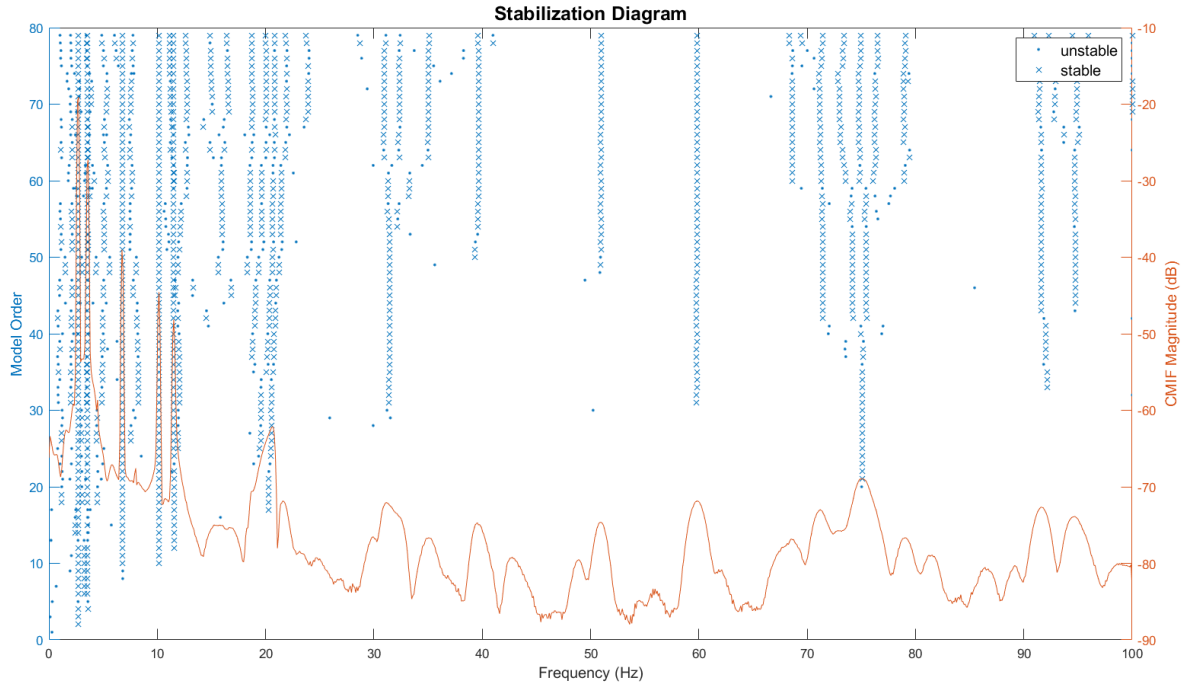

Figure 5.7: Stabilization diagram produced from the signal of the bridge in its undamaged state, influenced by 0.5 % noise.

Evaluating whether these frequencies are related to physical modes rather than spurious ones, and in such assessing whether a proper model order has been selected, is herein based on a comparison between the CSiBridge and the SSI-Cov results. This approach is usually not applicable in real-life applications. Extracting the true modes of a structure in such cases still largely depend on the experience and capability of the analyst. Nonetheless this comparison allows for the evaluation of the SSI-Cov algorithm's ability to identify the modes of a structure.

As mentioned, the four modes consistently identified by SSI-Cov correspond to modes 2, 3, 5 and 7 collected from the modal analysis performed in CSiBridge, which were presented in Table 5.1. Mode 3 and 5 have large MPMRs and are presumably therefore easily detected. Both mode 2, 5 and 7 however have lower MPMRs than mode 13. The reason why these are more easily identified by SSI-Cov can be attributed to two factors. For one, lower modes are more easily excited than higher modes. Mode 13 may not have been excited and therefore not recorded in the accelerograms. The frequency of the moving load is also a factor that affects which modes are perturbated. Nonetheless, increasing the model order might help SSI-Cov detect more modes. This however represents the challenge faced by the analyst, as an over-specification of the model order may also increase the detected number of spurious modes.

For the purpose of this work it is not imperative that all the modes of the bridge are identified. The different damage indicators can also be used for one mode only, although their level of confidence have been found to increase with several modes. The proper identification of some low order modes is considered sufficient for damage detection purposes, as low order modes are generally more descriptive of a structure than higher order modes in damage identification. What is imperative however, is that the same modes are identified in the different damage scenarios, as damage detection relies on comparisons between the same modes of the bridge in its different intact and damaged states.

In Figure 5.8 the mode shape calculated with SSI-Cov with damage by the abutment in the bridge

is presented. These were produced from accelerograms which were not contaminated with noise, in order to compare them to the mode shapes obtained from CSiBridge. Notably, the mode shapes were normalized during their extraction. They have since been interpolated to increase the quality of their resolution and presentation. The mode shapes identified by SSI-Cov are almost identical to the ones obtained from CSiBridge. This can be said for all the different damage locations as well. The comparability of the mode shapes from CSiBridge and SSI-Cov substantiate the generally accepted efficacy of the SSI-Cov algorithm.

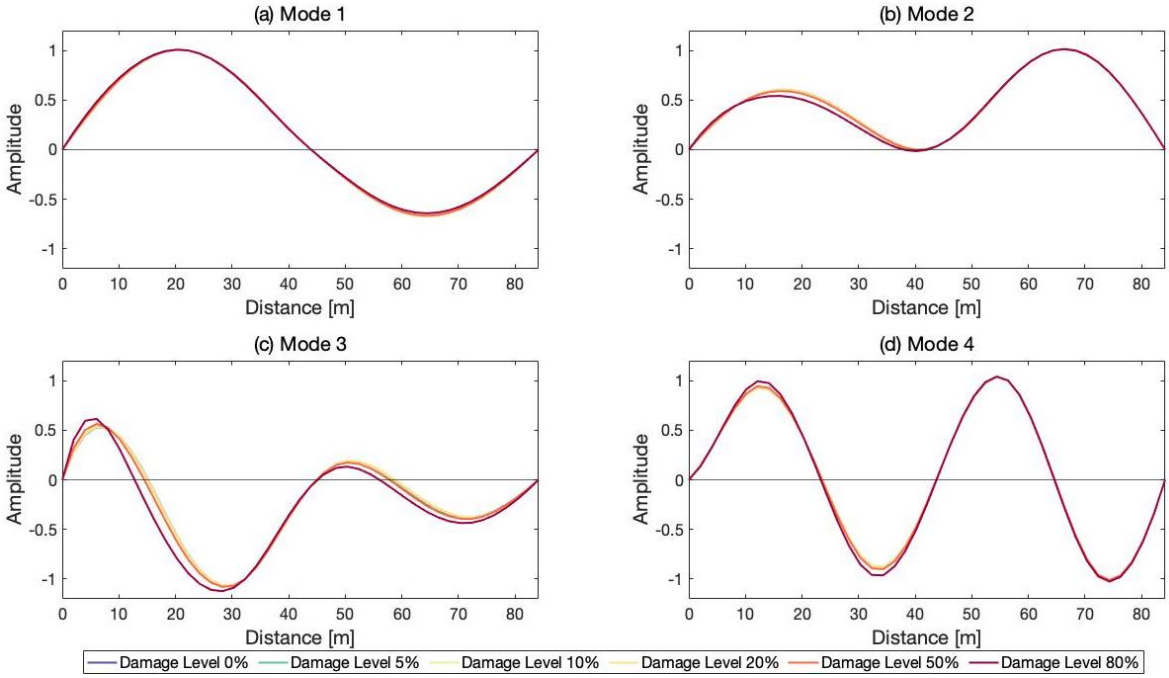

Figure 5.8: Mode shapes from SSI-Cov with varying level of damage by the abutment.

The introduction of noise to the accelerograms may however obscure the ability of SSI-Cov to detect different modes. As explained the automation of natural frequency and mode shape extraction from SSI-Cov was aided by the comparison and necessary normalization of mode shapes. To ensure that this procedure succeds in extracting the same modes for all noise levels, damage locations and damage levels, the identified mode shapes for all observations are plotted and inspected. Figure 5.9 presents the mode shapes of all modes for all damage levels and noise levels with damage at quarter-span. Each subfigure ((a), (b), (c) and (d)) thus contain 17 500 plots: 3500 for each of the five noise levels.

The correct mode shape is not extracted for all the 17 500 iterations. This is true for all the damage locations. Wrong mode shapes are only extracted when the noise is at 20 %, except only one instance where the noise level is 10 %. Arguably 20 % is a very high level of noise and the relative success of the SSI algorithm can still be considered high. The extraction of wrong modes more frequently occur for mode 4 than for the other modes. As higher modes are identified with more difficulty compared to lower modes, this makes sense. It can not be said for certain however that the wrong mode shapes are extracted because the right modes were not identified. First of all, the limit value α that was chosen for mode shape comparison may have been to high. Accordingly the extraction of mode shapes would rely on a model order of 25, which is likely too low to detect all modes with a noise level of 20 %. The significance of the deviation of some of the erroneous modes from the true modes however implies that this is not the case. In such, the model order will have been increased to 75 and the true modes are still not detected. Increasing the model order even

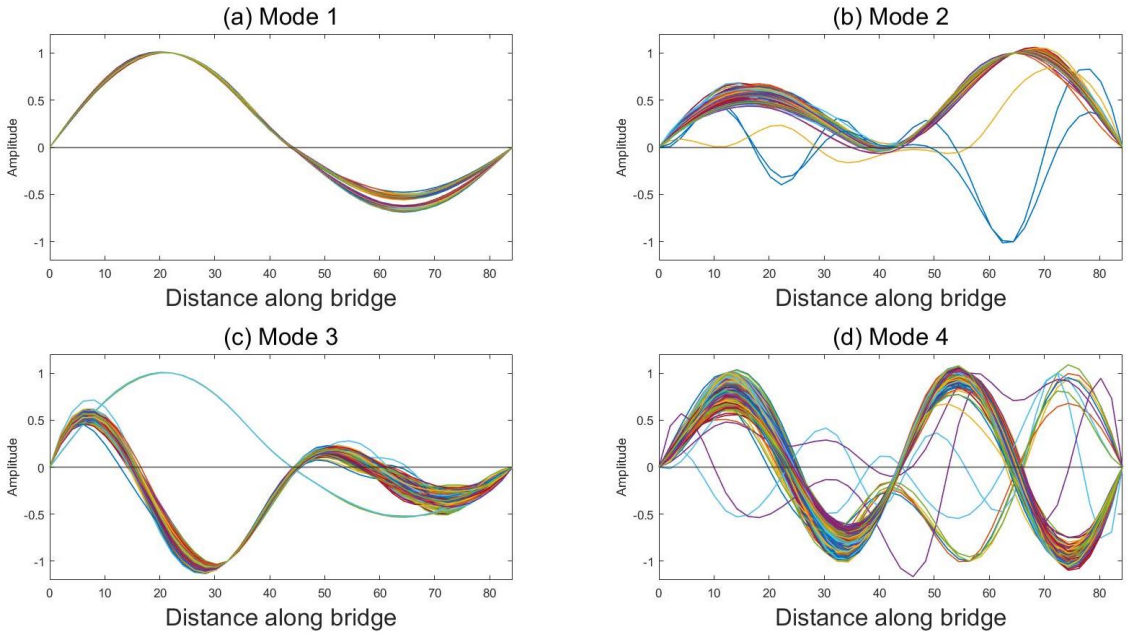

Figure 5.9: Plots of extracted mode shapes for all four modes. Each subfigure contains 17 500 plots; 500 for each of the seven damage levels times five levels of noise. Damage located at quarter-span.

further is a possibility, however this is computationally expensive and does not guarantee that the true modes will be detected.

The number of erroneous modes detected is limited to a worst case of maximum of 10 out of every 500 observations, or 2 %, for each damage level and location. Arguably this will not have a significant impact on the efficacy of the damage indicators. For brevity the erroneous modes are therefore not removed. This should however be applied in an SHM scheme as part of the data cleansing process. Table 5.2 summarizes the number of erroneous modes that are extracted for the different damage locations. The noise level is 20 % and the superscripts refer to the damage location.

Damage level	Mode 1	Mode 2	Mode 3	Mode 4
5 %		2^2, 1^4		1^1, 1^2, 1^3, 2^4
10 %		1^1, 1^2		4^2, 1^3, 1^4
20 %		1^1	8^2, 3^4	1^2
50 %		3^1, 1^4		8^1, 1^2, 1^4
80 %		2^2, 1^4		10^2, 6^4

Table 5.2: Summary of the number of erroneous modes that are detected for the different damage levels and at different damage locations. Noise level 20 %.

Figure 5.10 presents mode 1 from the bridge with damage by the abutment with increasing levels of noise in subfigures (a), (b), (c) and (d). At first glance it is evident that SSI-Cov handles the noise applied well. There seems to be little variation in the mode shapes between the different levels of noise. Each of these plots contain only one mode shape, from one observation, for each damage level.

[1]Abutment.
[2]Quarter-span.
[3]Mid-span.
[4]Column.

In Figure 5.11 mode 1 with no damage and increasing levels of noise is plotted for 500 observations. The effect of 20 % noise can be seen to affect some of the mode shapes to the same extent that damage does. This will likely affect the efficacy of damage detection, possibly masking subtle changes caused by damage, and will be further discussed.

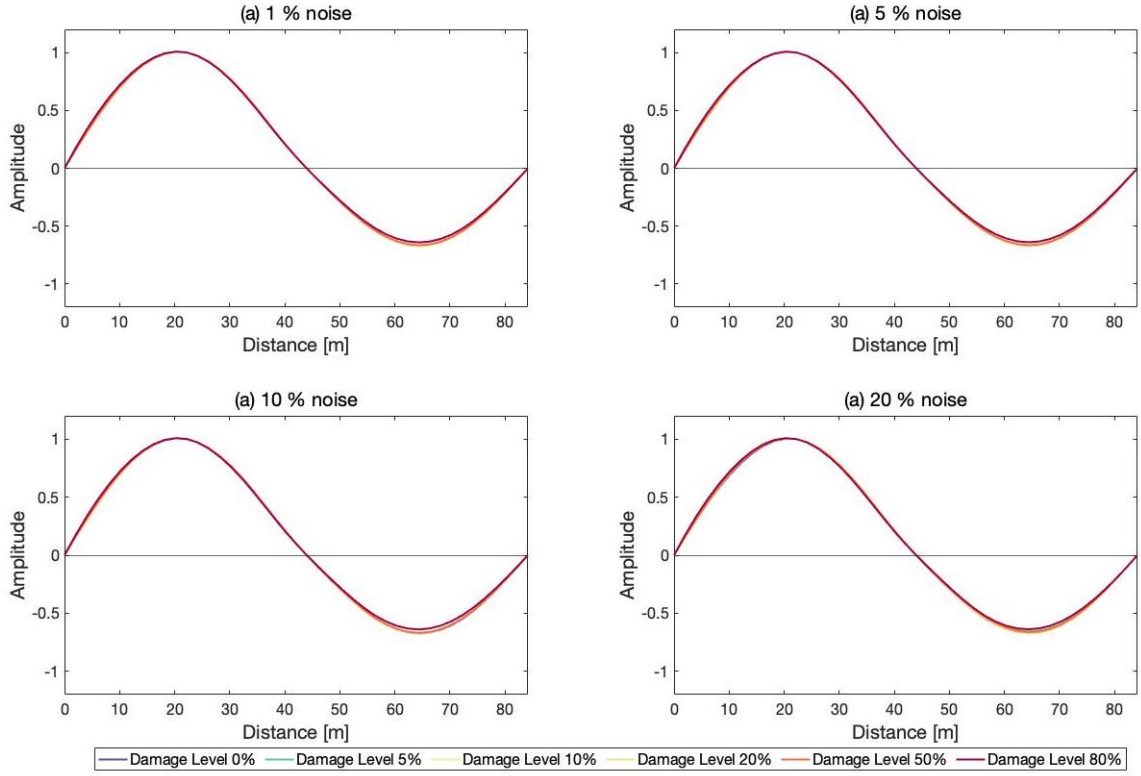

Figure 5.10: Mode shape 1 from SSI-Cov with all damage levels in abutment for varying noise levels.

5.3 Damage Detection Strategies

5.3.1 Development of Damage

The severity of the damage has an impact on how often damage is detected by the damage indicators. Therefore, the frequency of how often a threshold value is exceeded might be effective in monitoring the development of damage. In Figure 5.12 the frequency of exceedance by modal curvature, using a combination of two modes, is plotted for increasing damage at mid-span based on accelerograms from the sensor closest to this damage location, Sensor 3. The structure is undamaged for the first 500 observations in which the frequency parameter corresponds to the threshold value of 5 % on average, as presented in Figure 5.12 (a). These 500 observations are referred to as day 501 to 1000 as the 500 previous days were used as training data from which the threshold value is calculated. Furthermore, the frequency is calculated using 100 previous observations, as per Equation 4.3, so that days 501 to 600 remain empty. The bending stiffness of the mid-span element is subsequently reduced every 500 days, such that a 5 % reduction occurs in days 1001 to day 1500, and so on.

As shown in Figure 5.12 (b), the frequency of exceedance is now over the threshold line for all cases for this relatively low damage level meaning that the damage indicator remains larger than the threshold value for more than 5 % of the observations. The frequency of exceedance increases

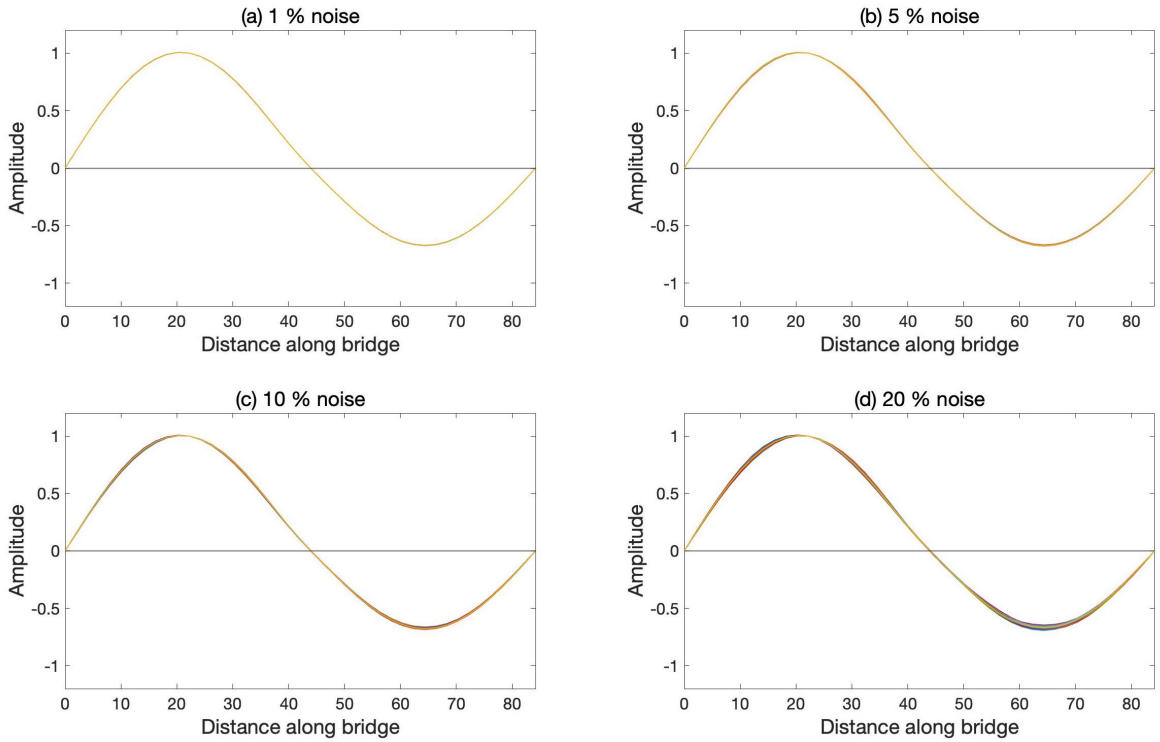

Figure 5.11: Mode shape 1 from SSI-Cov with no damage and 500 variations of each noise level.

even more in Figure 5.12 (c) where another 500 observations are included in which the damage is increased to 10 %. This trend continues, the frequency increases with increasing damage. With the frequency being calculated from the past 100 days a resulting slope when damage is increased occurs, as seen in Figure 5.12 (e), where 500 days of 50 % reduced bending stiffness is imposed and the frequency rises to 1, meaning that damage is detected for approximately all observations.

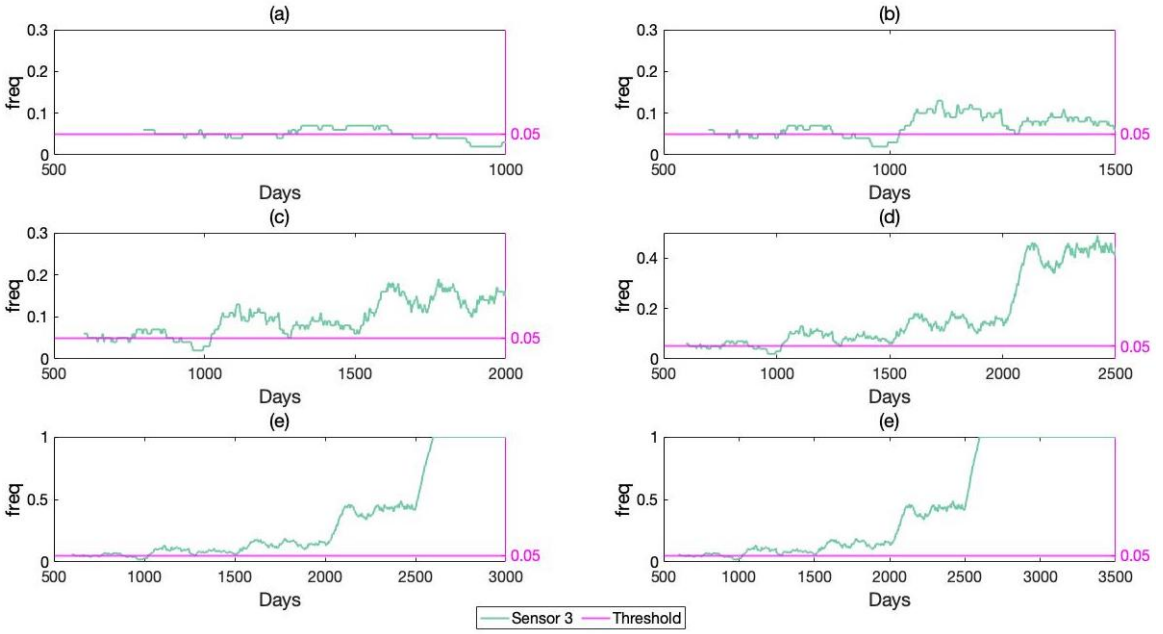

Figure 5.12: Development of damage by frequency of exceedance from Sensor 3 by modal curvature with two modes with increasing damage at mid-span, 5 % noise and 5 % threshold.

The data presented in Figure 5.12 is based on a 5 % threshold value unique for the sensor and noise level obtained from training data - the past 500 reference days. So, it is expected that the damage indicator will exceed the threshold value for 5 % of the observations when the structure is undamaged, resulting in an average frequency of exceedance of 0.05. There is 400 data points in the frequency of exceedance from which the structure is undamaged, and the average of these 400 is in fact 0.05 for Sensor 3. So, despite the noise, the training data is adequate for calculations of threshold value for this case. It should be noted that the average frequency of exceedance is not always 0.05 for the other sensors as a result of noise.

The frequency of exceedance is based on the number of times the damage indicator exceeds a given threshold value. The development of these discrete observations are presented in Figure 5.13. Three different threshold lines are plotted within the figure, corresponding to Sensor 3 for 5 % noise, for 2 %, 5 % and 10 % chance of false detection.

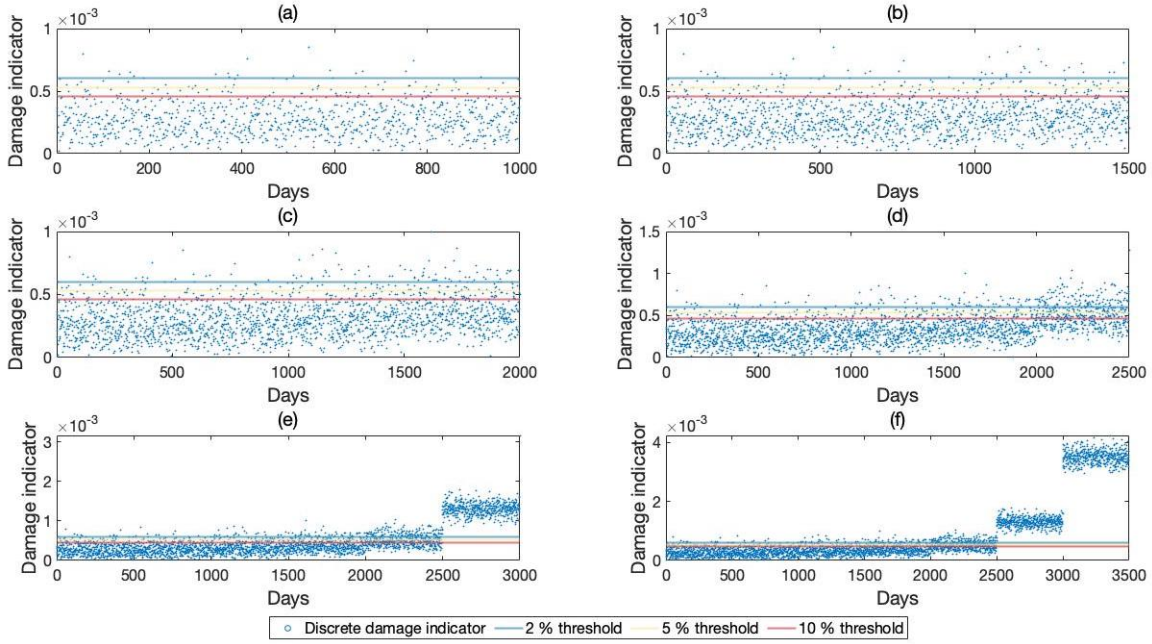

Figure 5.13: Development of damage indicator from Sensor 3 by modal curvature with two modes with increasing damage at mid-span and 5 % noise.

An increasing level of damage and number of observations are included in the subfigures of Figure 5.13, similar as in Figure 5.12, which is based on the same noise level and damage scenario. In this scatter plot, and for all upcoming scatter plots, all 3500 calculated observations are included, including the training data which will work as a reference. After 1000 days the structure goes from intact to a 5 % damage level at mid-span. Discerning this from the slight increase in the damage indicators in days 1000 – 1500 is difficult, and looking at the probability of detection, presented in Figure 5.14, it is evident that the probability of detection is only slightly increased at this damage level. Inspecting the frequency plot of Figure 5.12 (b), on the other hand, which is calculated using the same damage indicator data, it is found that the frequency of exceedance is increased beyond the accepted 5 % threshold value, or false alarm rate, in the same period of time. Both the frequency of exceedance and the discrete observations of Figure 5.13 and 5.14 display a general trend in which the damage indicator is increased with increasing damage. This agrees with expectation as all figures are based on the same data. The ability of predicting the existence of damage is however increased and possible at an earlier stage of

damage using the *freq* parameter compared to observing the scatter plot and probability plot, as the frequency of exceedance increases beyond accepted false alarm rates already at a 5 % level of damage. Exceedance of the damage indicator beyond the different thresholds values is not discernible until damage reaches levels of 20 % in the scatter plots, see subfigures 5.12 (d), (e) and (f).

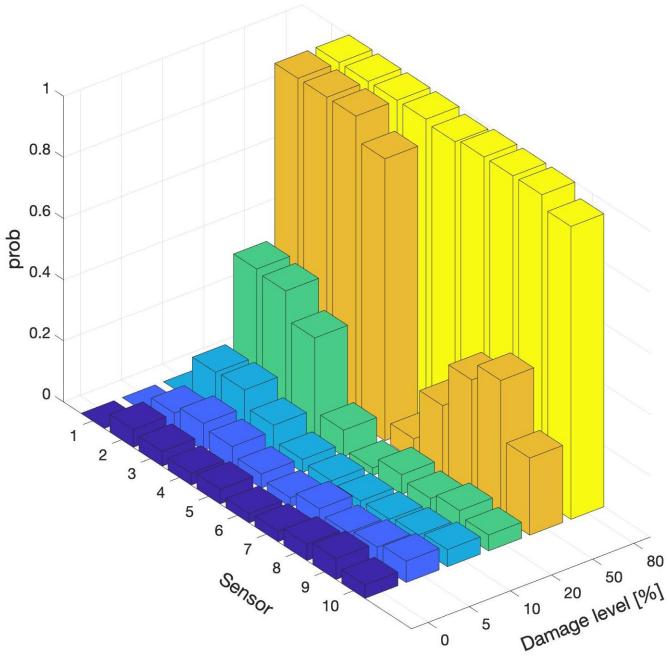

Figure 5.14: Probability of detection using modal curvature for two modes, increasing damage occurring at mid-span, noise level and threshold value 5 %.

5.3.2 Effect of Modes

The figures related to probability of detection presented in this chapter are plotted for a noise level and threshold of 5 % and a damage level of 20 %. Figure 5.15 presents the probability of detection for different combinations of modes and with varying damage locations using modal curvature. Irrespective of damage location, using only one mode has the highest probability of detection. Generally, probability of detection is decreased with an increasing number of modes. This is an interesting finding, as one from literature can infer that more modes equal better damage detection. When damage occurs at the abutment the inclusion of a third mode, see subfigure (c), decreases the probability of detection in the sensor associated with damage, marked in green; mode 3 significantly impacts the opposite abutment to the one where damage is introduced, that is at Sensor 10 rather than Sensor 1, increasing the probability of detection at this location and disrupting localization of damage. This can be related to the way the mode shapes change as a result of increased damage, as previously illustrated in Figure 5.2 (c). Here, the damage which is imposed by the abutment leads to changes in mode 3 in both spans of the bridge. Therefore, damage is not only detected by Sensor 1 which is closest to the damage when three modes are used but also by Sensor 10 which is the furthest away. Notably this may occur in any mode depending on where damage occurs, but may not necessarily have an impact. It can also explain why all sensors detect damage as the bending stiffness reduction is increased to 80 %. This is illustrated in Figure 5.16 which presents the frequency of detection using modal curvature with damage by the abutment.

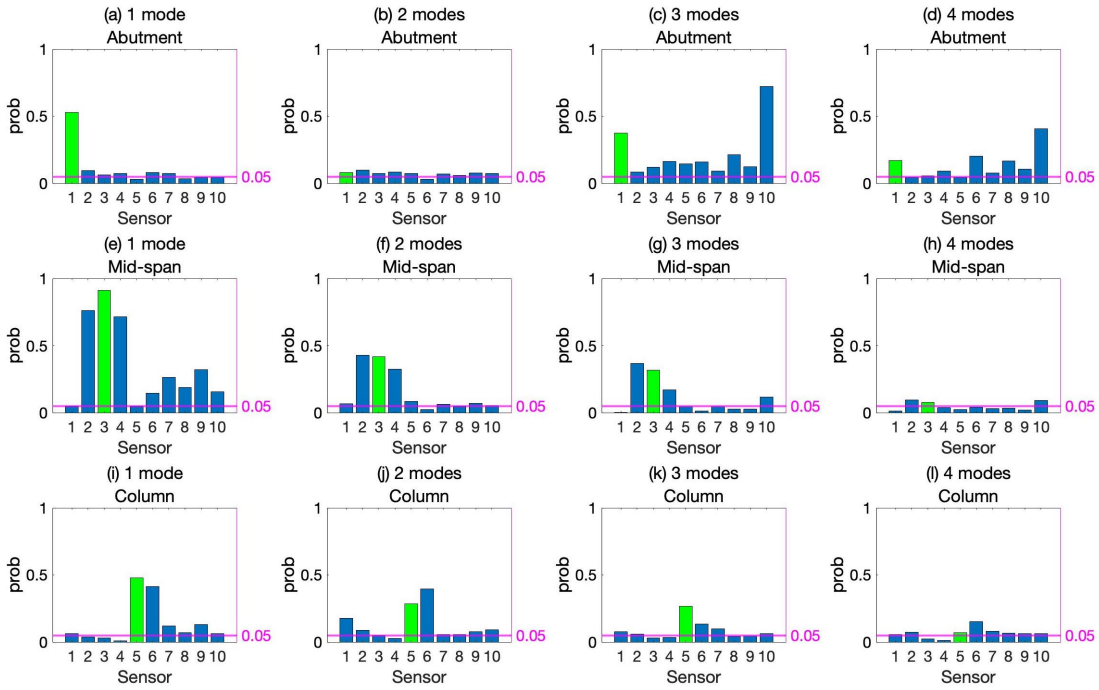

Figure 5.15: Probability of detection for modal curvature at different damage locations and with different combinations of modes.

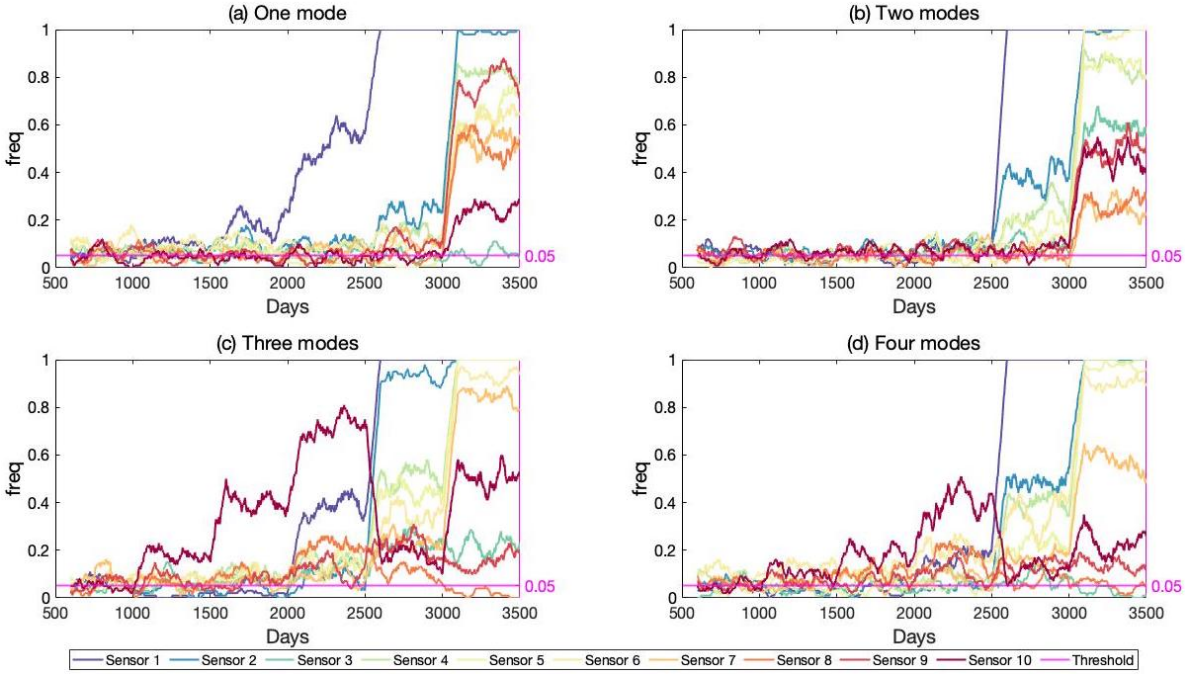

Figure 5.16: Frequency of exceedance using modal curvature with varying number of modes for damage by the abutment, 5 % noise and 5 % threshold.

Looking at Figure 5.16 one might rather say that detection is increased using more modes when damage occurs by the abutment, although detection occurs at the wrong location up until the damage level reaches 50 %. Damage is detected at an earlier stage with a combination of three and four modes. At 50 % damage a sudden drop in the detection at Sensor 10 is observed. Looking at the mode shape of mode 3, plotted for all damage levels by the abutment in Figure 5.17, this can be explained. These mode shapes were obtained from SSI-Cov with non-noisy accelerograms. Sensor 10

is located at 80.2 m. This part of the mode shapes is zoomed in on in Figure 5.17 (b). The general trend that can be observed is that the displacements forming the mode shape either decrease or increase consistently with increasing damage. This can be observed in subfigure (b) for all damage levels except 50 % round the location of Sensor 10. The amplitude of displacement of the mode shape at a damage level of 50 % is less than for all the other levels of damage. Therefore, there is a drop in the frequency of exceedance plot of Sensor 10 from day 2500 to day 3000 as the displacement at this location is almost identical to that of the undamaged mode shape when the bending stiffness is reduced by 50 % at the abutment. This issue occurs with all the damage indicators, but is reduced with the inclusion of a fourth mode. This is however at the expense of reduced detection.

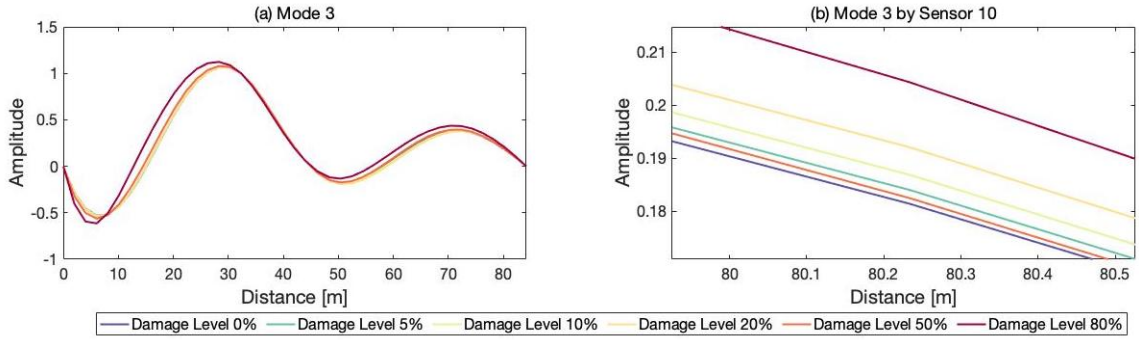

Figure 5.17: Mode 3 with varying damage by the abutment without noise.

From this, one can gather that effective damage detection and localization might be reduced with the inclusion of modes in which increasing levels of damage does not alter the mode shape consistently. It should be noted that inconsistent mode shape changes may not only occur as a result of SSI-Cov. In the mode shapes obtained directly from CSiBridge the same occurs, as discussed in Chapter 5.1. Hence, this may not only be an issue related to SSI-Cov or noise, but with modal analysis in general and the fact that mode shapes, being global properties, are used to detect local damage.

Accordingly one can presume that evaluating the effect of development of damage on the change of the different mode shapes utilized is important for effective damage detection. The extent to which inconsistent mode shape changes will affect damage detection is notably also dependent on level of noise. This becomes evident looking at Figures 5.18 and 5.19, which presents a scatter plot and a bar chart of the damage indicator of modal curvature in Sensor 10, using three modes for different noise and damage levels. There is a drop in the damage indicator from day 2501 to 3000 in Figures 5.18 (a) and (b), corresponding to 50 % damage. This is because the displacement in the third mode shape at this location increases for all damage levels except for 50 %.

At 1 % noise the effect of this phenomenon on the probability of detection is limited as the value of the damage indicator still is above the threshold value for most observations. When the noise level is at 5 % the effect is the most prominent. At noise levels of 10 % and 20 % however, the drop in probability is shifted from a damage level of 50 % to a damage level of 80 %. This also happens for modal strain energy, but not for modal flexibility, in this sensor.

The probability and frequency of detection with varying combinations of modes and with modal strain energy as a damage indicator is presented in Figures 5.20 and 5.21. When damage occurs at mid-span and by the column, the inclusion of more modes decreases the probability of

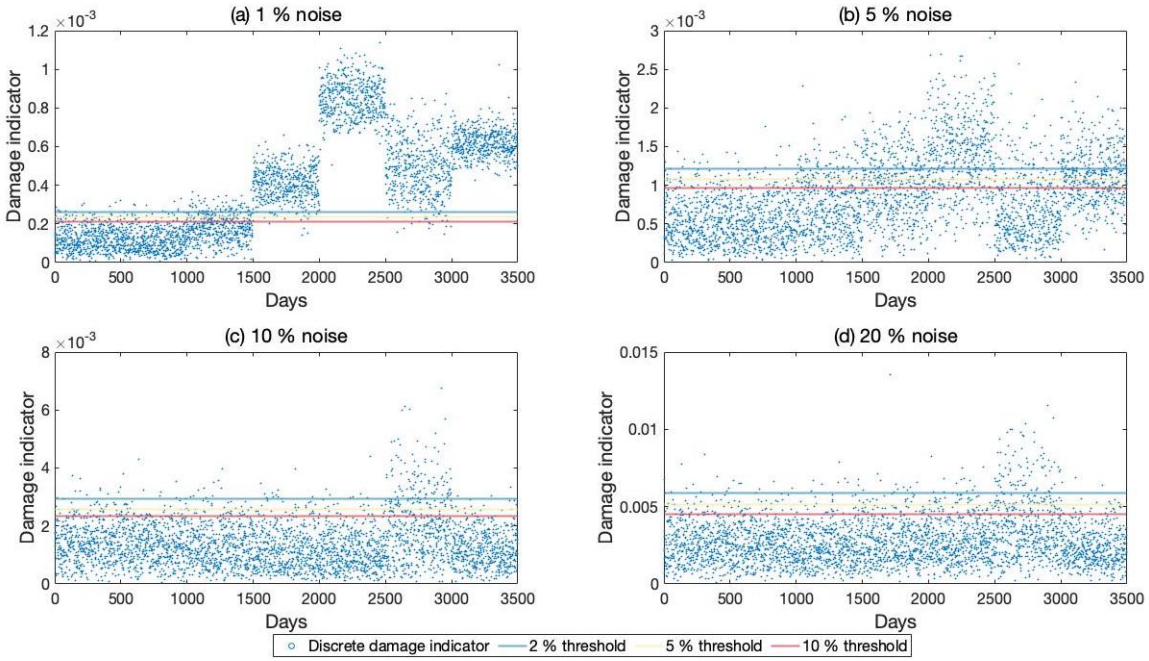

Figure 5.18: Scatter plot for modal curvature as damage indicator from three modes for Sensor 10 and damage by abutment with varying noise levels.

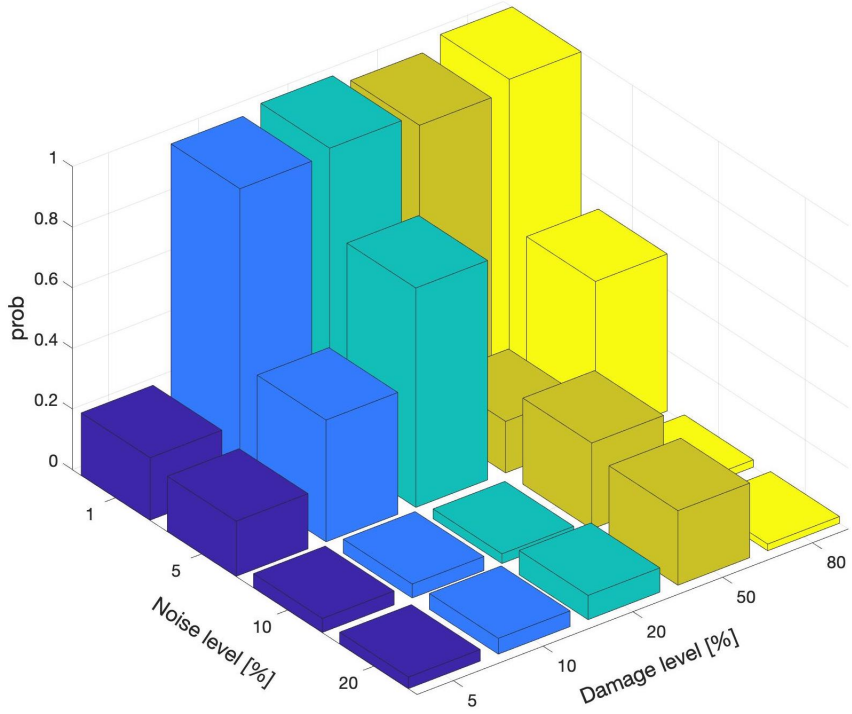

Figure 5.19: Bar chart for the modal curvature damage indicator at Sensor 10 with varying levels of noise and damage by abutment, using a combination of three modes.

detection. With damage by the abutment however, the pattern is opposite. The probability of detection increases to more than 90 % using three and four modes. Here, in similarity with the modal curvature results, inclusion of the third mode disrupts localization. This problem is however mitigated by the addition of a fourth mode. The same cannot be said for modal curvature.

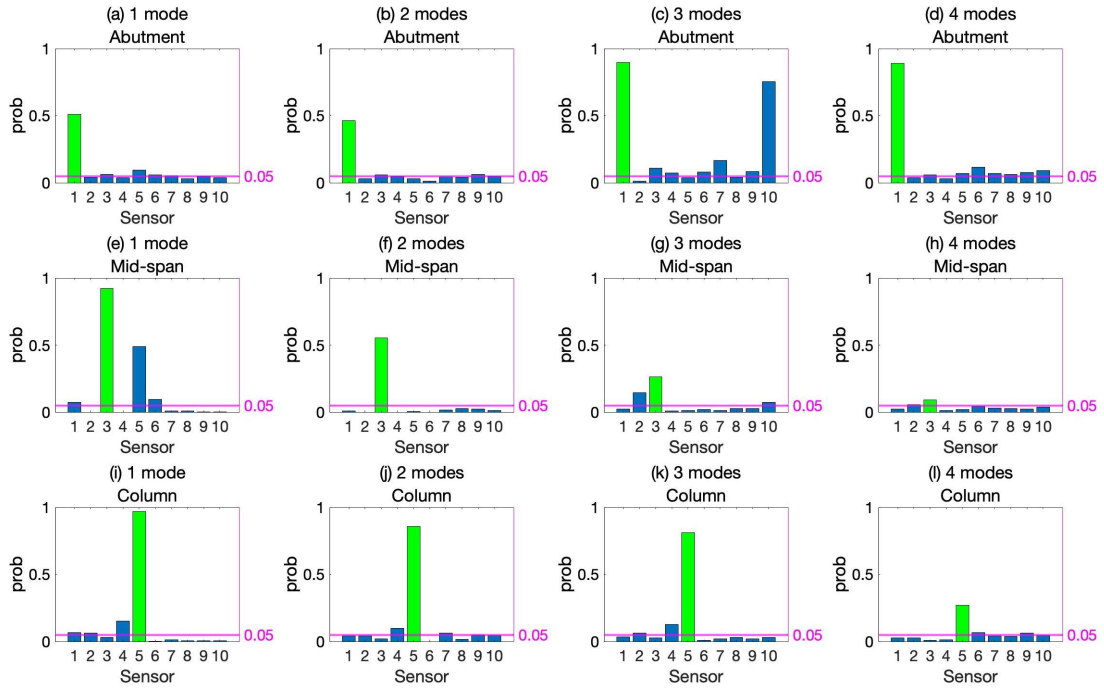

Figure 5.20: Probability of detection for modal strain energy at different damage locations and with different combinations of modes.

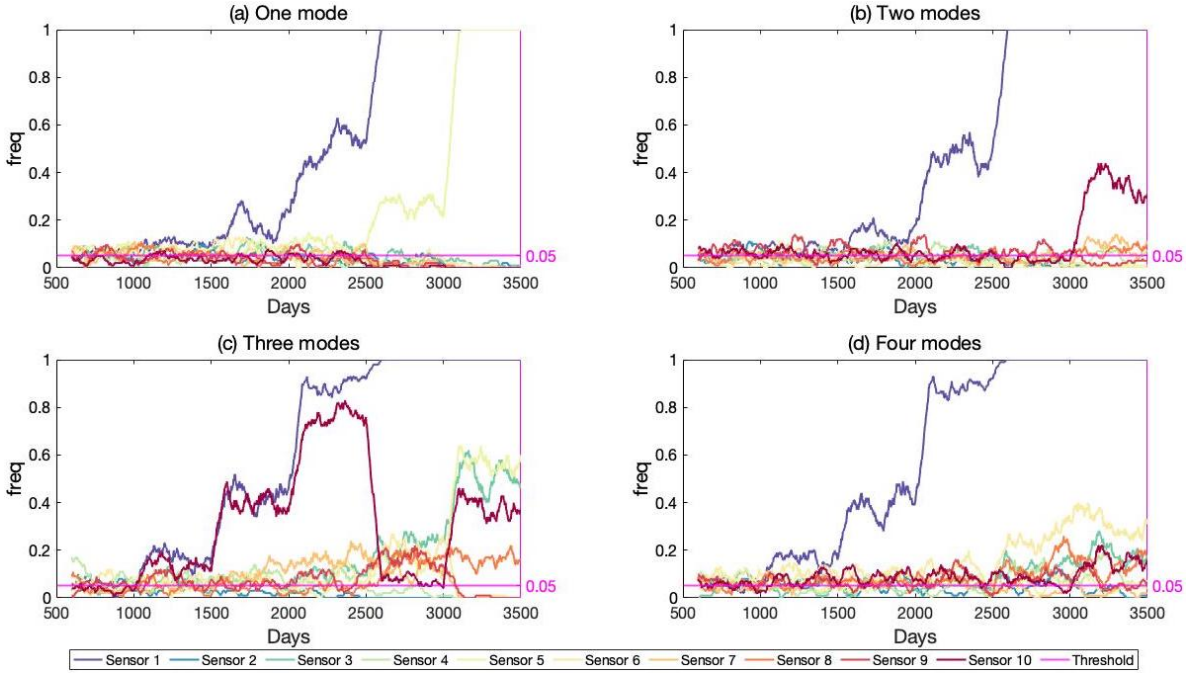

Figure 5.21: Frequency of exceedance using modal strain energy with varying number of modes for damage by the abutment, 5 % noise and 5 % threshold.

The modal flexibility, presented in Figure 5.22, behaves similarly as the modal strain energy as different combinations of modes are utilized. With damage by the abutment the probability of detection is increased with both three and four modes, compared to using two or less. Here as well Sensor 10 seems more affected than Sensor 1 where the damage actually occurs. When damage occurs at mid-span and by the column the probabilities of detection in a large amount of the sensors are high for all combinations of modes, however this decreases with an increasing number of modes.

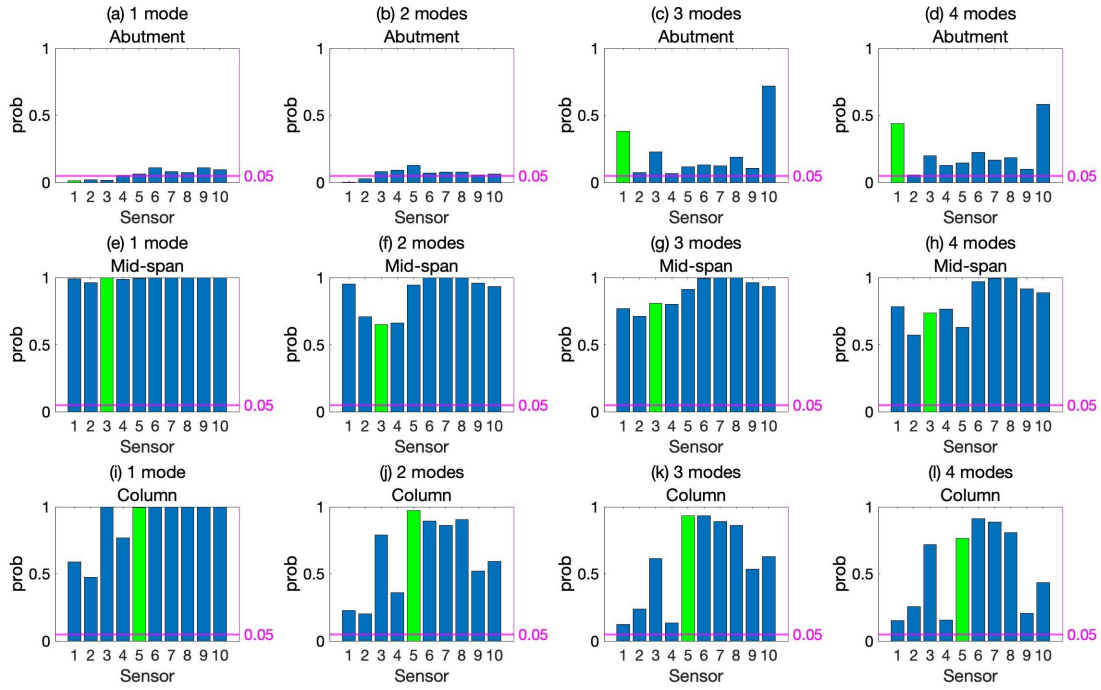

Figure 5.22: Probability of detection for modal flexibility at different damage locations and with different combinations of modes.

Subfigure (f) is particularly interesting, as the sensor associated with the damage location (Sensor 3) has the least probability of detection out of all sensors. When damage occurs by the column one can say that damage localization is improved with the use of more modes, particularly the combination of two and three.

The modal flexibility method performs poorly compared to both modal curvature and strain energy. The existence of damage is not detected by *freq* before damage reaches levels of 50 % and 80 % at the abutment, see subfigures 5.23 (a) and (b) where one and two modes are included respectively. As a third and fourth mode is included detection is drastically improved, even for lower levels of damage. Localization of damage is however negligable for all combinations of modes using modal flexiblity.

Overall, the number of modes that are included in the damage indicators have a significant impact on the probability of detecting damage and so the frequency of exceedance. This impact also depends on the location of the damage. With damage occurring by the abutment damage detection is generally increased using more modes, at the cost of decreased localization. This seems in part to be due to the large impact of the mode shape of mode 3 in the second span of the bridge. The same does not seem to apply when damage occurs elsewhere. In these cases both probability and frequency of detection is decreased with an increasing number of modes. This is illustrated in Figures 5.24, 5.25, 5.26 which depict the frequency of exceedance using modal curvature at different locations for one mode, three modes and four modes respectively.

Further, both modal curvature and modal strain energy performs well in locating the damage early on when only the first mode is evaluated, as seen in Figures 5.16 (a) and 5.21 (a). The frequency of exceedance in Sensor 1 clearly increases after 1500 days when the bending stiffness is decreased by 10 % at the abutment. Sensor 1 is located by this damage and thus the location of damage is detected effectively as no other sensors can be used to detect damage at this stage.

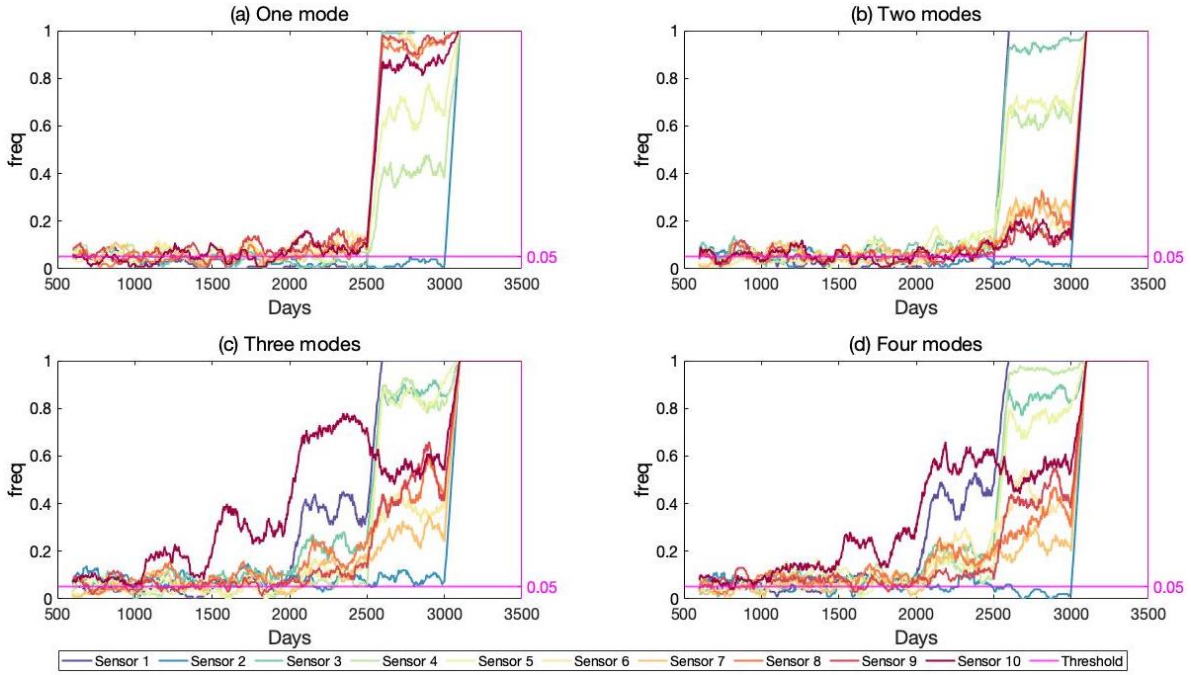

Figure 5.23: Frequency of exceedance using modal flexibility with varying number of modes for damage by the abutment, 5 % noise and 5 % threshold.

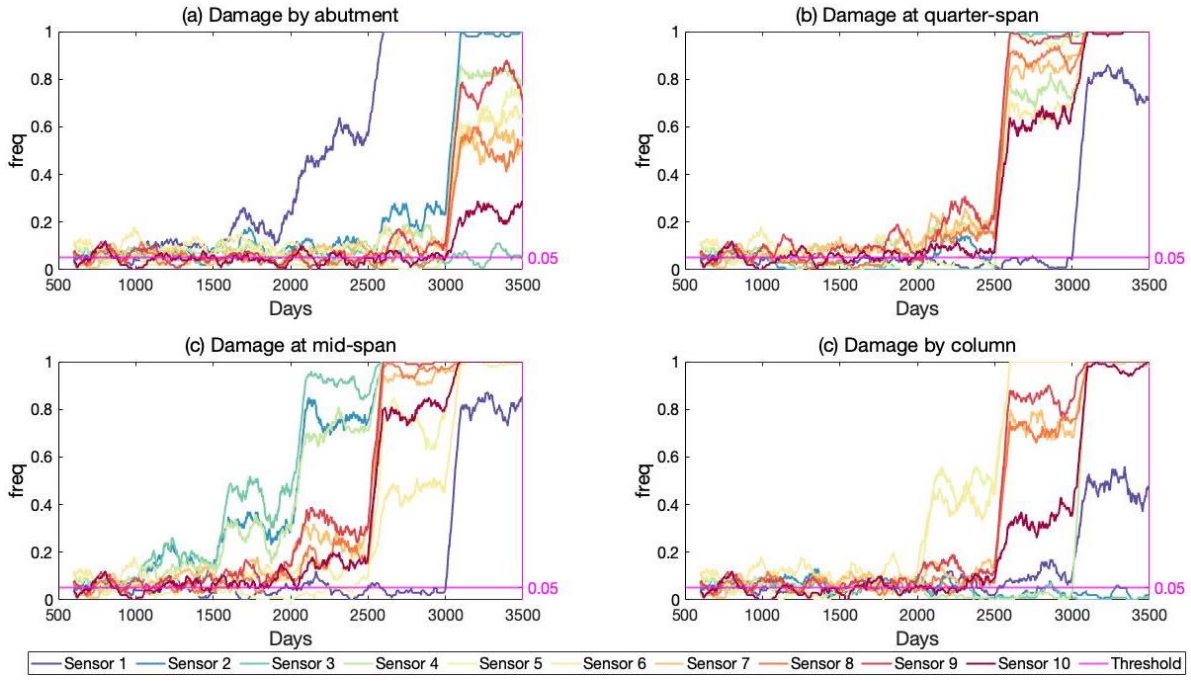

Figure 5.24: Frequency of exceedance using modal curvature with one mode for all damage locations, 5 % noise and 5 % threshold.

The only mode evaluated on its own herein is the first mode, so it is not known what results would be obtained by looking at any of the other modes singularly or any other combination of modes. Inclusion of a third mode generally reduces the performance, so it is checked what influence mode three has on the *freq* in Figures 5.27 and 5.28, using modal strain energy with damage by the abutment and at mid-span respectively.

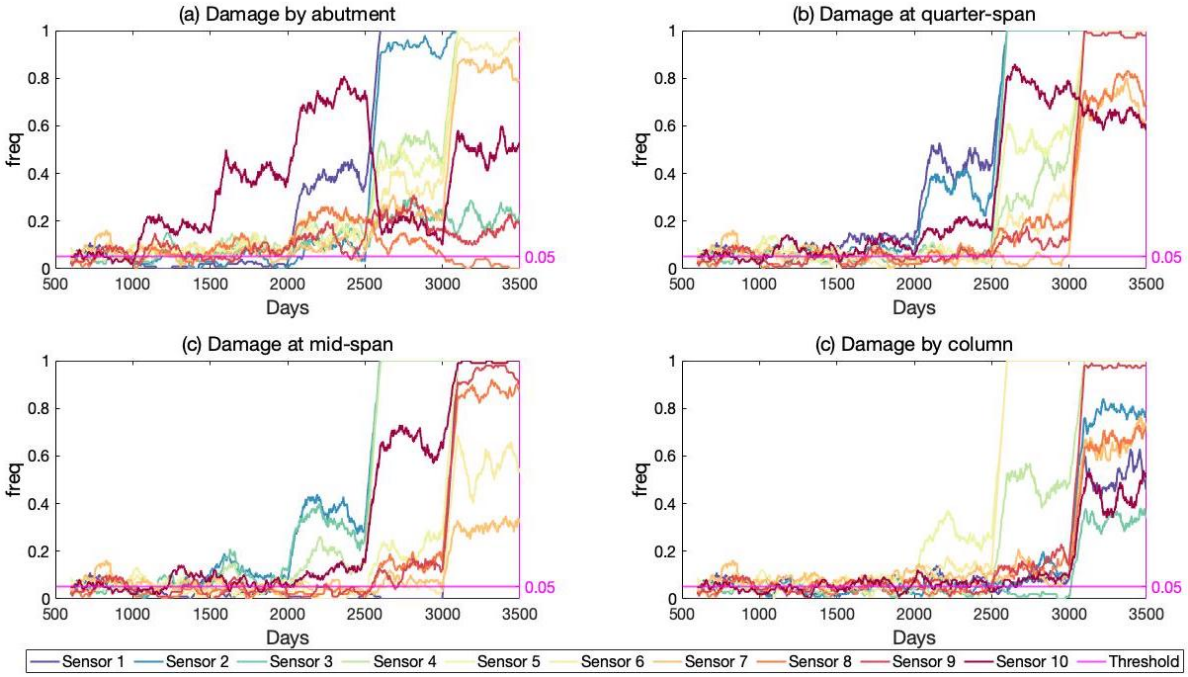

Figure 5.25: Frequency of exceedance using modal curvature with three modes for all damage locations, 5 % noise and 5 % threshold.

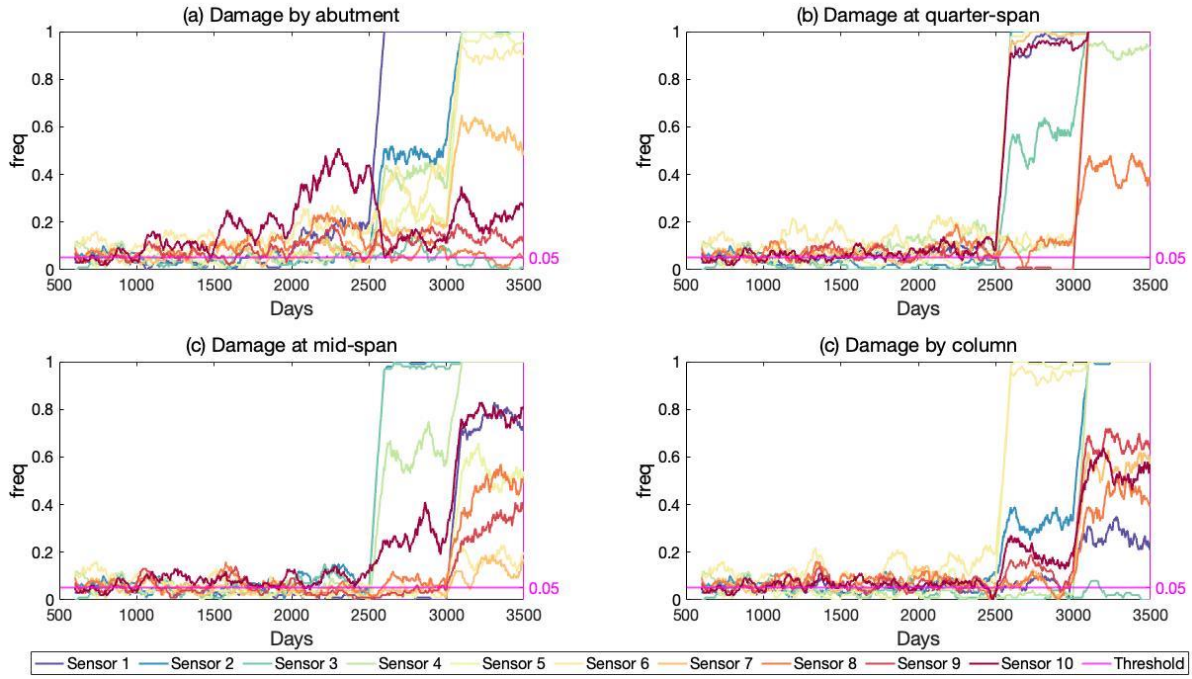

Figure 5.26: Frequency of exceedance using modal curvature with four modes for all damage locations, 5 % noise and 5 % threshold.

It can be seen from Figures 5.27 (c) and (f) that a reduced bending stiffness by the abutment results in changes in the response of the third mode shape and thus the modal strain energy by the far end observed by Sensor 10. However, when all four modes are included, the results from Sensor 1 is equally good and the unwanted frequency increase from Sensor 10 is removed, seen in Figure 5.27 (d). The performance is notably reduced when mode three is excluded in Figure 5.27 (e) where only the first, second and fourth mode is used, so mode three clearly contributes with valuable information. The frequency parameter increases later and for several sensors, leading to later detection and poor

localization. The same occurs when the damage is located at quarter-span in Figure 5.28, although the performance is good with only one mode.

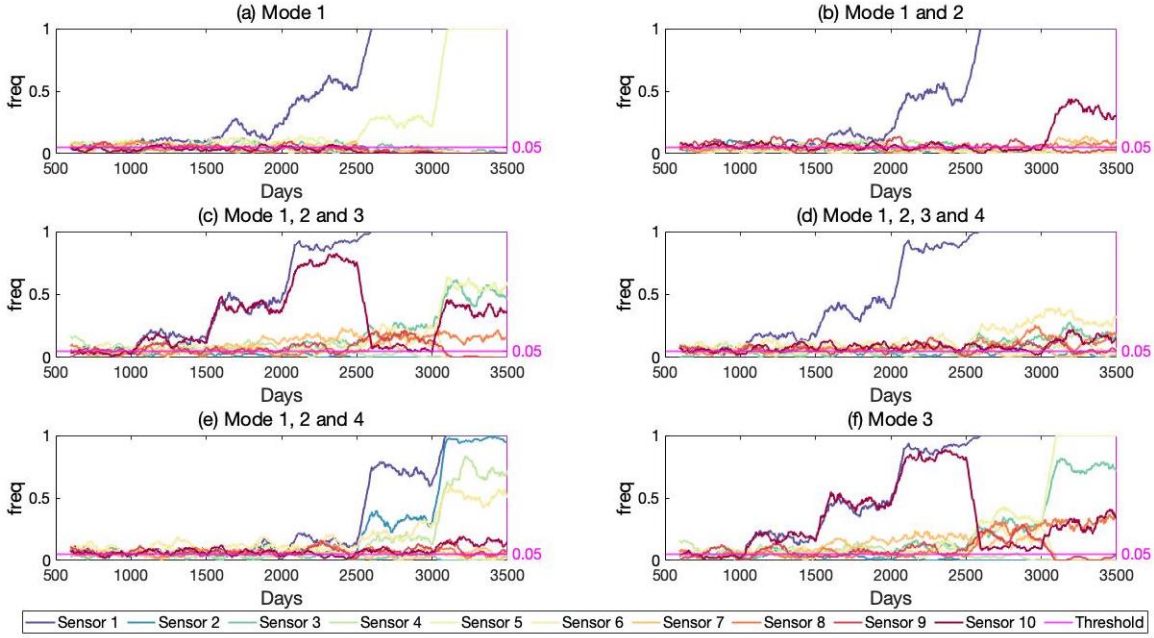

Figure 5.27: Frequency of exceedance from modal strain energy varying numbers and combinations of modes caused by damage by abutment with 5 % noise and 5 % threshold.

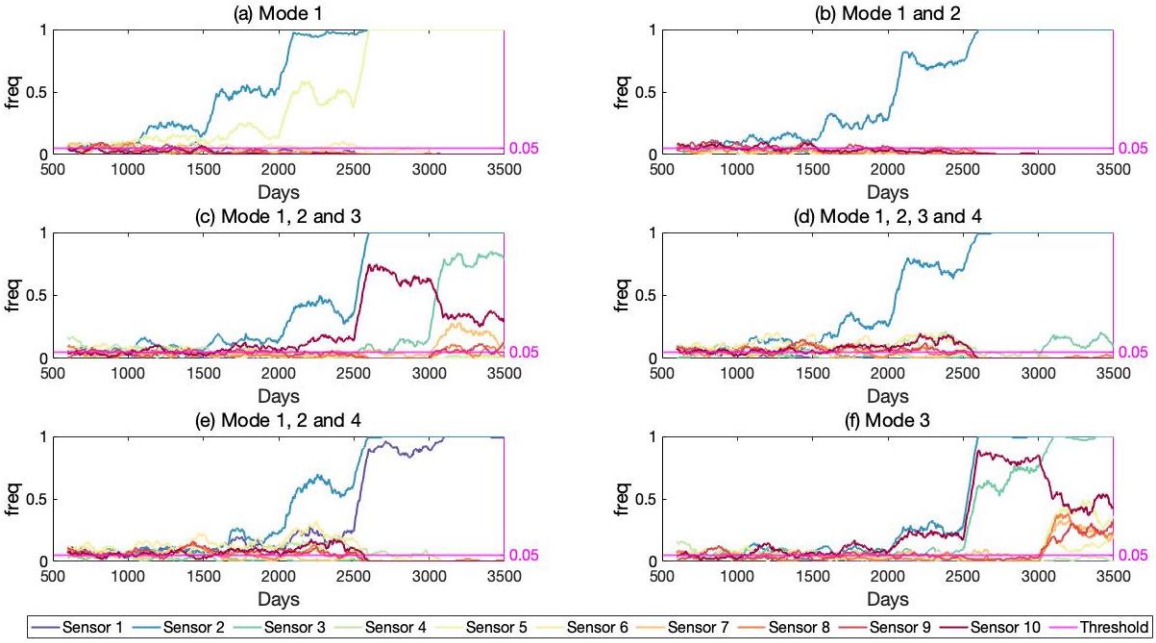

Figure 5.28: Frequency of exceedance from modal strain energy varying numbers and combinations of modes caused by damage at quarter-span with 5 % noise and 5 % threshold.

The ideal number of modes included in the calculations may vary depending on the noise level. The previously discussed Figures 5.16, 5.21 and 5.23 all have a noise level of 5 % and may be compared to Figures 5.29, 5.30 and 5.31 where the noise level is increased to 20 %.

All three damage indicators only detect damage for the higher damage levels with a 20 % noise level but the results of three modes are no longer polluted with the indication of damage from

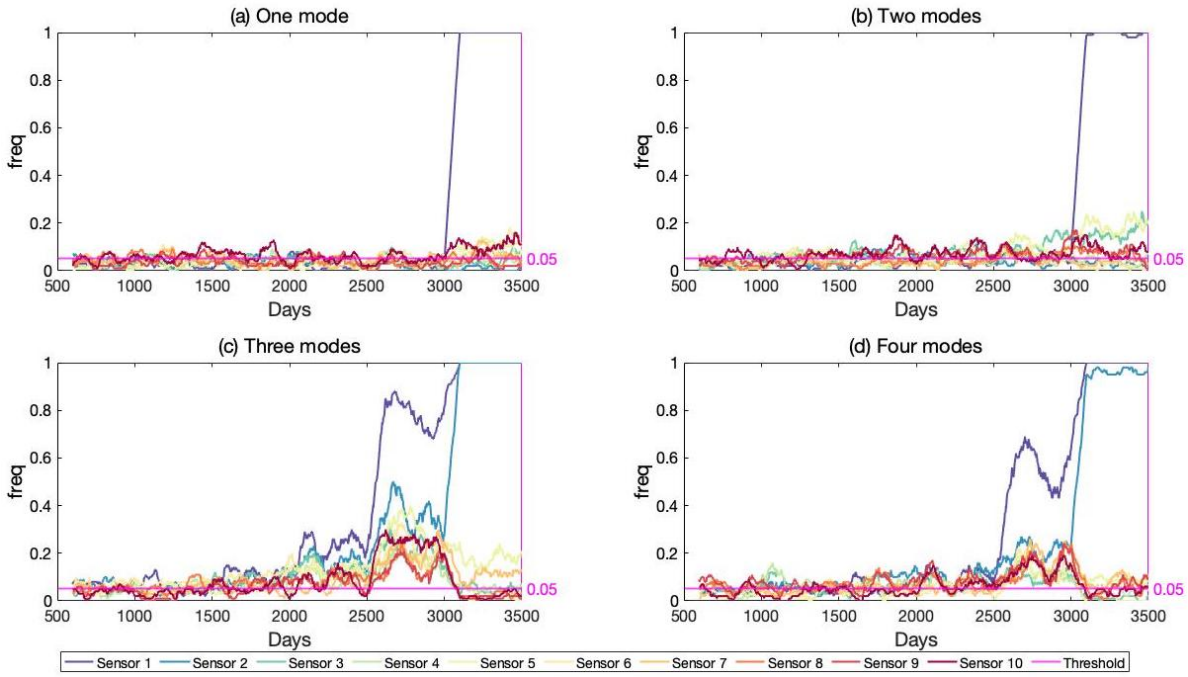

Figure 5.29: Frequency of exceedance using modal curvature with varying number of modes for damage by the abutment, 20 % noise and 5 % threshold.

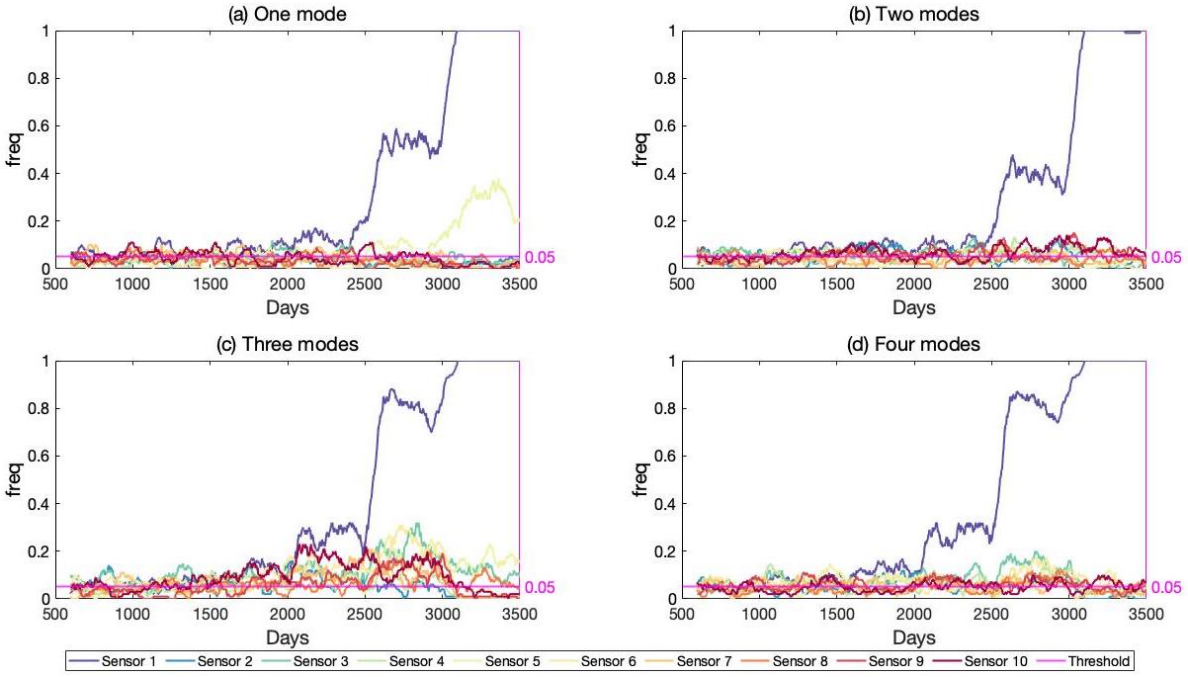

Figure 5.30: Frequency of exceedance using modal strain energy with varying number of modes for damage by the abutment, 20 % noise and 5 % threshold.

Sensor 10. Therefore, localization of damage is now more accurate although it is found at a higher damage severity. Three modes must now be included in the modal curvature method if damage is to be detected before it reaches the 80 % damage level by the abutment, however, this at the cost of clear localization. The performance of the modal strain energy and modal flexibility methods for localization of damage is improved by this high noise level. So, it is found that more modes are favourable for all damage indicators for damage by the abutment for all noise levels and especially important for 20 %. It should be noted that this is not true for the other locations of damage.

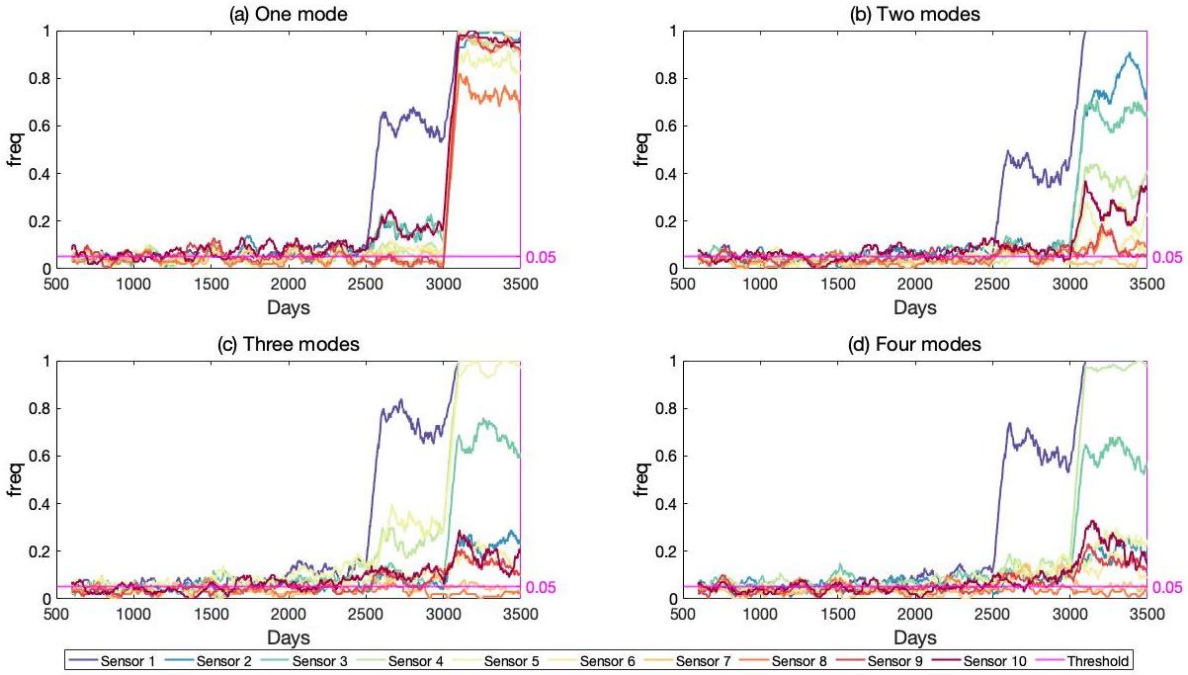

Figure 5.31: Frequency of exceedance using modal flexibility with varying number of modes for damage by the abutment, 20 % noise and 5 % threshold.

For all damage locations, except by the abutment, it is found that the best results are obtained by the use of only one mode. An example of this is illustrated in Figure 5.32 obtained by modal strain energy for damage at quarter span. The same trend is found by the other damage indicators and for damage by the column and at mid-span aswell; one mode generally leads to better results regarding both detection and localization and the efficacy decreases with increasing number of modes.

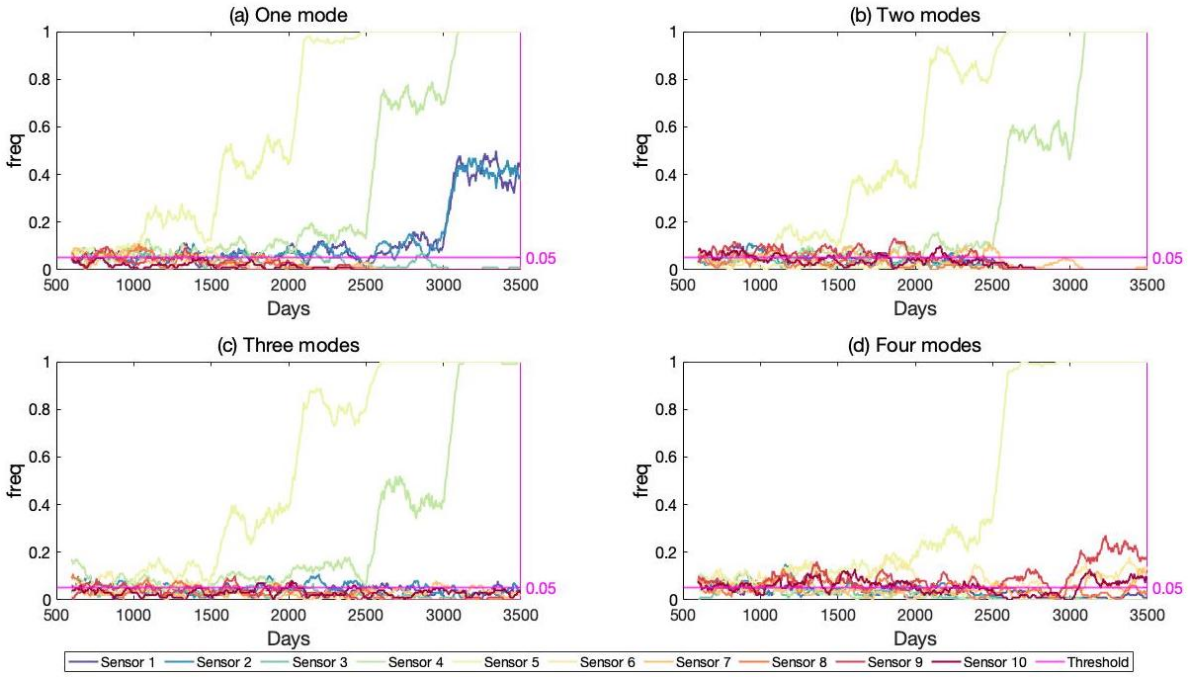

Figure 5.32: Frequency of exceedance using modal strain energy with varying number of modes for damage at quarter-span, 5 % noise and 5 % threshold.

Figures 5.24, 5.33 and 5.34 present damage at all locations and the frequency of exceedance by all three damage indicators with one mode only and 5 % noise. Damage is detected at a 5 % reduction in bending stiffness by modal strain energy for all locations of damage by the closest sensor where the damage is located. This is not the case when two or more modes are included in which detection is delayed, see Figure 5.53. Detection also happens at a lower damage level and more frequently by modal curvature and modal flexibility when one mode is used as compared to two modes, illustrated in Figures 5.51 and 5.55. For damage by the abutment, however, the detection performance is further improved for all damage indicators by the inclusion of a third and fourth mode though the localization performance is disturbed to various degrees.

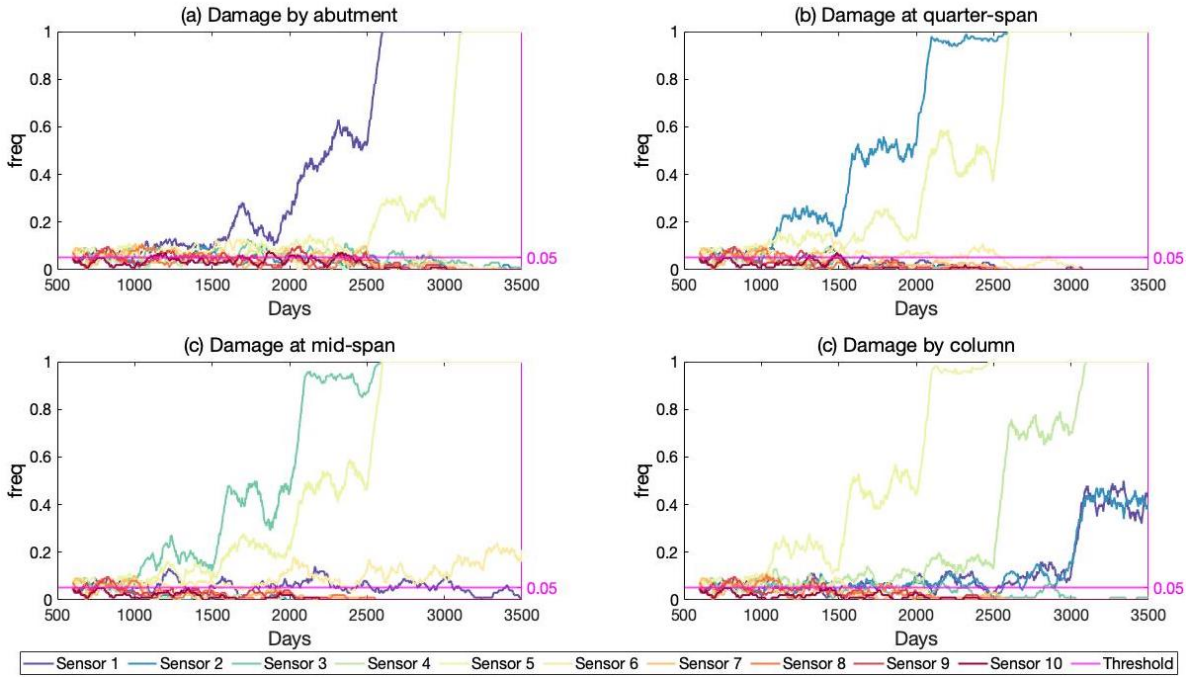

Figure 5.33: Frequency of exceedance using modal strain energy with one mode and varying damage locations, 5 % noise and 5 % threshold.

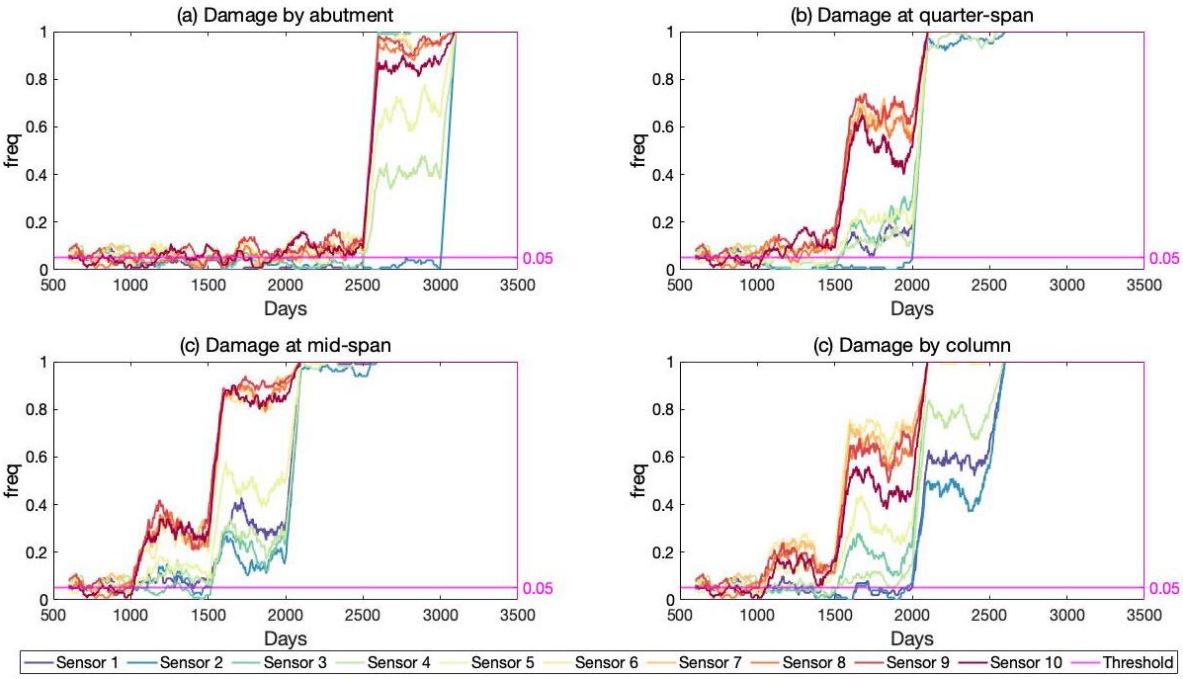

Figure 5.34: Frequency of exceedance using modal flexibility with one mode and varying damage locations, 5 % noise and 5 % threshold.

5.3.3 Effect of Noise

The effect of noise on damage detection for the different damage indicators is highly relevant. The existence of noise on vibration signals in real-life applications of SHM is considered one of the major drawbacks of these techniques. Although five different levels of noise were evaluated, the results with 0.5 % noise are excluded as they do not deviate significantly from the 1 % noise level results. The probability of detecting damage is only slightly increased in some cases. A 0.5 % influence of noise may also be considered unrealistically low.

In Figure 5.35 the probability of detection with modal curvature for some levels of damage by the abutment as well as at mid-span is presented. The frequency of detection is also presented in Figure 5.36 for damage occurring at quarter-span.

At first glance noise clearly has an impact on the probability of modal curvature to detect damage. For damage levels of 5 % and 10 % the probability of detection is insignificant when the noise level is increased beyond 1 %. With 50 % damage, the probability of detection is high in Sensor 1 where the damage occurs for all the presented noise levels. Localization interestingly seems to improve at higher levels of noise, at the expense of a slightly decreased probability of detection as the noise level reaches 10 %. This is also demonstrated in the frequency plot. With a noise level of 1 % damage detection and localization is clear from a 5 % damage level. The frequency of detection is generally decreased with increasing levels of noise. By increasing from 5 % to 10 % noise, see subfigures 5.36 (b) and (c), increased noise does not impair detection, but improves localization.

Figure 5.37 also presents the probability of detection with modal curvature for different levels of noise, but at different locations, namely by the column and at quarter-span. The remarks made on Figure 5.35 can be transferred to Figure 5.37; for low levels of damage, namely 5 % and 10 %, damage detection is disrupted with a noise level of 5 % or more. For the higher damage level of 50

%, on the other hand, increased noise leads to increased localization.

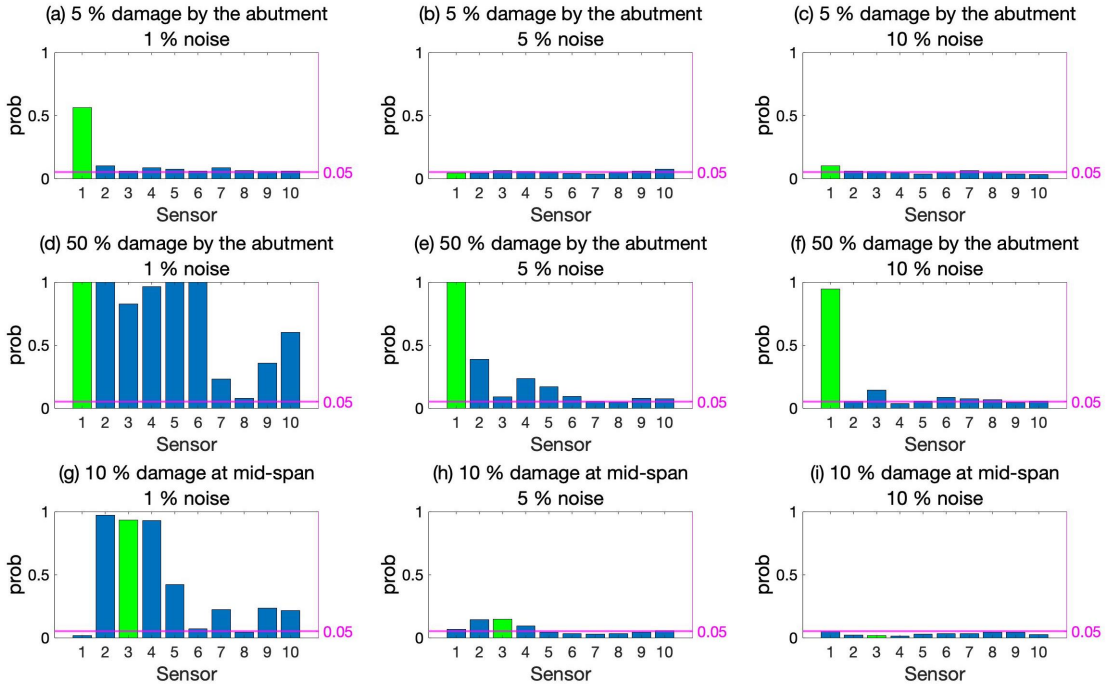

Figure 5.35: Probability of detection with modal curvature using two modes for different levels of noise and damage by the abutment as well as at mid-span.

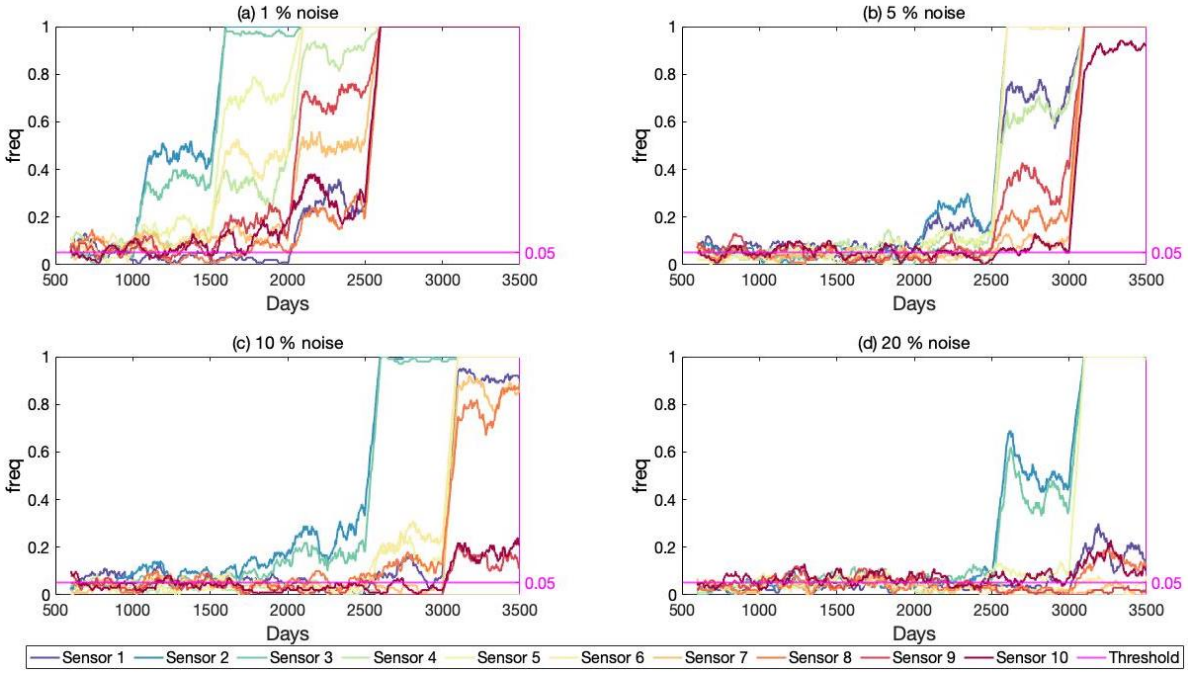

Figure 5.36: Frequency of exceeding the 5 % threshold value using modal curvature with varying noise levels and increasing damage at quarter-span using two modes.

Using both modal flexibility and modal strain energy as a damage indicator the same pattern can be discerned as from modal curvature, see Figures 5.38, 5.39, 5.40 and 5.41. Damage detection is generally decreased with increasing levels of noise, as is expected. As can also be seen in previous figures that include the modal strain energy, this damage indicator remains superior to the others in

localization of damage, regardless of the level of noise.

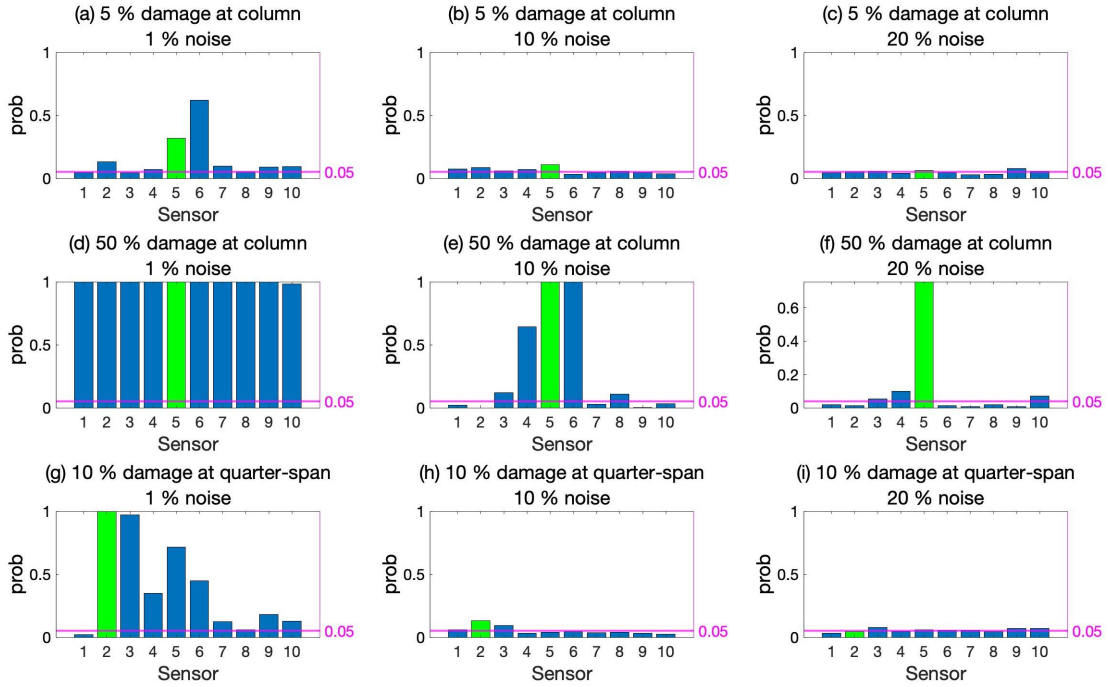

Figure 5.37: Probability of detection with modal curvature for different levels of noise and damage by the column as well as at quarter-span.

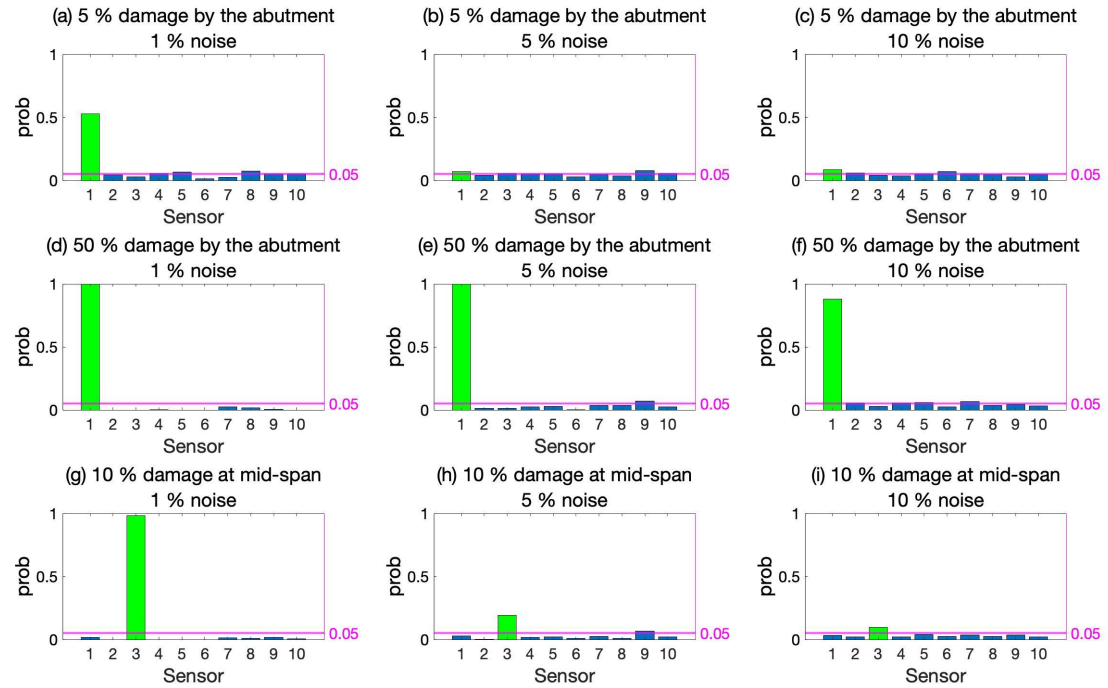

Figure 5.38: Probability of detection with modal strain energy for different levels of noise and damage by the abutment as well as at mid-span.

For all damage indicators, when the damage level is low (5 % and 10 %), the probability as well as the frequency of damage detection is decreased to insignificant levels as noise is increased beyond 1 %. Notably, the probability of detecting a 5 % level of damage is low even with 1 % noise. When

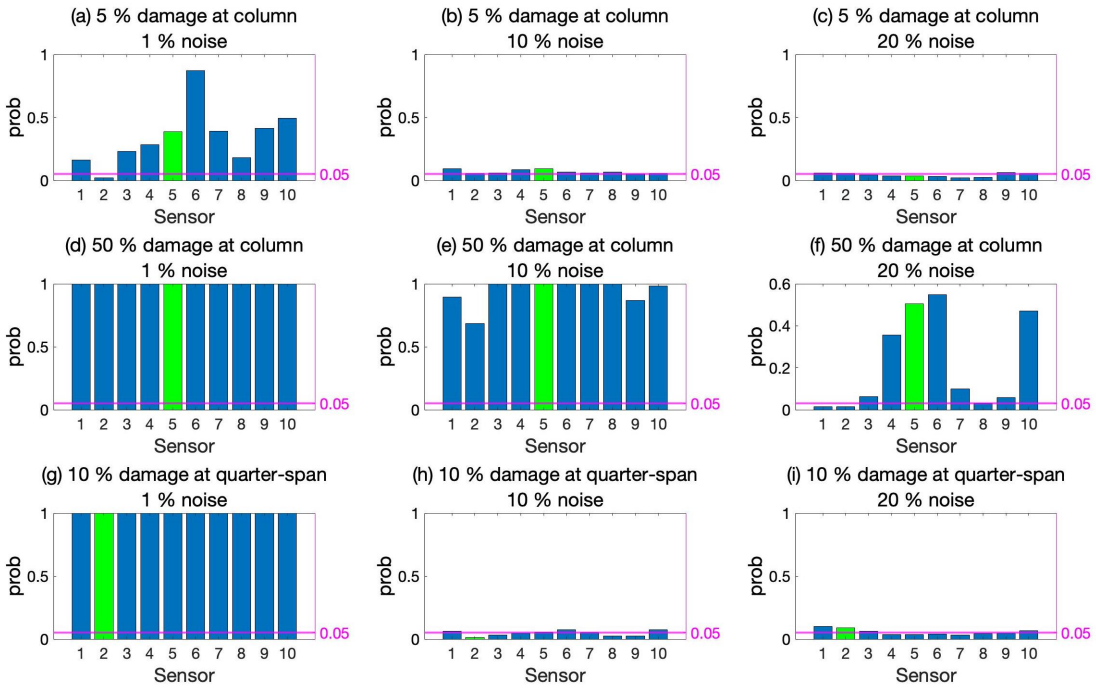

Figure 5.39: Probability of detection with modal flexibility for different levels of noise and damage by the column as well as at quarter-span.

the damage level increases to 50 %, more noise actually seems favorable for the modal curvature; localization is improved as the probability of detection remains high in the sensor located by the damage, as it occurs both by the abutment and by the column. The same is true for the modal flexibility, although not to the same extent.

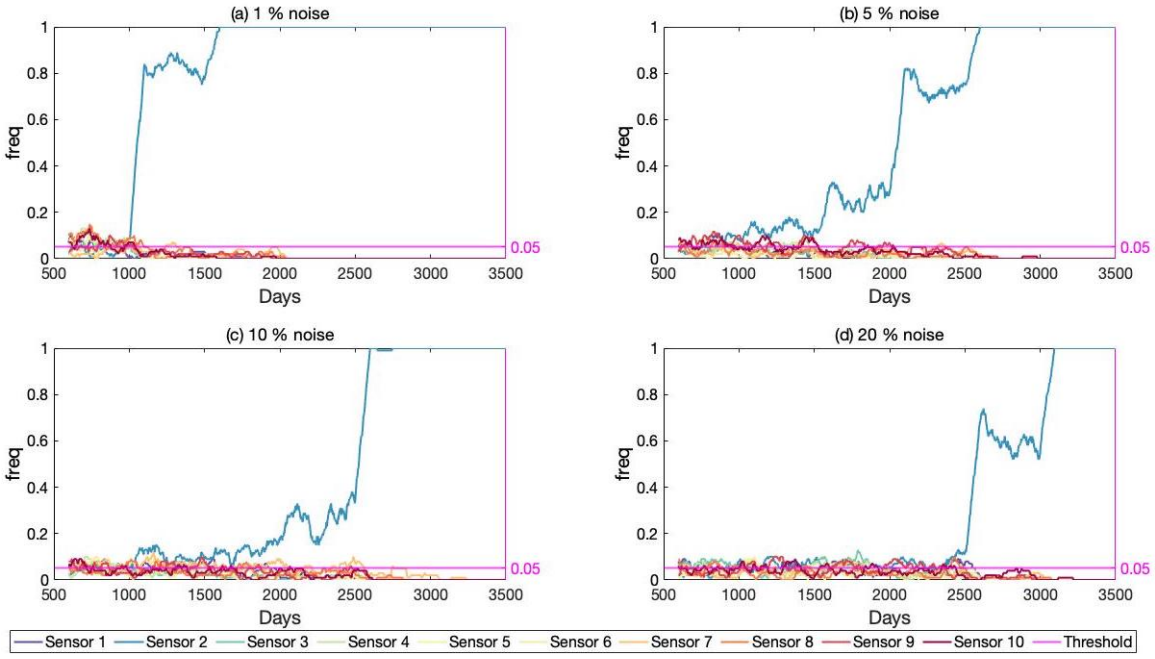

Figure 5.40: Frequency of exceeding the 5 % threshold value using modal strain energy with varying noise levels, with increasing damage at quarter-span by looking at two modes.

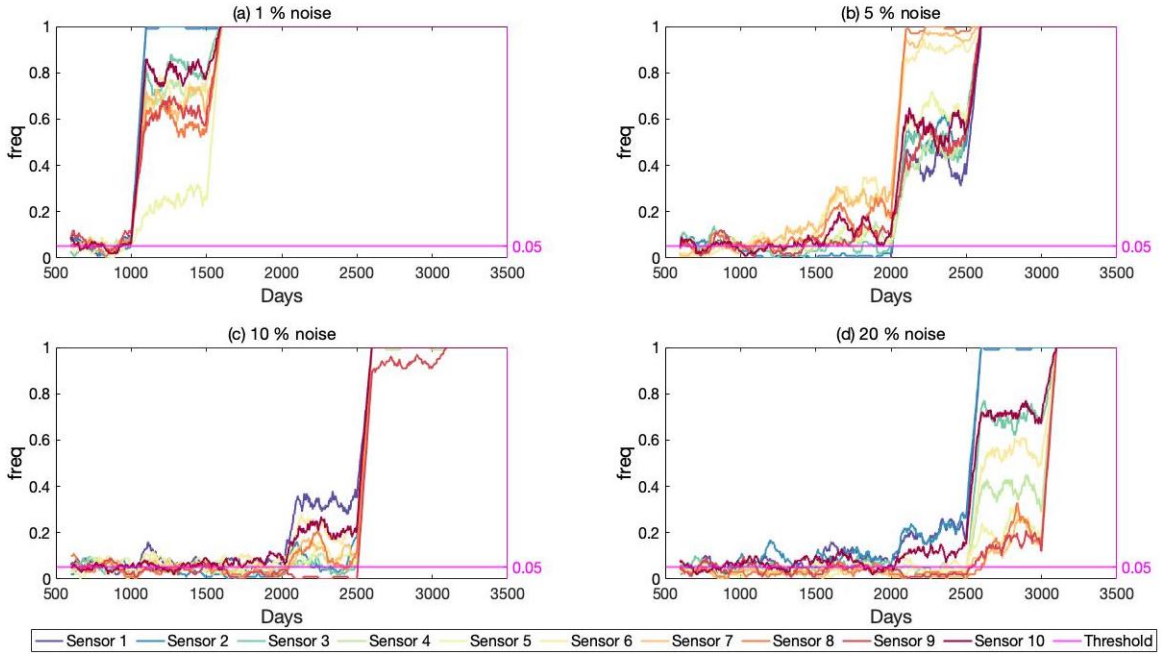

Figure 5.41: Frequency of exceeding the 5 % threshold value using modal flexibility with varying noise levels, with increasing damage at quarter-span by looking at two modes.

Higher noise levels result in a larger variance in the damage indicators, as seen in Figures 5.42, 5.43, 5.44, 5.45, 5.46 and 5.47, where the indication of damage at quarter-span is plotted discretely for all three damage indicators for two sensor locations. For the purpose of visualizing the variance in the data, the scale is kept constant for all subfigures within each figure. Consequently, the early increase in the damage indicator for the lower noise levels is not visually clear. Moreover, some data is not included at high noise levels in order for all the subfigures to fit the same scale. These are only a few data which deviate considerably, as a result of noise, from the remainder of the calculated damage indicators.

The performance of all three damage indicators is highly affected by noise when evaluating the observations discretely. This is illustrated in Figures 5.42, 5.43, 5.44, 5.45, 5.46 and 5.47 based on Sensor 2, which is close to this damage at quarter-span, and Sensor 3 placed 12.1 m away from damage. As noise levels increase the variance of the daily damage indicator values increases, as is expected. This affects the calculated threshold values as well as the probability and frequency of detection. Increased levels of noise delays damage detection to when damage becomes more severe.

For the lowest noise level and damage severity considered herein, damage is detected by the sensor closest to damage when modal strain energy is used to obtain the discrete damage indicator based on two modes as in Figure 5.42 (a). Detection is delayed for the higher noise levels. The discrete damage indicator exceeds the thresholds for several of the observations after 1500 days, corresponding to a damage severity of 10 %, for 5 and 10 % noise as seen in Figures 5.42 (b) and (c). From Figure 5.42 and 5.43 it can be observed that the discrete damage indicator is decreasing with increasing damage for the sensor placed further away from damage and increasing for the closer. This happens for all noise levels and leads to effective localization.

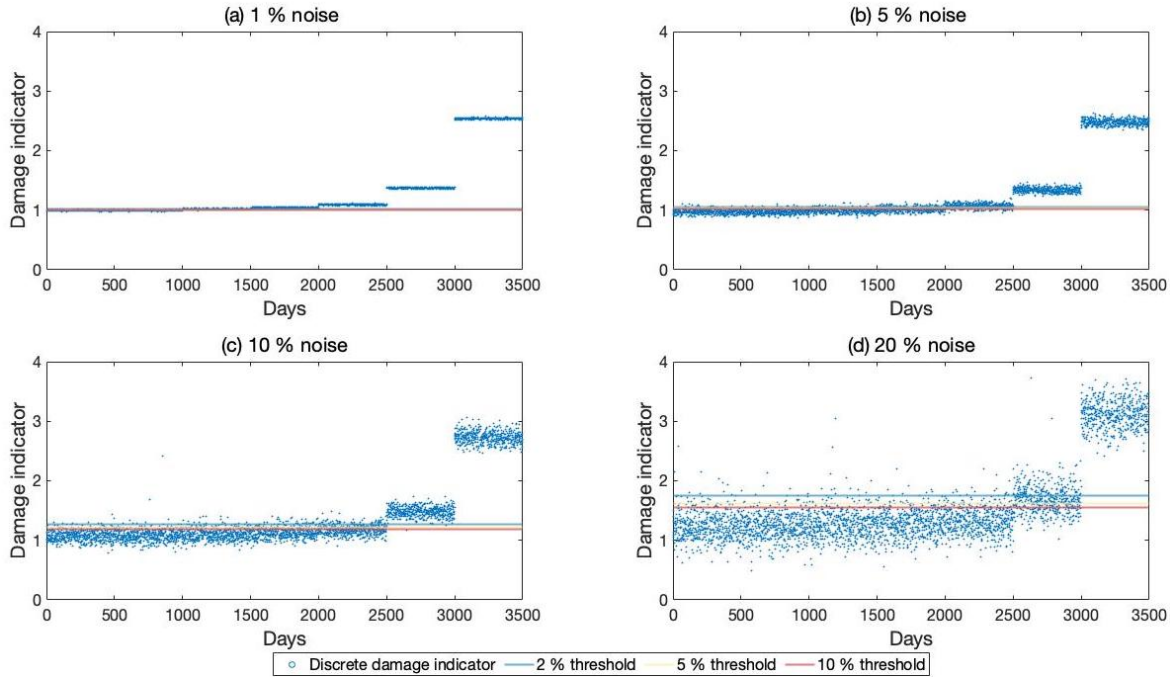

Figure 5.42: Scatter plot of damage indicator from modal strain energy, from Sensor 2 and damage at quarter-span for varying noise levels with corresponding threshold values.

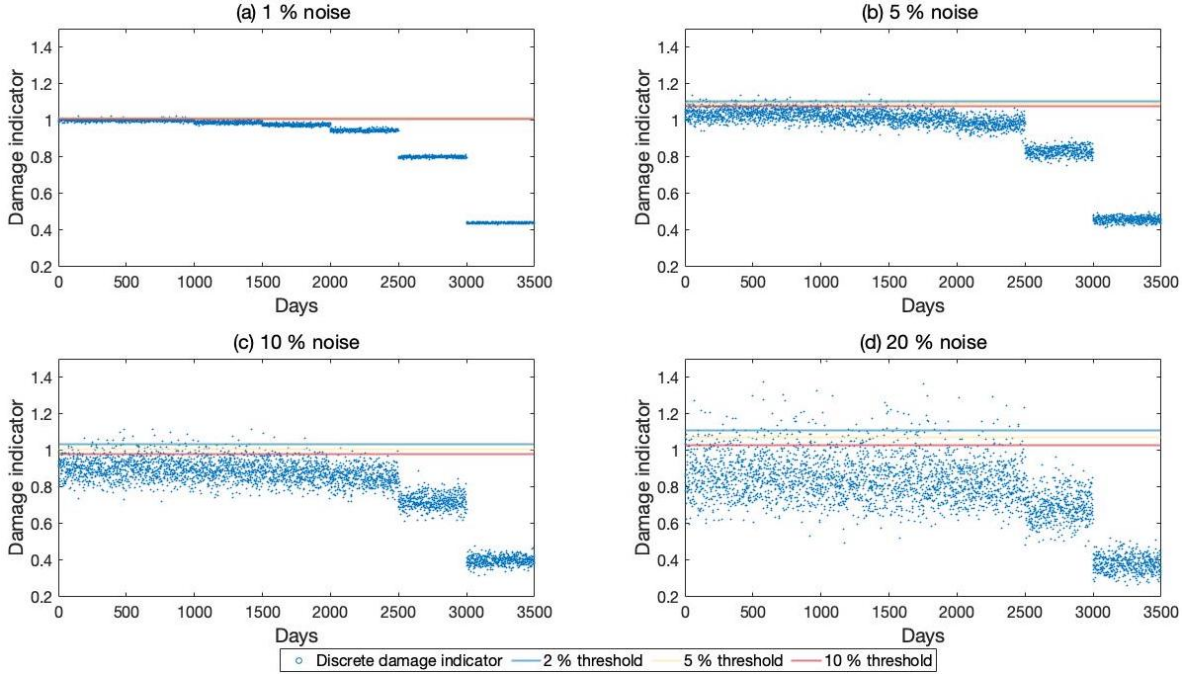

Figure 5.43: Scatter plot of damage indicator from modal strain energy, from Sensor 3 and damage at quarter-span for varying noise levels with corresponding threshold values.

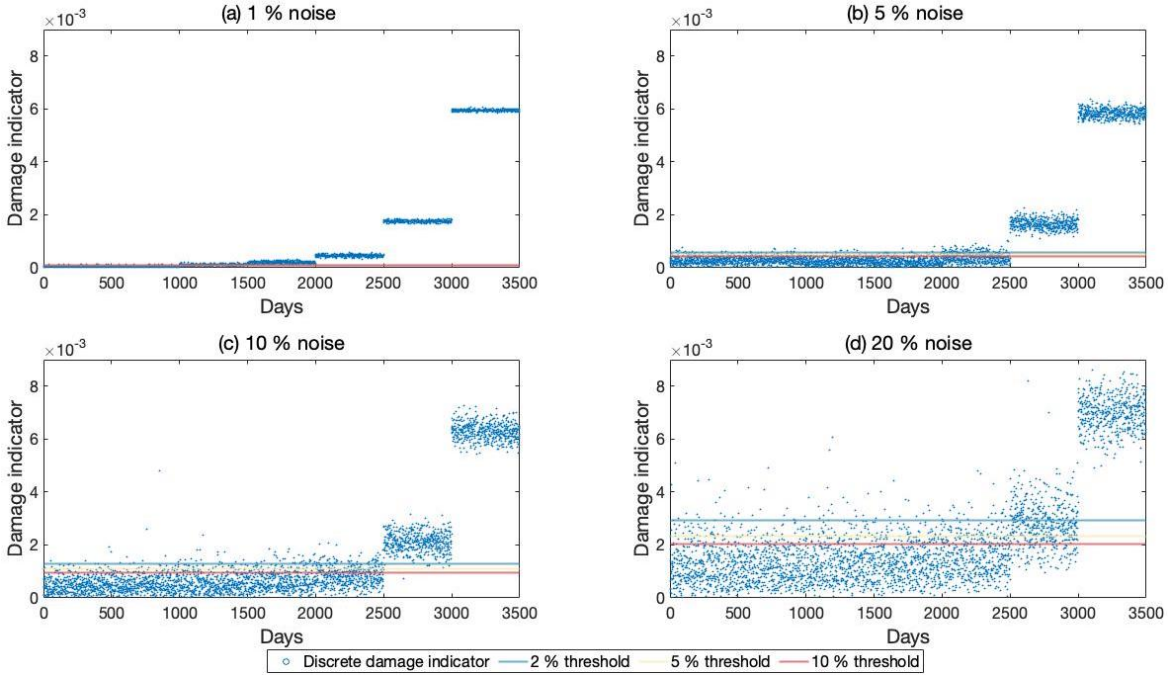

Figure 5.44: Scatter plot of damage indicator from modal curvature, from Sensor 2 and damage at quarter-span for varying noise levels with corresponding threshold values.

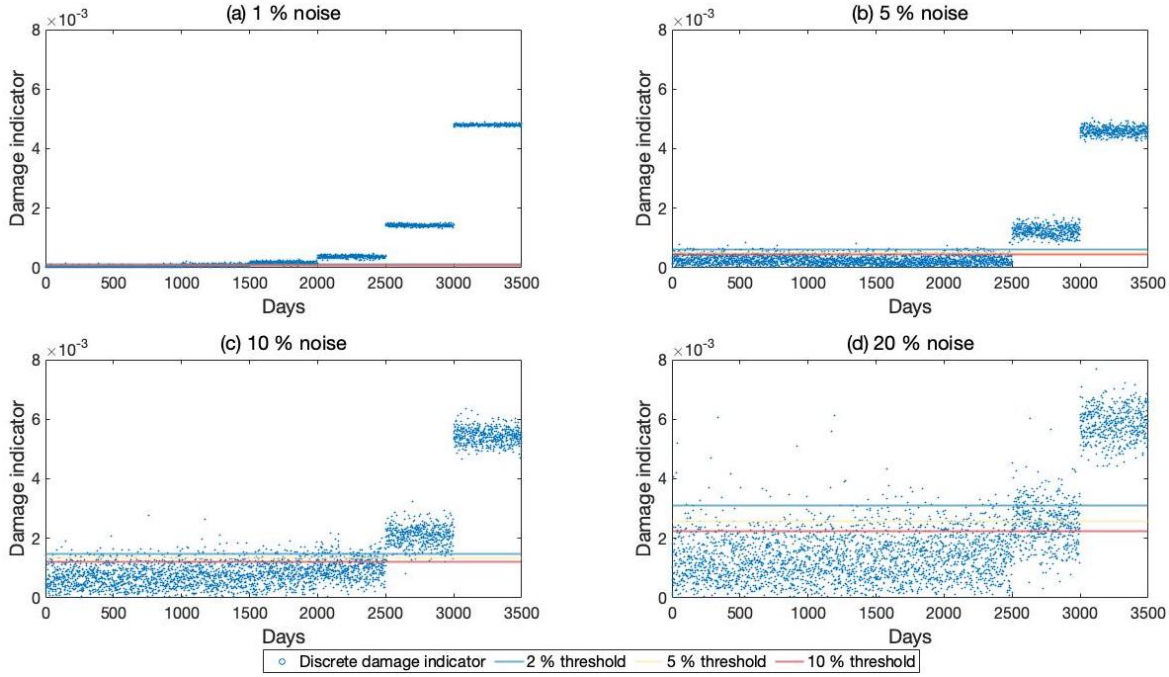

Figure 5.45: Scatter plot of damage indicator from modal curvature, from Sensor 3 and damage at quarter-span for varying noise levels with corresponding threshold values.

Damage is detected at even the lowest severity of damage, initiated at day 1000, by both sensors for the lowest noise level evaluated, 1 % noise, presented in Figures 5.44 (a) and 5.45 (a) for modal curvature and in Figures 5.46 (a) and 5.47 (a) for modal flexibility. The detection of damage is effectively delayed with higher noise levels. With modal curvature and flexibility there is little between the two sensors, and so the location of damage may not be determined as confidently as previously done by modal strain energy. However, when looking closely on the modal curvature data, damage is more frequently detected by Sensor 2, which becomes more clear when the frequency of

exceedance is plotted, see Figure 5.36. It should be noted that neither of the sensors discussed are significantly far away from damage compared to the other sensors and so the indication of location is not directly wrong. As seen in Figure 5.36, damage is less frequently indicated by the other sensors on the structure from modal curvature. Modal flexibility, on the other hand, has a poor localization performance for all noise levels compared to the other two methods as illustrated in Figure 5.41.

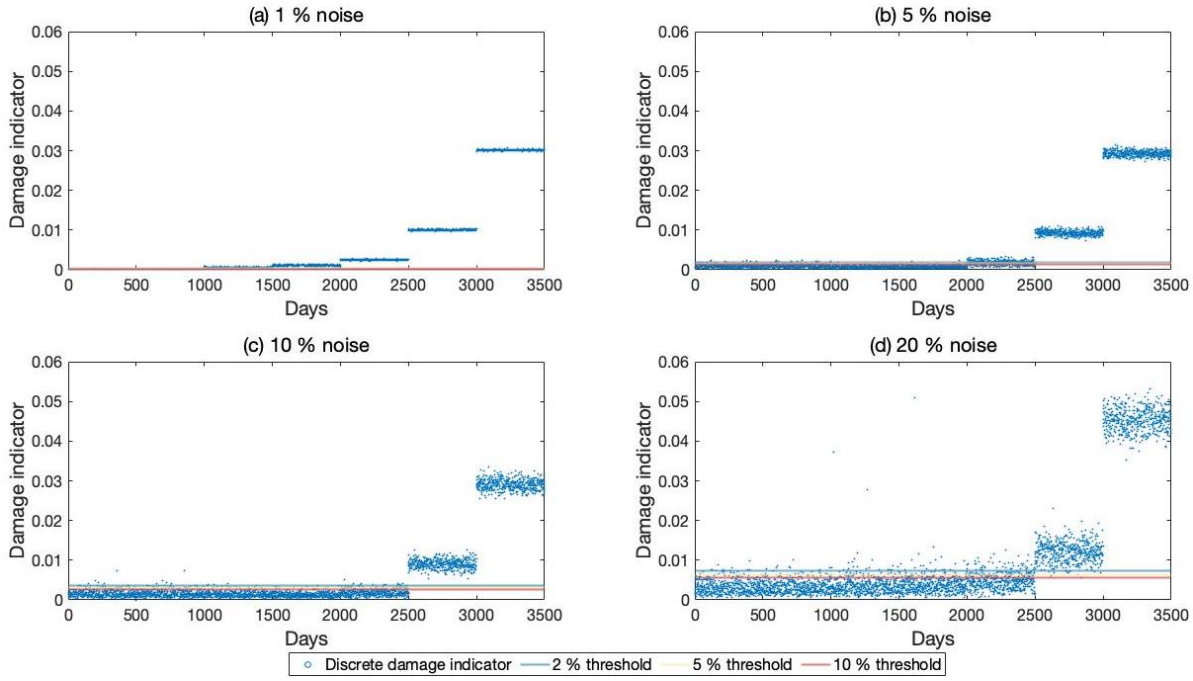

Figure 5.46: Scatter plot of damage indicator from modal flexibility, from Sensor 2 and damage at quarter-span for varying noise levels with corresponding threshold values.

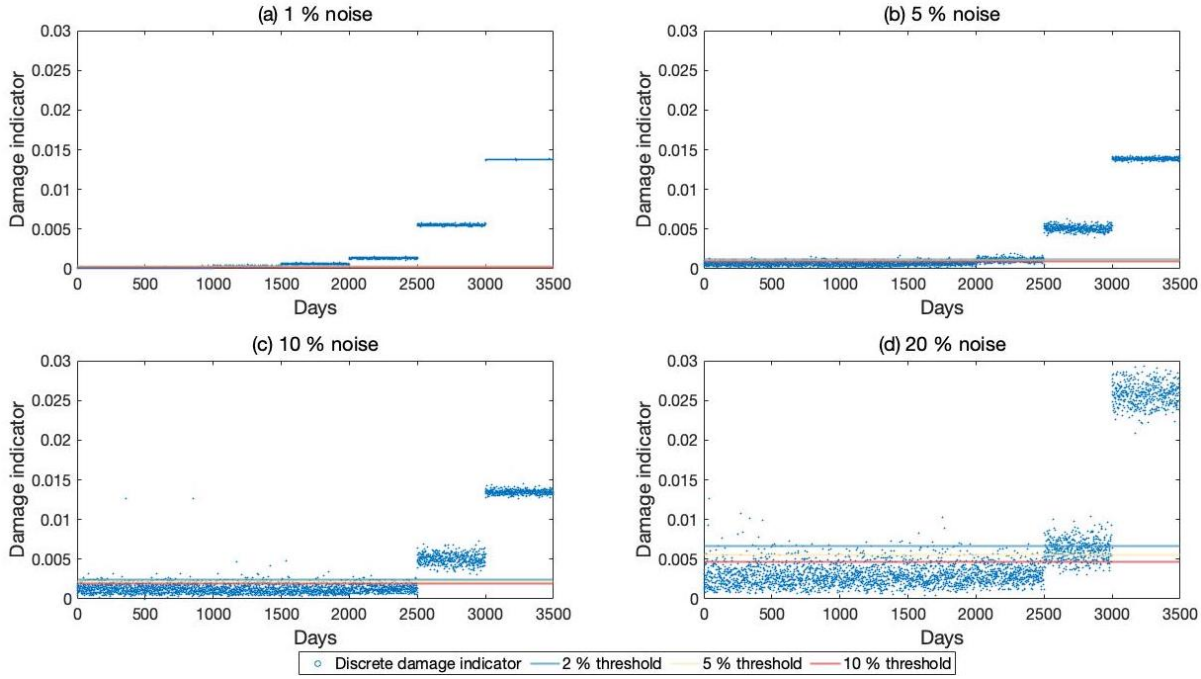

Figure 5.47: Scatter plot of damage indicator from modal flexibility, from Sensor 3 and damage at quarter-span for varying noise levels with corresponding threshold values.

Noise has varying impact on the modal curvature as damage indicator depending on the location of damage. This is illustrated in Figures 5.48 and 5.49 where the *freq* is plotted for the four damage locations with only the closest sensor to the respective damage locations.

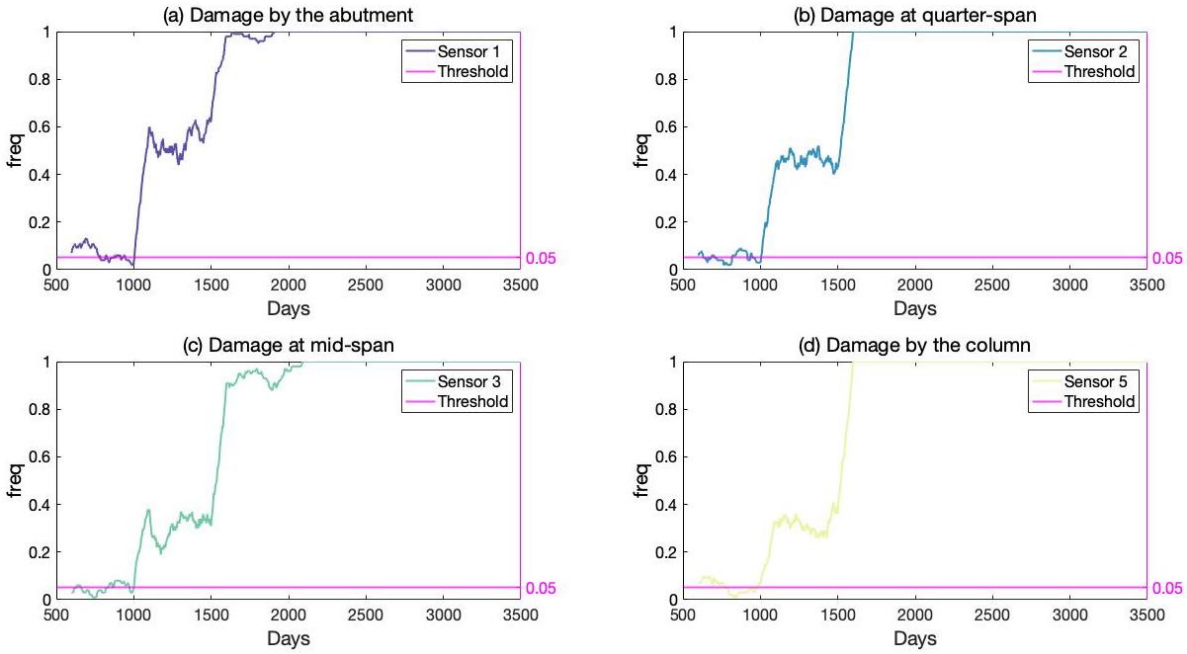

Figure 5.48: Frequency of exceedance by modal curvature from two modes. Varying damage locations with the closest sensor of each location respectively. 1 % noise and 5 % threshold.

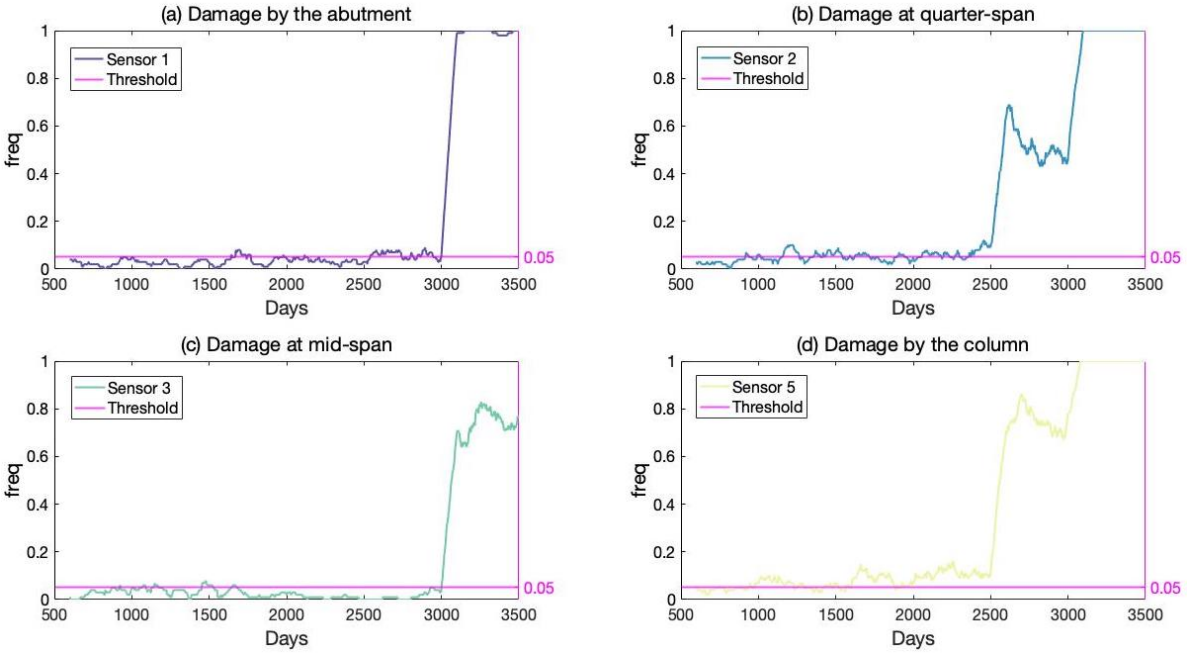

Figure 5.49: Frequency of exceedance by modal curvature from two modes. Varying damage locations with the closest sensor of each location respectively. 20 % noise and 5 % threshold.

The lowest noise level considered, 1 %, is used in the former Figure, illustrating that damage is immediately detected, that is at a level of 5 %, relatively frequently at all locations. For the latter, however, where the noise level is increased to 20 % which is the highest considered herein, the

detection is delayed to occur at 80 % damage by abutment and at mid-span, in Figures 5.49 (a) and (c). Interestingly, the frequency of exceedance is decreasing with increasing damage at mid-span up until day 3000. This does not happen for the lower noise level and is thus concluded to be an effect of noise. The *freq* parameter starts to increase at 50 % damage for damage at quarter-span and by the column, see subfigures (b) and (d).

Overall noise has a large impact on all the damage indicators. Increasing noise levels delays damage detection. Moreover, damage occurring at different locations are affected differently. An interesting finding is the increased damage localization ability of modal curvature and modal flexibility with increasing noise. Considering this, increased levels of noise may seem preferable for these indicators. Detection is however delayed - generally damage is not detectable until a bending stiffness reduction of 50 % is reached when the noise level is at 20 %. At noise levels of 5 % and 10 % the efficacy of the *freq* parameter becomes evident. Damage is clearly detectable from a level of 20 % and even 10 %. This is a lot more difficult to discern when considering the discrete data. The preferable combination of modes does not seem to be affected by noise.

5.3.4 Effect of Damage Location

Where the damage occurs in a structure has already been found to have an effect on damage detection and localization. In Figure 5.50 the probability of detection for modal curvature is presented with different levels of damage and at different damage locations.

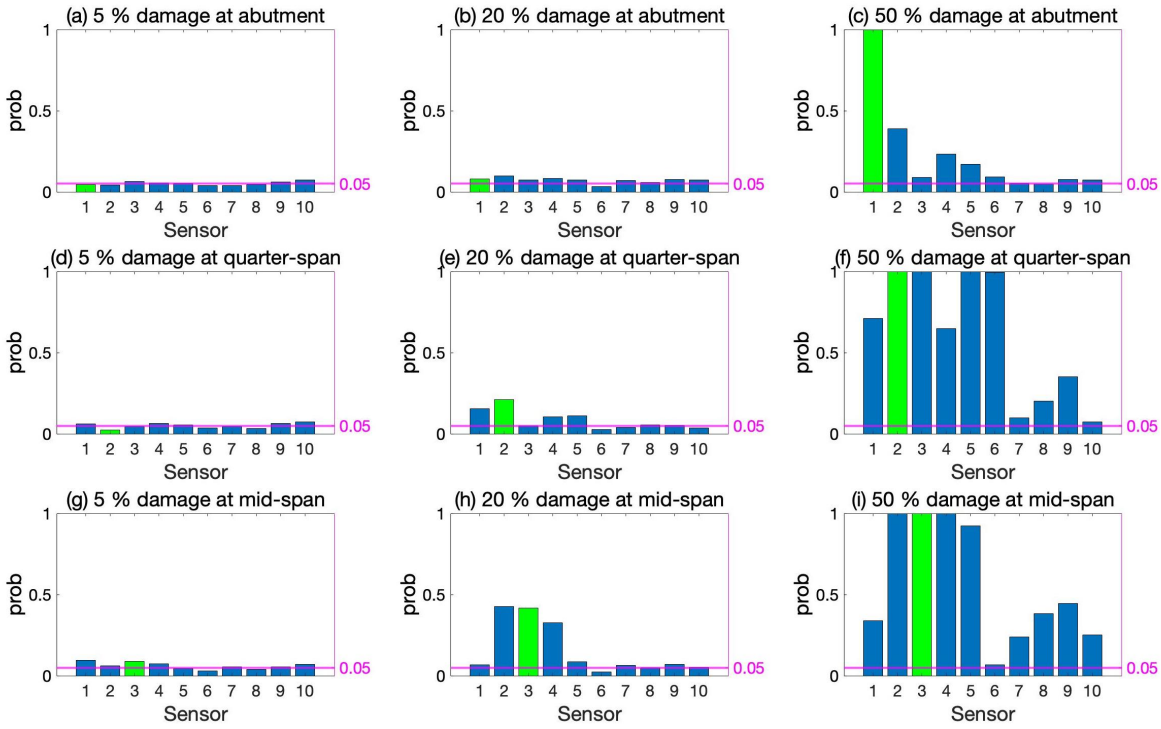

Figure 5.50: Probability of detection for modal curvature with different levels of damage and at different damage locations. A combination of two modes is utilized and the noise and threshold is at 5 %.

The frequency of exceedance for the same parameters is presented in Figure 5.51. The modal curvature has a probability of detecting damage less than 10 % when the damage level is 5 % at all the damage locations considered. The same occurs when the damage is increased to 10 %, although this

is not presented here. As damage increases to 20 %, the probability of detection is slightly increased when damage occurs at quarter-span and particularly at mid-span. The probability of detecting damage is higher when damage occurs at mid-span as compared to the other damage locations. When the damage is increased to 50 %. At the sensors corresponding to the damage locations, marked in green, the probability of detection is 100 %. This is also true for other sensors when damage occurs at quarter- and mid-span. The modal curvature can thus be said to perform poorly in damage localization although it is evident that the probability of detection is higher in the sensors in the left span of the bridge where the damage occurs. The location of the damage also seems to impact the ability of this damage indicator in localizing damage. When damage occurs by the abutment the localization of damage is better than when it occurs at quarter- or mid-span when two modes are used.

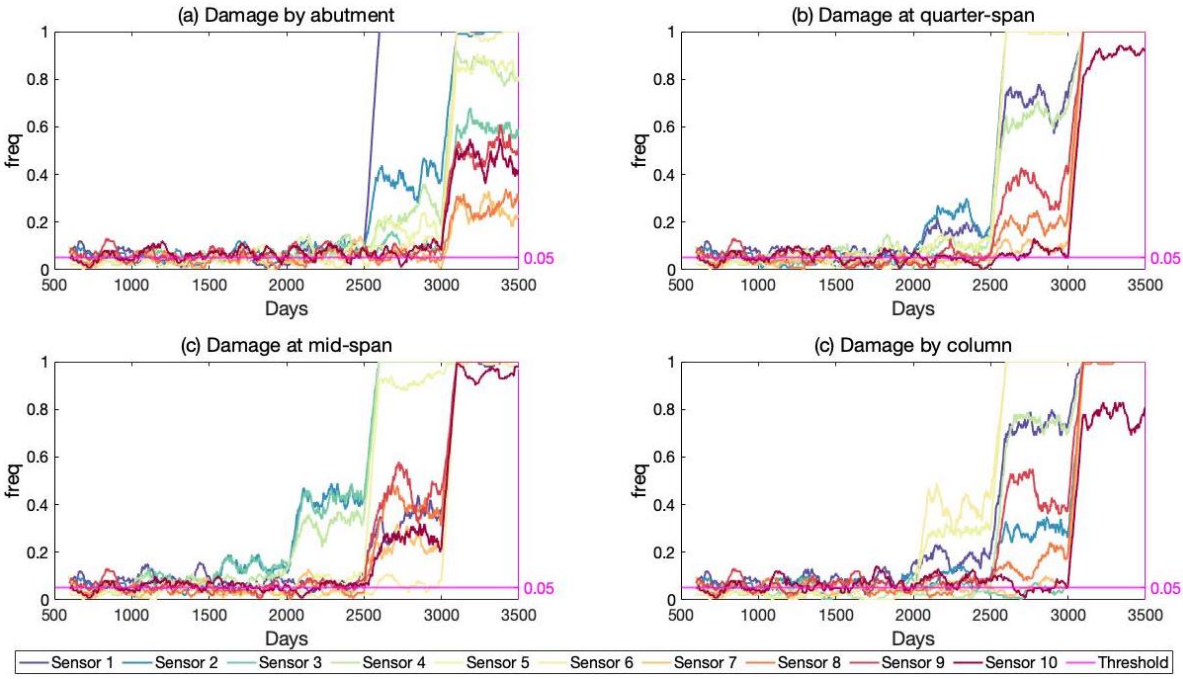

Figure 5.51: Frequency of exceedance using modal curvature with two modes for all damage locations, 5 % noise and 5 % threshold.

Comparing the probability and frequency of detection using modal curvature with a combination of two modes, a clear benefit can be seen using *freq* when damage occurs at quarter- and mid-span. Whereas the probability of detection at these damage locations is below 50 % for a damage level of 20 %, the frequency of detection at this damage level exceeds that of lower damage levels. With damage occurring at mid-span a 10 % damage level is also detectable. Using modal curvature it is clearly more difficult to detect damage occurring by the abutment, compared to the other damage locations.

Considering modal strain energy, presented in Figures 5.52 and 5.53, damage localization is significantly increased compared to modal curvature. The probability of detection remains poor when the damage level is at 5 %. The same can be said for 10 %, although this is not included in the probability plot. In the frequency plot however a damage level of 5 % is detectable when damage occurs both at quarter-span and by the column. 10 % is also detectable as damage occurs by the abutment and at mid-span. When the damage level is increased to 20 %, the probability of detection is increased to roughly 50 % for all damage locations. At this damage level modal strain energy outperforms modal curvature. Interestingly, the modal strain energy seems more sensitive to

damage when it occurs at quarter-span. When the damage level is increased to 50 % modal strain energy accurately predicts damage and location with 100 % confidence. The frequency of detection however, clearly indicate damage already at a level of 10 % for all damage locations.

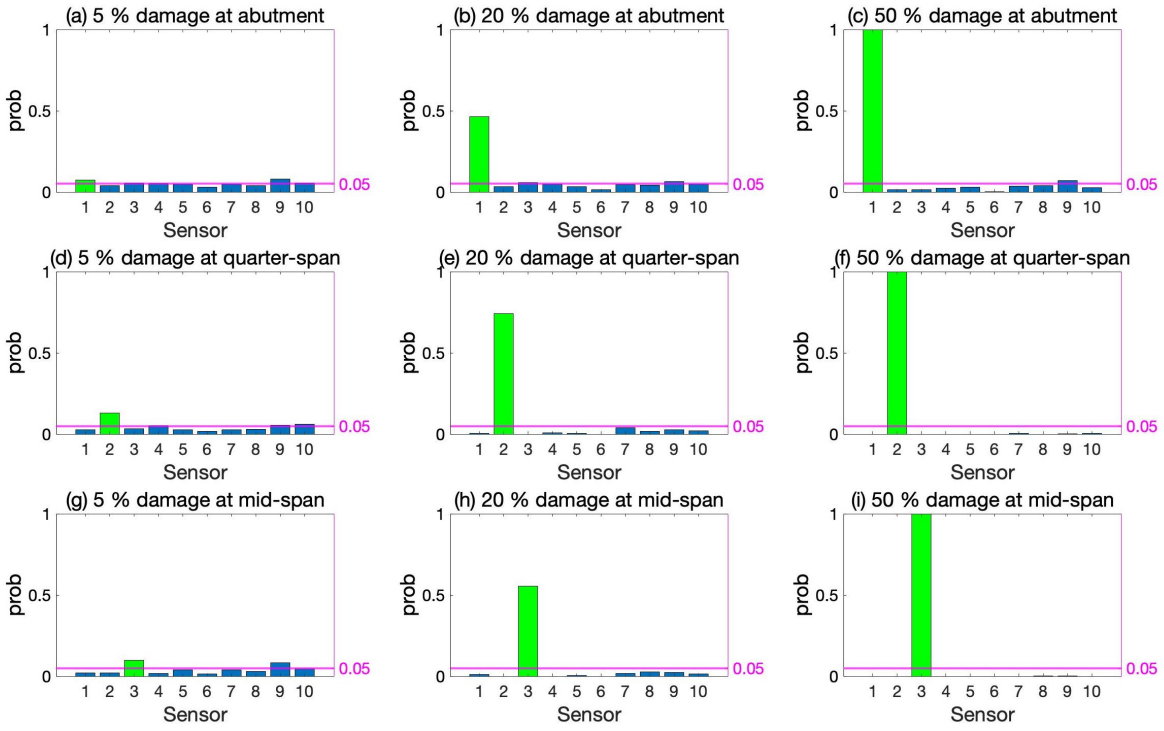

Figure 5.52: Probability of detection for modal strain energy with different levels of damage and at different damage locations. A combination of two modes is utilized and the noise and threshold is at 5 %.

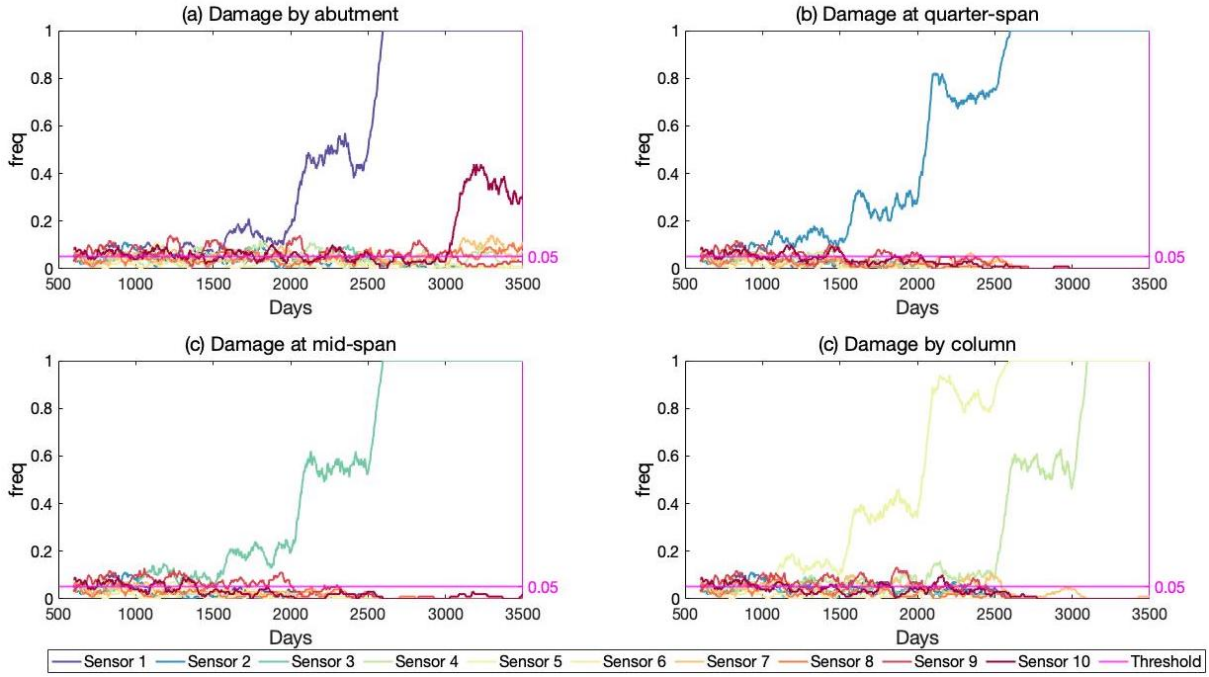

Figure 5.53: Frequency of exceedance using modal strain energy with two modes for all damage locations, 5 % noise and 5 % threshold.

Figure 5.54 presents the probability of detection for modal flexibility, and Figure 5.55 presents the frequency of detection for modal flexibility. The probability of detecting damage with this damage indicator is increased with 20 % damage as compared to the other damage indicators when damage occurs by quarter-span and at mid-span. The localization of damage however is distorted. The sensors associated with the damage locations, illustrated in green, interestingly have the least probability of detection. When damage occurs at the abutment the probability of detection at Sensor 1 is close to zero. The modal flexibility performs poorly when 20 % damage occurs at this location. The same can be said for the frequency of detection at this location. At the other damage locations however, frequency of exceedance also predicts damage at a damage level of 10 %. A damage level of 5 % is also detectable at mid-span and by the column. As the damage increases to 50 %, all sensors have a 100 % probability of detection when damage occurs at quarter- and mid-span. Localizing damage from these results is not feasible.

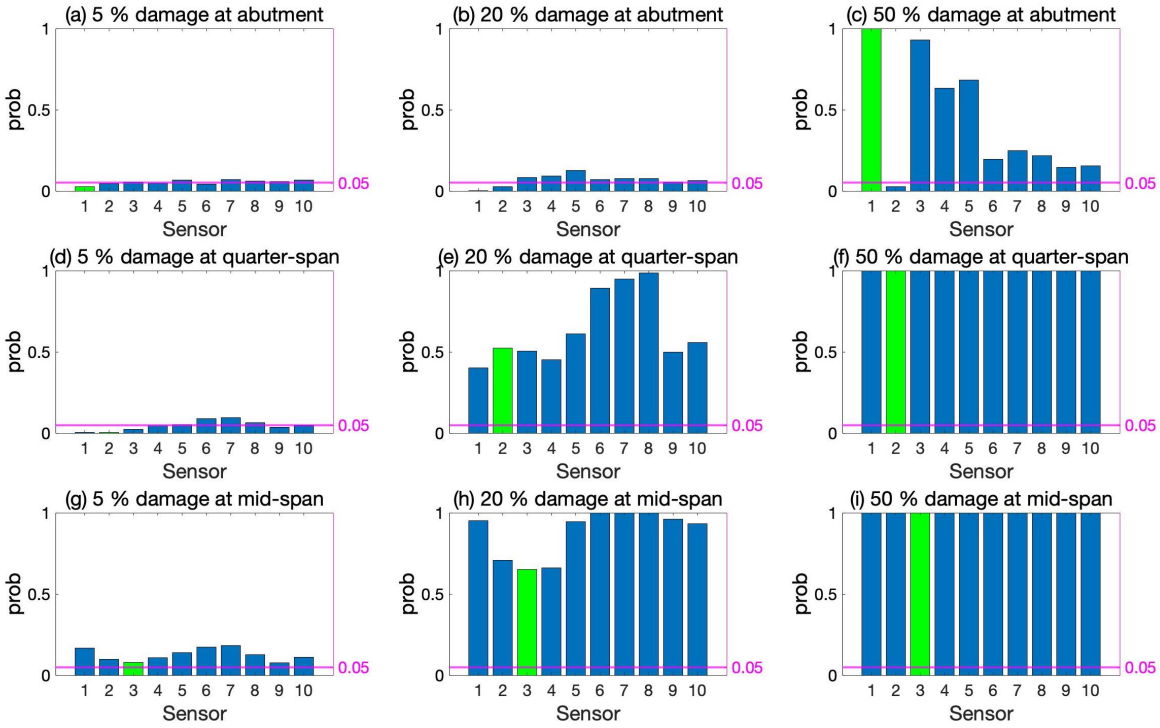

Figure 5.54: Probability of detection for modal flexibility with different levels of damage and at different damage locations. A combination of two modes is utilized and the noise and threshold is at 5 %.

All damage locations and a 5 % noise level is utilized by modal flexibility and illustrated in both Figure 5.55 and 5.56, though in the latter all sensors but the closest to the respective damage is removed. It may be concluded that the performance of modal flexibility is equally good as modal strain energy in detecting damage at mid-span and by the column at this noise level, as seen in Figures 5.56 (c) and (d) for modal flexibility and in Figures 5.53 (c) and (d). Damage is detected at 50 % and 20 % damage by the abutment and at quarter-span, repsectively, by the closest sensor to each location in Figures 5.56 (a) and (b). For the latter, it can be seen in Figure 5.55 (b) that damage is detected already at 20 % by several of the other sensors, which are further away from the damage. Interestingly, the *freq* parameter is decreasing in the closest sensor to damage when damage is located by the abutment or at quarter-span before it increases. So, localization is not feasible by this method for neither of the locations.

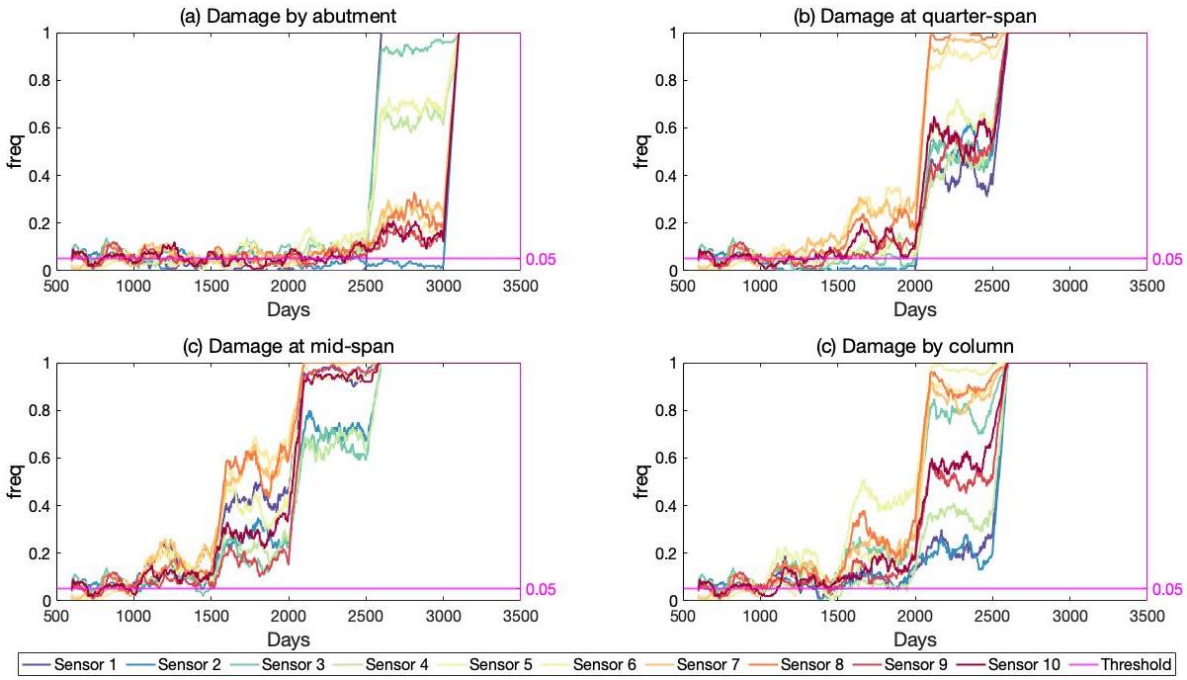

Figure 5.55: Frequency of exceedance using modal flexibility with two modes for all damage locations, 5 % noise and 5 % threshold.

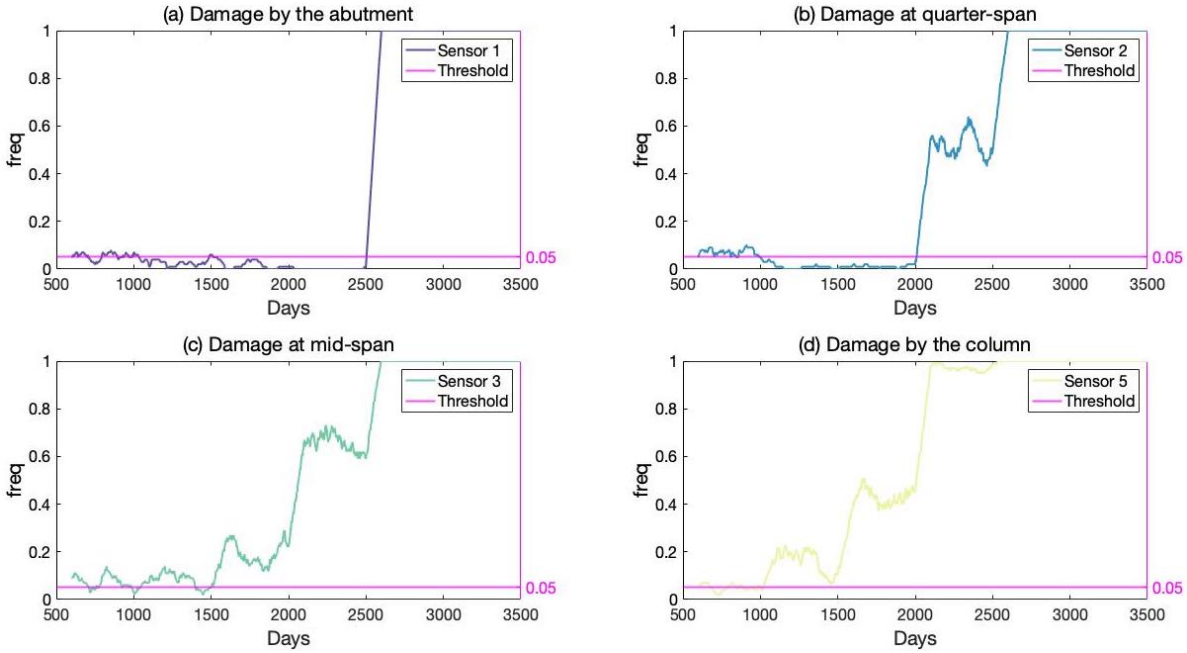

Figure 5.56: Frequency of exceedance by modal flexibility from two modes. Varying damage locations with the closest sensor of each location respectively. 5 % noise and 5 % threshold.

To summarize, the probability of detecting damage is increased with increasing damage for all the different damage indicators and all damage locations. For a damage level of both 5 % and 10 % all of the damage indicators can be said to fail in predicting damage when their discrete damage detection is evaluated. Considering frequency of detection on the other hand these damage levels are detectable using both modal strain energy and modal flexibility, dependent on the damage location; damage occurring by the abutment is more difficult to detect compared to the other locations for all of the damage indicators. Notably, these conclusions are drawn from results where a combination of two modes was utilized. Previously it was found that using three modes was preferable for detecting

damage by the abutment. Considering the preferable number of modes is therefore important.

5.3.5 Effect of Threshold Values

Noise has an effect on the training data which the thresholds are calculated from. If a threshold value corresponding to a low chance of false detection is selected, only a few erroneous observations may have a large effect on the threshold value. The impact of these errors will arguably be reduced if a higher threshold for false detection is selected. The threshold value of 2 % chance of false detection corresponds to the 11^{th} highest value of the damage indicator from the 500 reference days so that only 10 observations e.g. 2 % exceeds the threshold. For a 10 % chance of false detection, on the other hand, the 51^{st} highest valued damage indicator is established as threshold value. Therefore, there is a smaller chance that noise will impact a significant number of these observations leading to perhaps a more correct threshold value.

The frequency of which the damage indicator of modal curvature from Sensor 3 exceeds the 2 %, 5 % and 10 % threshold value is illustrated in Figures 5.57, 5.12 and 5.58, respectively. In subfigure (a) in all the mentioned figures the structure is undamaged. Here the development of the frequency of detection should averagely reflect the threshold line. This happens both for 5 % and 10 % thresholds, but the frequency rarely exceeds the 2 % threshold line. Accordingly the variance of the training data is greater than the remaining 500 days of data where the structure is also intact. Nevertheless the frequency of detection as damage is imposed is equally effective for all threshold values.

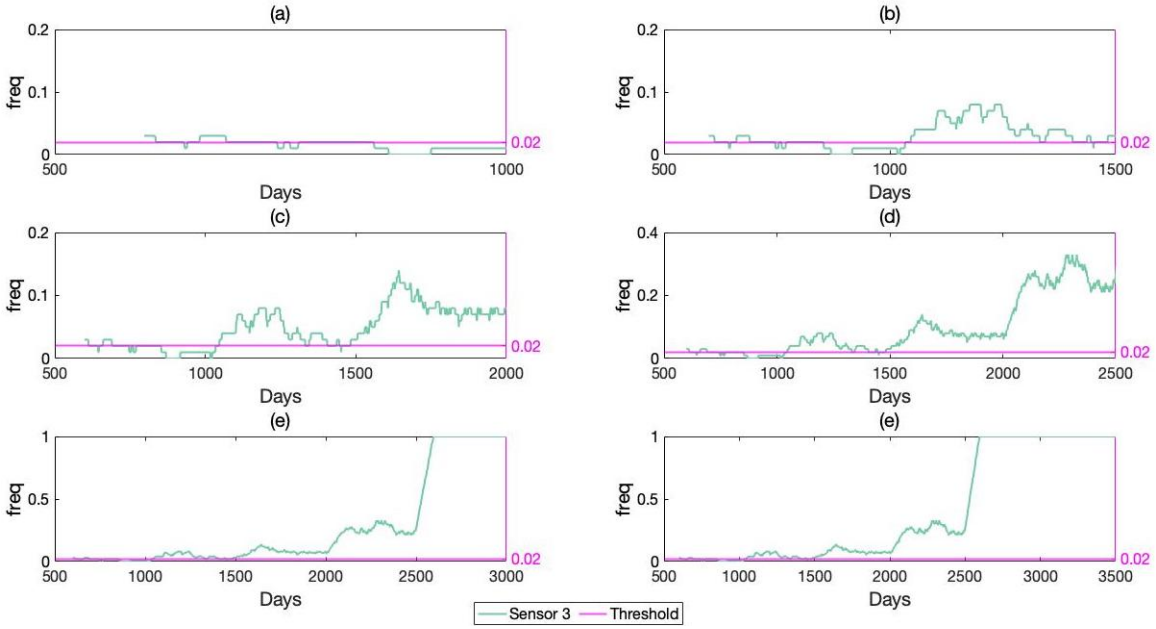

Figure 5.57: Development of damage by frequency of exceedance from Sensor 3 by modal curvature with two modes with increasing damage at mid-span, 5 % noise and 2 % threshold.

Furthermore, the threshold values are unique for each sensor, noise level and threshold level. The percentage of false detection determining the threshold values therefore has low impact on the detection and localization performance of all three methods discussed herein when presented by the *freq* parameter.

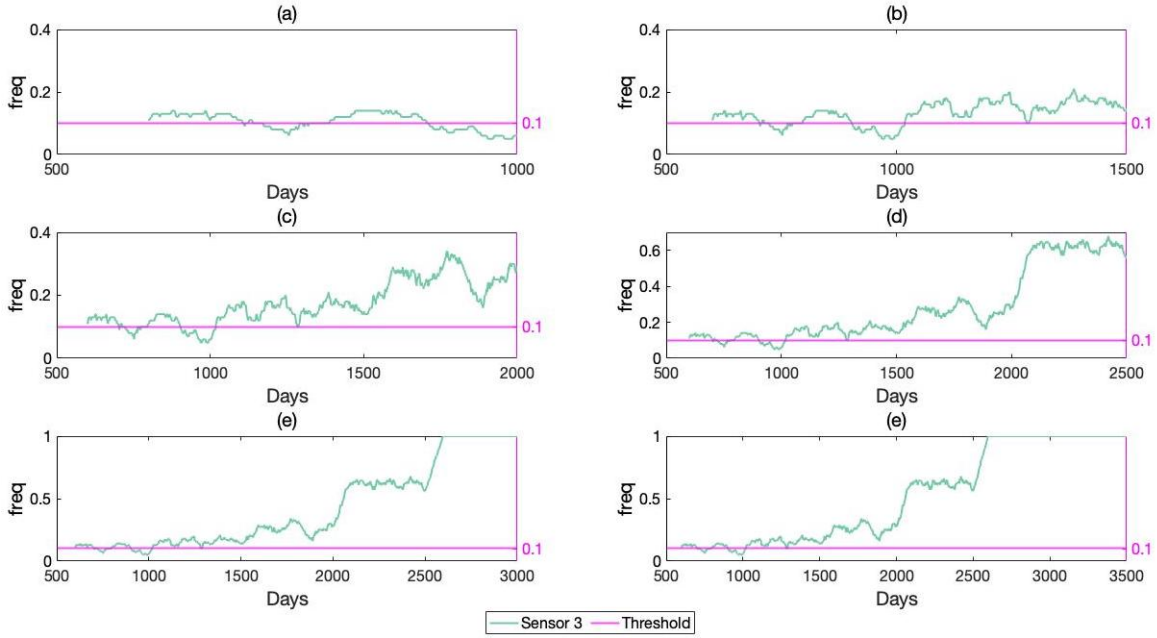

Figure 5.58: Development of damage by frequency of exceedance from Sensor 3 by modal curvature with two modes with increasing damage at mid-span, 5 % noise and 10 % threshold.

5.3.6 Comparison of Damage Indicators

The different damage indicators, namely modal curvature, modal strain energy and modal flexibility, perform very differently. Figure 5.59 presents the frequency of exceedance for the different indicators using only the first mode with a 5 % noise level and damage by the column.

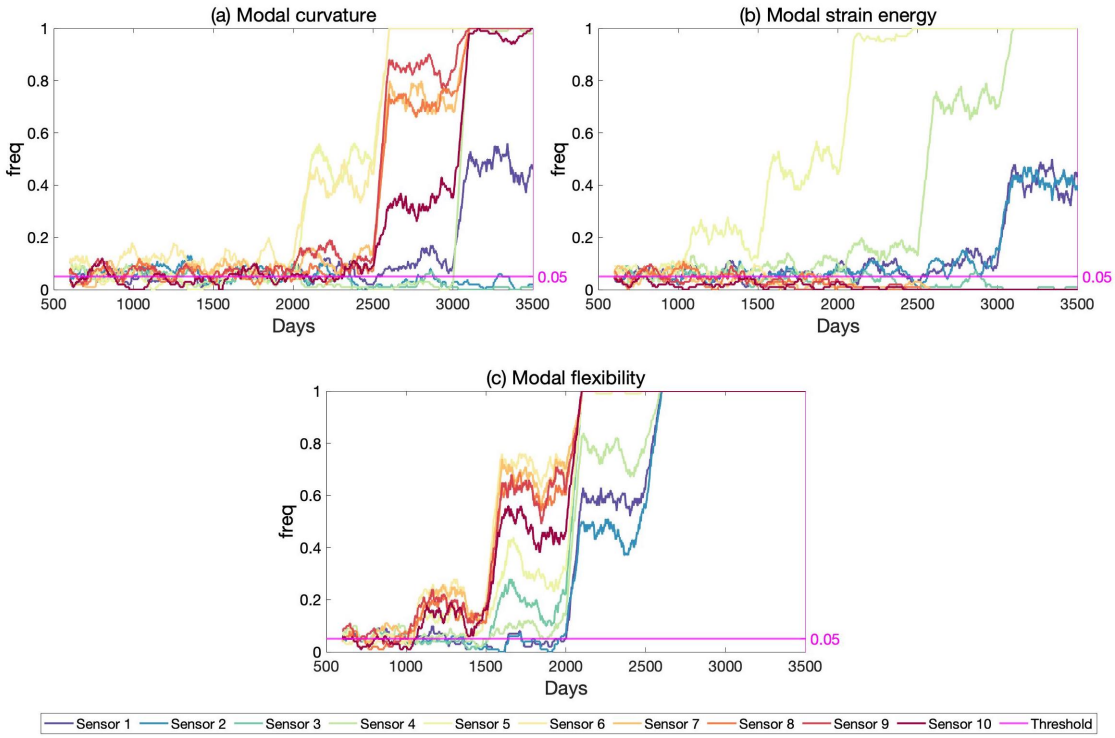

Figure 5.59: Frequency of exceedance for modal curvature, modal strain energy and modal flexibility with damage occurring by the column. The first mode and a noise level of 5 % is utilized.

Both modal strain energy and modal flexibility detect a 5 % damage level, with modal strain energy being exceedingly good in localizing the damage. Modal curvature however does not detect damage until the bending stiffness is reduced by 20 %. As the noise level is increased to 10 %, see Figure 5.60, modal flexibility still detects 5 % damage, whereas detection with modal strain energy is delayed to a 10 % damage level. The modal flexibility can thus be said to exceed the other methods in handling noise. Interestingly, the performance of modal curvature is increased at this noise level with damage being detected earlier than when a 5 % noise level is applied.

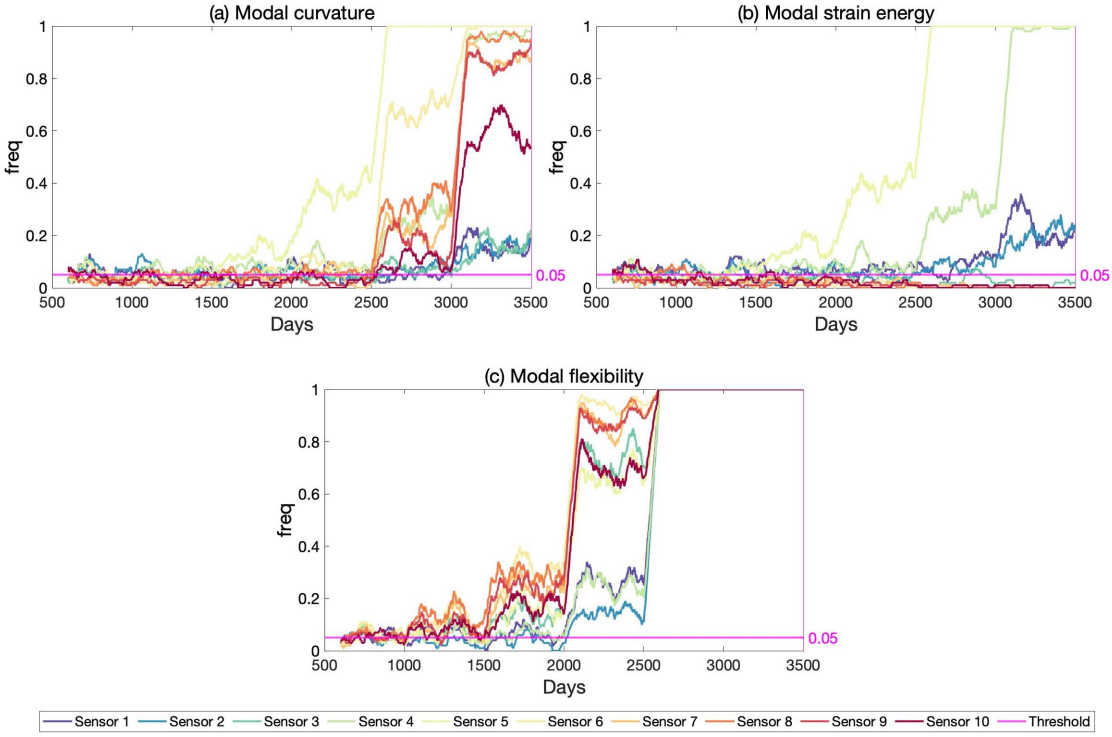

Figure 5.60: Frequency of exceedance for modal curvature, modal strain energy and modal flexibility with damage occurring by the column. The first mode and a noise level of 10 % is utilized.

The frequency of exceedance for a noise level of 20 % i presented in Figure 5.61 for the three same locations and damage indicators. Here as well the modal flexibility outperforms the other two damage indicators in terms of early detection, substantiating its sensitivity to damage. At this point localization is however even poorer than before – Sensor 10 which indicates damage at early levels is not associated with the damage location. Modal curvature and modal strain energy remain efficient in localization of damage.

When damage occurs at mid-span the same observations hold true, except the performance of modal curvature which is increased at a noise level of 5 %, see Figure 5.62. At 10 % noise the performance of modal curvature when damage occurs at mid-span is however decreased compared to when damage occurs by the column.

When damage is imposed at quarter-span, damage is detected earlier at 10 % noise than 5 % noise with modal curvature, similar to when damage occurs by the column. This can be observed in Figures 5.63 and 5.64. Notably results with damage occurring by the abutment deviate from the other locations when only the first mode is considered. Here, as previously discovered, using several modes improved damage detection. Considering the results where a combination of four modes was

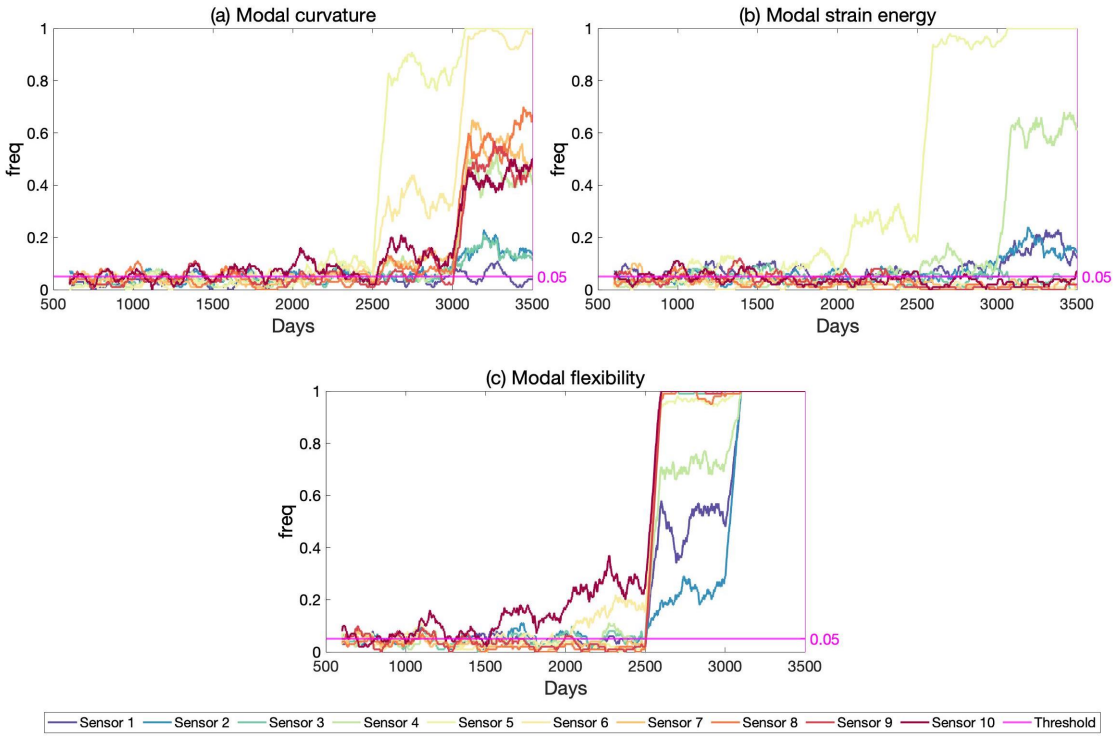

Figure 5.61: Frequency of exceedance for modal curvature, modal strain energy and modal flexibility with damage occurring by the column. The first mode and a noise level of 20 % is utilized.

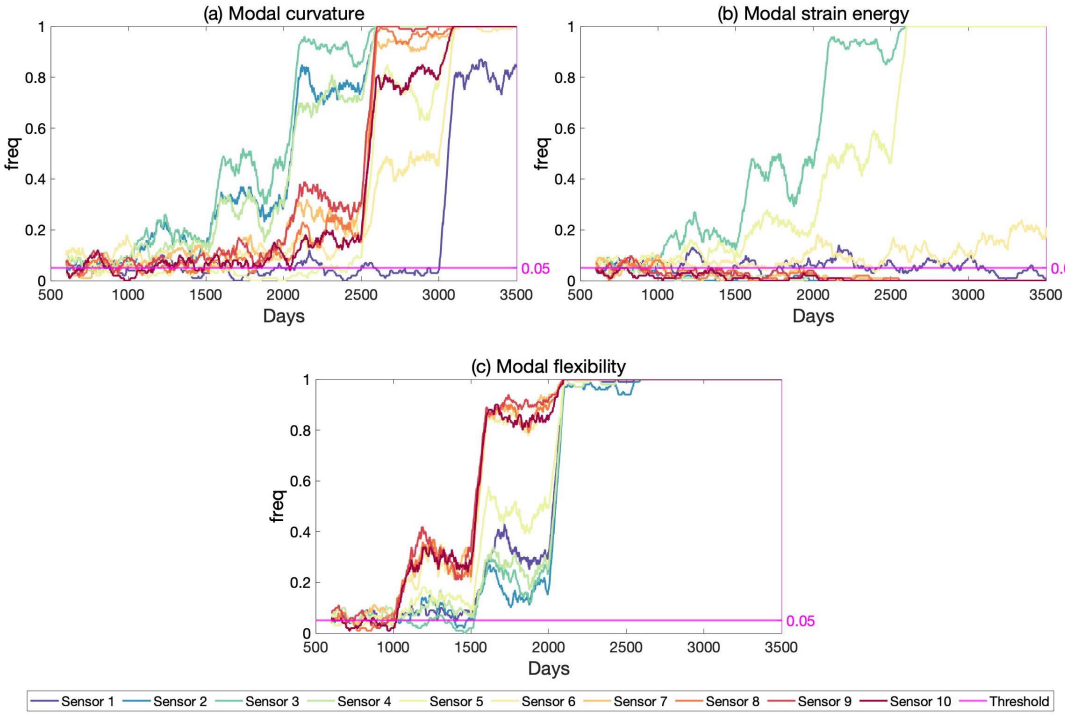

Figure 5.62: Frequency of exceedance for modal curvature, modal strain energy and modal flexibility with damage occurring at mid-span. The first mode and a noise level of 5 % is utilized.

utilized for the different indicators these still deviate from the results of the other locations. Damage detection is delayed at all noise levels for both modal curvature and modal flexibility, while the performance of modal strain energy remains equal to its performance when damage occurs elsewhere. Notably, localization is improved as noise increases for the modal flexibility with damage occurring by the abutment as previously demonstrated.

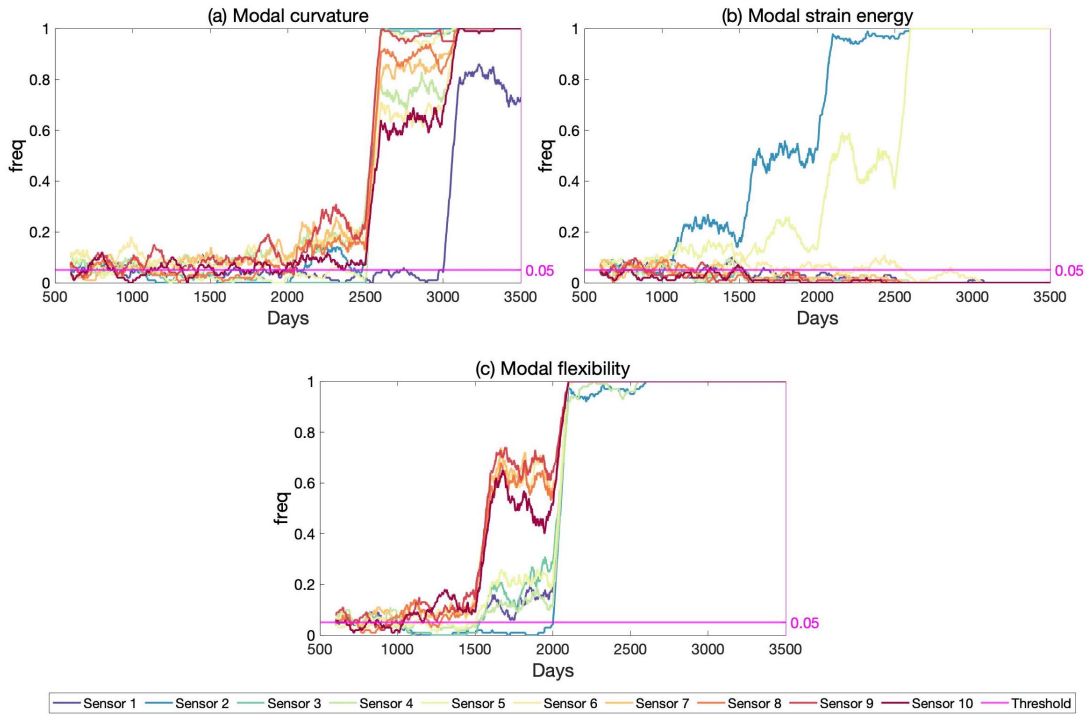

Figure 5.63: Frequency of exceedance for modal curvature, modal strain energy and modal flexibility with damage occurring at quarter-span. The first mode and a noise level of 5 % is utilized.

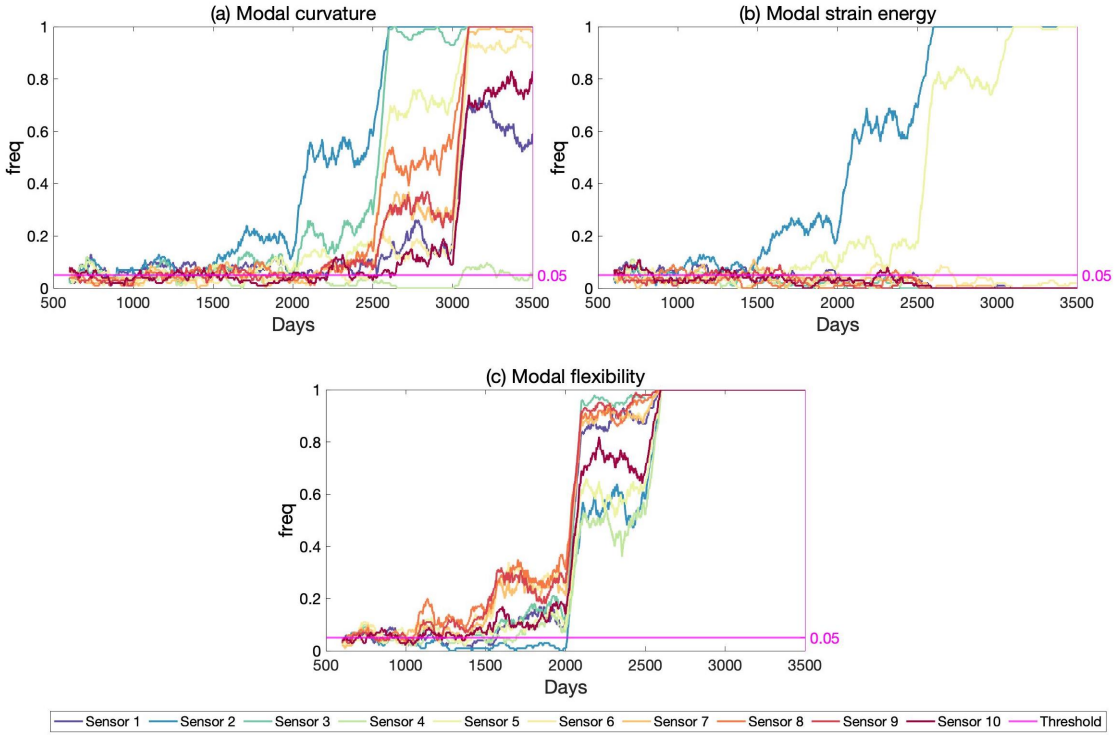

Figure 5.64: Frequency of exceedance for modal curvature, modal strain energy and modal flexibility with damage occurring at quarter-span. The first mode and a noise level of 10 % is utilized.

As was seen in Figure 5.40, the frequency of exceedance from modal strain energy based on two modes is reduced with increasing damage for all other sensors except Sensor 2, which is closest to this damage at quarter-span. The reason for this is previously illustrated in Figures 5.42 and 5.43

where the discrete damage indicators from Sensor 2 and 3, respectively, is scattered. The former presents an increasing damage indicator with increasing damage. For the latter however, which is further away from damage, the damage indicator is decreasing instead. This is reasonable as this damage indicator is based on calculating the fractional strain of sub-elements of the bridge divided by the total strain that the bridge undergoes as presented previously in Equation 3.23. As the bending stiffness of an element is decreased the strain is increased, leading to an increase in the total length and strain which the relatively constant strain of the undamaged sub-elements is divided by. This is a positive effect for localization of damage as it results in the frequency parameter creeping towards zero for all other locations than the damaged. This also occurs for other damage locations and combinations of modes, as the figures of the current subchapter presents, though damage may be detected by a few of the other sensors as well as the one closest to the respective damage location.

To summarize, both the modal strain energy and the modal flexibility demonstrate consistency in damage detection performance (as well as localization for modal strain energy) regardless of where damage occurs, although the sensitivity of modal flexibility is decreased when damage is imposed by the abutment. Modal flexibility does however portray the highest sensitivity to damage out of all the indicators, particularly as noise levels reach 10 % and 20 %. Even at 20 % noise it is able to detect a 10 % bending stiffness reduction, although localization is not feasible.

Chapter 6

Conclusions

The work presented herein was performed with the intent of investigating whether assessing different damage indicators for vibration-based damage detection in a long-term monitoring scheme can be an effective tool for damage identification in civil structures. This was done by simulating damage in a railway bridge modelled in a FEA software and varying several parameters to investigate their effect on the efficacy of damage detection and localization. The efficacy of the damage indicators is evaluated both discretely and with a proposed long-term framework, leading to the following conclusions:

- Noise present in the vibratory signals have an effect on the efficacy of all the different damage indicators. Increased levels of noise delays damage detection in all cases. Modal flexibility, showcasing high sensitivity to damage, is the least affected out of the three indicators evaluated. In some cases, localization is improved when modal curvature and modal flexibility is considered, as noise increases from 5 % to 10 %. Localization with modal strain energy is efficient regardless of noise.

- Where damage occurs is also demonstrated to impact the efficacy of the different indicators. When damage occurs by the abutment of the bridge, damage detection is delayed when considering modal flexibility compared to other locations and indicators. Moreover damage by the abutment is more easily detected when several modes are utilized; when damage occurs elsewhere using only the first mode is preferable. Moreover, where damage occurs impacts how the different mode shapes change. This is in some cases found to decrease the efficacy of damage localization.

- Which and how many modes are utilized in the calculations of the different damage indicators are found to have an effect on their efficacy. This is also found to be dependent on where damage occurs, but using only one lower mode is generally provides the most effective detection of damage. The development of the different mode shapes as damage increases is also considered important. Modes in which the displacements that is the mode shape increases or decreases consistently with increasing damage provide more reliable damage detection.

- Out of the three different damage indicators, namely modal curvature, strain energy and flexibility, it is found that modal strain energy provides the most effective approach. Whereas modal flexibility showcases high sensitivity to damage, localization is not feasible. Modal curvature is more effective in this manner, however it demonstrates high sensitivity to noise. Modal strain energy on the other hand demonstrates consistency in both detection and localization of damage regardless of its location.

- Applying the different damage indicators in a long-term monitoring scheme using the proposed *freq* parameter exceeds traditional approaches of discrete-time evaluation. Damage can more

confidently be detected at earlier stages as *freq* is able to demonstrate persistent detection over time. Reliability and consistency in damage detection is maintained at a higher level with the proposed long-term monitoring framework.

6.1 Recommendations for Further Work

Evaluating the efficacy of damage detection using modal curvature, modal strain energy and modal flexibility is an extensive task in this context, where several parameters are varied (e.g. noise levels, combinations of modes and more) over longer periods of time creating comprehensive sets of data. One recommendation for further work is to perform a multivariate analyses. In doing so the efficacy of the different damage indicators may be more thoroughly evaluated in terms of the varied parameters and their relations. Moreover, such an analysis may reveal a correlation between damage severity and the frequency of detection which could further improve the efficacy of the methods by allowing for quantification of damage.

Notably parameters of noise, damage level and damage location cannot be selected in real-life applications and such an analyses would solely be indicative of when damage detection is most effective in terms of these parameters and presumably for this individual structure. Nevertheless a generalized scheme for the performance of such an analysis may be utilized on any numerical model and can in such be a tool for increasing the effectiveness of evaluating the health of real-life structures.

The health of the structure investigated was mitigated by reducing the bending stiffness of certain elements at different locations of the bridge. Whether the conclusions drawn here can be transferred to damage which affects structural properties differently, as well as to different types of structures, would be beneficial to investigate in order for long-term vibration-based damage detection to be an attractive and feasible option for structural health monitoring.

Bibliography

[1] A. Rytter, "Vibration based inspection of civil engineering structures ph. d," *Aalborg University, Aalborg, Denmark*, 1993.

[2] E. P. Carden and P. Fanning, "Vibration based condition monitoring: a review," *Structural health monitoring*, vol. 3, no. 4, pp. 355–377, 2004.

[3] W. Fan and P. Qiao, "Vibration-based damage identification methods: a review and comparative study," *Structural health monitoring*, vol. 10, no. 1, pp. 83–111, 2011.

[4] D. Goyal and B. Pabla, "The vibration monitoring methods and signal processing techniques for structural health monitoring: a review," *Archives of Computational Methods in Engineering*, vol. 23, no. 4, pp. 585–594, 2016.

[5] X. Kong, C.-S. Cai, and J. Hu, "The state-of-the-art on framework of vibration-based structural damage identification for decision making," *Applied Sciences*, vol. 7, no. 5, p. 497, 2017.

[6] C.-P. Fritzen, M. Klinkov, and P. Kraemer, "Vibration-based damage diagnosis and monitoring of external loads," in *New Trends in Structural Health Monitoring*, pp. 149–208, Springer, 2013.

[7] G. W. Roberts, X. Meng, and A. H. Dodson, "Integrating a global positioning system and accelerometers to monitor the deflection of bridges," *Journal of Surveying Engineering*, vol. 130, no. 2, pp. 65–72, 2004.

[8] J. Barnes, C. Rizos, M. Kanli, A. Pahwa, D. Small, G. Voigt, N. Gambale, and J. Lamance, "High accuracy positioning using locata's next generation technology," in *Proceedings of the 18th International Technical Meeting of the Satellite Division of The Institute of Navigation (ION GNSS 2005)*, pp. 2049–2056, 2005.

[9] F. Moschas and S. Stiros, "Measurement of the dynamic displacements and of the modal frequencies of a short-span pedestrian bridge using gps and an accelerometer," *Engineering Structures*, vol. 33, no. 1, pp. 10–17, 2011.

[10] P. A. Psimoulis and S. C. Stiros, "Measuring deflections of a short-span railway bridge using a robotic total station," *Journal of Bridge engineering*, vol. 18, no. 2, pp. 182–185, 2013.

[11] C. R. Farrar, G. Park, D. W. Allen, and M. D. Todd, "Sensor network paradigms for structural health monitoring," *Structural Control and Health Monitoring: The Official Journal of the International Association for Structural Control and Monitoring and of the European Association for the Control of Structures*, vol. 13, no. 1, pp. 210–225, 2006.

[12] A. B. Noel, A. Abdaoui, T. Elfouly, M. H. Ahmed, A. Badawy, and M. S. Shehata, "Structural health monitoring using wireless sensor networks: A comprehensive survey," *IEEE Communications Surveys & Tutorials*, vol. 19, no. 3, pp. 1403–1423, 2017.

[13] C. R. Farrar and K. Worden, "An introduction to structural health monitoring," *Philosophical Transactions of the Royal Society A: Mathematical, Physical and Engineering Sciences*, vol. 365, no. 1851, pp. 303–315, 2007.

[14] E. Reynders, "System identification methods for (operational) modal analysis: review and comparison," *Archives of Computational Methods in Engineering*, vol. 19, no. 1, pp. 51–124, 2012.

[15] R. Brincker and C. Ventura, *Introduction to operational modal analysis*. John Wiley & Sons, 2015.

[16] R. Brincker, L. Zhang, and P. Andersen, "Modal identification from ambient responses using frequency domain decomposition," in *Proc. of the 18*'International Modal Analysis Conference (IMAC), San Antonio, Texas*, 2000.

[17] R. Brincker, C. Ventura, and P. Andersen, "Damping estimation by frequency domain decomposition," in *Proceedings of the 19th international modal analysis conference (IMAC)*, vol. 1, pp. 698–703, Orlando, FL, USA, 2001.

[18] L. Zhang, T. Wang, and Y. Tamura, "Frequency-spatial domain decomposition technique with application to operational modal analysis of civil engineering structures," in *Proc. of the 1st Internatıonal Operatıonal Modal Analysis Conference, Copenhagen*, 2005.

[19] L. Hermans, H. Van der Auweraer, and P. Guillaume, "A frequency-domain maximum likelihood approach for the extraction of modal parameters from output-only data," in *Proceedings of the 23rd International Conference on Noise and Vibration Engineering, ISMA*, pp. 963–972, 1998.

[20] P. Guillaume, P. Verboven, and S. Vanlanduit, "Frequency-domain maximum likelihood identification of modal parameters with confidence intervals," in *Proceedings of the international seminar on modal analysis*, vol. 1, pp. 359–366, Katholieke Universiteit Leuven, 1998.

[21] B. Peeters, H. Van der Auweraer, P. Guillaume, and J. Leuridan, "The polymax frequency-domain method: a new standard for modal parameter estimation?," *Shock and Vibration*, vol. 11, no. 3, 4, pp. 395–409, 2004.

[22] P. Cawley, "Structural health monitoring: Closing the gap between research and industrial deployment," *Structural Health Monitoring*, vol. 17, no. 5, pp. 1225–1244, 2018.

[23] C. R. Farrar, S. W. Doebling, and D. A. Nix, "Vibration–based structural damage identification," *Philosophical Transactions of the Royal Society of London. Series A: Mathematical, Physical and Engineering Sciences*, vol. 359, no. 1778, pp. 131–149, 2001.

[24] S. W. Doebling, C. R. Farrar, M. B. Prime, and D. W. Shevitz, "Damage identification and health monitoring of structural and mechanical systems from changes in their vibration characteristics: a literature review," tech. rep., Los Alamos National Lab., NM (United States), 1996.

[25] O. Salawu, "Detection of structural damage through changes in frequency: a review," *Engineering structures*, vol. 19, no. 9, pp. 718–723, 1997.

[26] C. Farrar and G. James Iii, "System identification from ambient vibration measurements on a bridge," *Journal of Sound and Vibration*, vol. 205, no. 1, pp. 1–18, 1997.

[27] T. Wolff and M. Richardson, "Fault detection in structures from changes in their modal parameters," in *Proceedings of the 7th international modal analysis conference*, vol. 1, pp. 87–94, 1989.

[28] L. M. Khoo, P. R. Mantena, and P. Jadhav, "Structural damage assessment using vibration modal analysis," *Structural Health Monitoring*, vol. 3, no. 2, pp. 177–194, 2004.

[29] A. Pandey, M. Biswas, and M. Samman, "Damage detection from changes in curvature mode shapes," *Journal of Sound and Vibration*, vol. 145, no. 2, pp. 321–332, 1991.

[30] M. A. Wahab and G. De Roeck, "Damage detection in bridges using modal curvatures: application to a real damage scenario," *Journal of Sound and Vibration*, vol. 226, no. 2, pp. 217–235, 1999.

[31] C. P. Ratcliffe, "A frequency and curvature based experimental method for locating damage in structures," *Journal of Vibration and Acoustics*, vol. 122, no. 3, pp. 324–329, 2000.

[32] J. Chance, G. Tomlinson, and K. Worden, "A simplified approach to the numerical and experimental modelling of the dynamics of a cracked beam," in *Proceedings - SPIE the International Society for Optical Engineering*, pp. 778–778, Citeseer, 1994.

[33] M. P. Limongelli and P. F. Giordano, "Vibration-based damage indicators: a comparison based on information entropy," *Journal of Civil Structural Health Monitoring*, pp. 1–16, 2020.

[34] E. Sazonov and P. Klinkhachorn, "Optimal spatial sampling interval for damage detection by curvature or strain energy mode shapes," *Journal of Sound and Vibration*, vol. 285, no. 4-5, pp. 783–801, 2005.

[35] J. J. Moughty and J. R. Casas, "A state of the art review of modal-based damage detection in bridges: Development, challenges, and solutions," *Applied Sciences*, vol. 7, no. 5, p. 510, 2017.

[36] W. Fan and P. Qiao, "A strain energy-based damage severity correction factor method for damage identification in plate-type structures," *Mechanical Systems and Signal Processing*, vol. 28, pp. 660–678, 2012.

[37] D. Dessi and G. Camerlengo, "Damage identification techniques via modal curvature analysis: overview and comparison," *Mechanical Systems and Signal Processing*, vol. 52, pp. 181–205, 2015.

[38] N. Stubbs, J. Kim, and K. Topole, "An efficient and robust algorithm for damage localization in offshore platforms," in *Proceedings of the ASCE 10th structures congress*, vol. 1, pp. 543–546, 1992.

[39] Z. Shi, S. Law, and L. Zhang, "Structural damage localization from modal strain energy change," *Journal of Sound and Vibration*, vol. 218, no. 5, pp. 825–844, 1998.

[40] S. Law, Z. Shi, and L. Zhang, "Structural damage detection from incomplete and noisy modal test data," *Journal of Engineering Mechanics*, vol. 124, no. 11, pp. 1280–1288, 1998.

[41] H. Guan and V. M. Karbhari, "Improved damage detection method based on element modal strain damage index using sparse measurement," *Journal of Sound and Vibration*, vol. 309, no. 3-5, pp. 465–494, 2008.

[42] S. W. Doebling, C. R. Farrar, M. B. Prime, *et al.*, "A summary review of vibration-based damage identification methods," *Shock and vibration digest*, vol. 30, no. 2, pp. 91–105, 1998.

[43] V. Dawari and G. Vesmawala, "Modal curvature and modal flexibility methods for honeycomb damage identification in reinforced concrete beams," *Procedia Engineering*, vol. 51, pp. 119–124, 2013.

[44] S. W. Doebling, C. R. Farrar, M. Prime, and D. Shevitz, "A review of damage identification methods that examine changes in dynamic properties," *Shock and Vibration Digest*, vol. 30, no. 2, pp. 91–105, 1998.

[45] A. Aktan, K. Lee, C. Chuntavan, and T. Aksel, "Modal testing for structural identification and condition assessment of constructed facilities," in *Proceedings - SPIE the International Society for Optical Engineering*, pp. 462–462, The International Society for Optics and Photonics, 1994.

[46] A. Pandey and M. Biswas, "Damage detection in structures using changes in flexibility," *Journal of Sound and Vibration*, vol. 169, no. 1, pp. 3–17, 1994.

[47] A. Pandey and M. Biswas, "Damage diagnosis of truss structures by estimation of flexibility change," *Modal Analysis: The International Journal of Analytical and Experimental Modal Analysis*, vol. 10, no. 2, pp. 104–117, 1995.

[48] T. Toksoy and A. Aktan, "Bridge-condition assessment by modal flexibility," *Experimental Mechanics*, vol. 34, no. 3, pp. 271–278, 1994.

[49] S. W. Doebling, *Measurement of structural flexibility matrices for experiments with incomplete reciprocity*. PhD thesis, University of Colorado, 1995.

[50] S. W. Doebling, L. D. Peterson, and K. F. Alvin, "Estimation of reciprocal residual flexibility from experimental modal data," *AIAA journal*, vol. 34, no. 8, pp. 1678–1685, 1996.

[51] T. W. Lim, "Submatrix approach to stiffness matrix correction using modal test data," *AIAA journal*, vol. 28, no. 6, pp. 1123–1130, 1990.

[52] T. W. Lim, "Structural damage detection using modal test data," *AIAA journal*, vol. 29, no. 12, pp. 2271–2274, 1991.

[53] H. Gysin, "Critical application of an error matrix method for location of finite element modeling inaccuracies," in *Proc. of the 4th International Modal Analysis Conference*, pp. 1339–1351, 1986.

[54] Y. Park, "Weighted-error-matrix application to detect stiffness damage by dynamic characteristics measurement," *Journal of Modal Analysis*, vol. 6, no. 2, pp. 101–107, 1988.

[55] O. Salawu and C. Williams, "Structural damage detection using experimental modal analysis a comparison of some methods," in *Proceedings of the International Modal Analysis Conference*, pp. 254–254, Society for Experimental Mechanics, 1993.

[56] L. Peterson, K. Alvin, S. Doebling, and K. Park, "Damage detection using experimentally measured mass and stiffness matrices," tech. rep., A1AA-93-1482-CP, 1993.

[57] I. Newman, "A conceptualization of mixed methods: A need for inductive/deductive approach to conducting research.," 2000.

[58] B. K. Hayes, R. G. Stephens, J. Ngo, and J. C. Dunn, "The dimensionality of reasoning: Inductive and deductive inference can be explained by a single process.," *Journal of Experimental Psychology: Learning, Memory, and Cognition*, vol. 44, no. 9, p. 1333, 2018.

[59] W. M. Trochim and J. P. Donnelly, "Research methods knowledge base," 2001.

[60] M. L. Smith, "Naturalistic research," *The Personnel and Guidance Journal*, vol. 59, no. 9, pp. 585–589, 1981.

[61] R. M. Thomas, *Blending qualitative and quantitative research methods in theses and dissertations*. Corwin Press, 2003.

[62] M. Hennink, I. Hutter, and A. Bailey, *Qualitative research methods*. SAGE Publications Limited, 2020.

[63] H. R. Bernard and H. R. Bernard, *Social research methods: Qualitative and quantitative approaches*. Sage, 2013.

[64] J. Maxwell, "Understanding and validity in qualitative research," *Harvard educational review*, vol. 62, no. 3, pp. 279–301, 1992.

[65] R. Adcock and D. Collier, "Measurement validity: A shared standard for qualitative and quantitative research," *American political science review*, pp. 529–546, 2001.

[66] A. J. Onwuegbuzie, "Expanding the framework of internal and external validity in quantitative research.," 2000.

[67] G. Guest, K. M. MacQueen, and E. E. Namey, "Validity and reliability (credibility and dependability) in qualitative research and data analysis," *Applied thematic analysis. London: Sage Publications*, pp. 79–106, 2012.

[68] A. Smaling, "Varieties of methodological intersubjectivity—the relations with qualitative and quantitative research, and with objectivity," *Quality and Quantity*, vol. 26, no. 2, pp. 169–180, 1992.

[69] S. J. Lee, "Quantitative versus qualitative research methods—two approaches to organisation studies," *Asia Pacific Journal of Management*, vol. 9, no. 1, pp. 87–94, 1992.

[70] L. Leung, "Validity, reliability, and generalizability in qualitative research," *Journal of family medicine and primary care*, vol. 4, no. 3, pp. 324–327, 2015.

[71] A. S. Lee and R. L. Baskerville, "Conceptualizing generalizability: New contributions and a reply," *MIS quarterly*, pp. 749–761, 2012.

[72] Z.-F. Fu and J. He, *Modal analysis*. Elsevier, 2001.

[73] S. Adhikari, *Damping models for structural vibration*. PhD thesis, Citeseer, 2001.

[74] A. K. Chopra *et al.*, *Dynamics of structures*, p. 455. Pearson Education Upper Saddle River, NJ, 2012.

[75] A. Alipour and F. Zareian, "Study rayleigh damping in structures; uncertainties and treatments," in *Proceedings of 14th World Conference on Earthquake Engineering, Beijing, China*, pp. 1–8, 2008.

[76] A. K. Chopra *et al.*, *Dynamics of structures*, p. 457. Pearson Education Upper Saddle River, NJ, 2012.

[77] J. Brownjohn, F. Magalhaes, E. Caetano, and A. Cunha, "Ambient vibration re-testing and operational modal analysis of the humber bridge," *Engineering Structures*, vol. 32, no. 8, pp. 2003–2018, 2010.

[78] B. Peeters and G. De Roeck, "One-year monitoring of the z24-bridge: environmental effects versus damage events," *Earthquake engineering & structural dynamics*, vol. 30, no. 2, pp. 149–171, 2001.

[79] P. Van Overschee and B. De Moor, *Subspace identification for linear systems: Theory—Implementation—Applications*. Springer Science & Business Media, 1996.

[80] B. Peeters and G. De Roeck, "Stochastic system identification for operational modal analysis: a review," *J. Dyn. Sys., Meas., Control*, vol. 123, no. 4, pp. 659–667, 2001.

[81] Y. Xie, P. Liu, and G.-P. Cai, "Modal parameter identification of flexible spacecraft using the covariance-driven stochastic subspace identification (ssi-cov) method," *Acta Mechanica Sinica*, vol. 32, no. 4, pp. 710–719, 2016.

[82] A. Otto, "Ooma toolbox." https://www.mathworks.com/matlabcentral/fileexchange/68657-ooma-toolbox. Accessed: 25.01.2021.

[83] K. A. Kvåle, O. Øiseth, and A. Rønnquist, "Operational modal analysis of an end-supported pontoon bridge," *Engineering Structures*, vol. 148, pp. 410–423, 2017.

[84] S. Li, J.-T. Wang, A.-Y. Jin, and G.-H. Luo, "Parametric analysis of ssi algorithm in modal identification of high arch dams," *Soil Dynamics and Earthquake Engineering*, vol. 129, p. 105929, 2020.

[85] L. Hermans and H. Van der Auweraer, "Modal testing and analysis of structures under operational conditions: industrial applications," *Mechanical systems and signal processing*, vol. 13, no. 2, pp. 193–216, 1999.

[86] E. Reynders, J. Houbrechts, and G. De Roeck, "Fully automated (operational) modal analysis," *Mechanical Systems and Signal Processing*, vol. 29, pp. 228–250, 2012.

[87] H. Van der Auweraer and B. Peeters, "Discriminating physical poles from mathematical poles in high order systems: use and automation of the stabilization diagram," in *Proceedings of the 21st IEEE Instrumentation and Measurement Technology Conference (IEEE Cat. No. 04CH37510)*, vol. 3, pp. 2193–2198, IEEE, 2004.

[88] C. R. Farrar and D. A. Jauregui, "Comparative study of damage identification algorithms applied to a bridge: I. experiment," *Smart materials and structures*, vol. 7, no. 5, pp. 704–719, 1998.

[89] V. Dawari and G. Vesmawala, "Structural damage identification using modal curvature differences," *IOSR J Mech Civ Eng*, vol. 4, pp. 33–38, 2013.

[90] A. Alvandi and C. Cremona, "Assessment of vibration-based damage identification techniques," *Journal of sound and vibration*, vol. 292, no. 1-2, pp. 179–202, 2006.

[91] Z. Shi, S. Law, and L. Zhang, "Structural damage detection from modal strain energy change," *Journal of engineering mechanics*, vol. 126, no. 12, pp. 1216–1223, 2000.

[92] A. C. Altunışık, F. Y. Okur, S. Karaca, and V. Kahya, "Vibration-based damage detection in beam structures with multiple cracks: modal curvature vs. modal flexibility methods," *Nondestructive Testing and Evaluation*, vol. 34, no. 1, pp. 33–53, 2019.

[93] S. Quqa, L. Landi, and P. P. Diotallevi, "On the use of singular vectors for the flexibility-based damage detection under the assumption of unknown structural masses," *Shock and Vibration*, vol. 2018, 2018.

[94] Y. Ni, H. Zhou, K. Chan, and J. Ko, "Modal flexibility analysis of cable-stayed ting kau bridge for damage identification," *Computer-Aided Civil and Infrastructure Engineering*, vol. 23, no. 3, pp. 223–236, 2008.

List of Appendices

A – Script for application of SSI-Cov and extraction of mode shapes and natural frequencies.

B – Script for interpolation of mode shapes and curvature calculation.

C – Script for sorting calculated curvatures with increasing damage for different noise levels.

D – Script for calculating modal curvature damage indicator, frequency of exceedance and threshold values.

E – Script for calculating modal strain energy damage indicator, frequency of exceedance and threshold values.

F – Script for calculating modal flexibility damage indicator.

G – Script for calculating threshold values and frequency of exceedance for modal flexibility damage indicator.

Appendix A

```
clc
clear all
close all

%Declare input vars
iChannels = 10; %no of sensors
iNoiseInstances = 500; %no of species in noise population
dBeta = [0.005,0.01,0.05,0.1,0.2]; %noise levels

%Files for undamaged structure:
%strInFiles = ["UD","UD_Ref"]

%Files for damage by the abutment:
strInFiles = ["abutment_I30.95","abutment_I30.9","abutment_I30.8","abutment_I30.5","↙
abutment_I30.2"];

%Files for damage at quarter-span:
% strInFiles = ["quarter_I30.95","quarter_I30.9","quarter_I30.8","quarter_I30.5","↙
quarter_I30.2"];

%Files for damage at mid-span:
% strInFiles = ["middle_I30.95","middle_I30.9","middle_I30.8","middle_I30.5","middle_I30.↙
2"];

%Files for damage by the column:
% strInFiles = ["column_I30.95","column_I30.9","column_I30.8","column_I30.5","column_I30.↙
2"];

%Cells to store variables from SSI
dBetaFileResult =cell(iNoiseInstances,1); %cell to save the 500 noisy acceleration data
A_cov_500 = cell(iNoiseInstances,1);
C_cov_500 = cell(iNoiseInstances,1);
IDs_cov_500 = cell(iNoiseInstances,1);
fn_cov_500 = cell(iNoiseInstances,1);
zeta_cov_500 = cell(iNoiseInstances,1);
Phi_cov_500 = cell(iNoiseInstances,1);
fn_cov_500_res = cell(iNoiseInstances,1);
Phi_cov_500_res = cell(iNoiseInstances,1);
Phi_cov_500_norm = cell(iNoiseInstances,1);
Ref_Phi = cell(1,1);
Ref_Phi_norm = cell(1,1);
Max = cell(iNoiseInstances,1);
D1 = cell(iNoiseInstances,1);
D2 = cell(iNoiseInstances,1);
D3 = cell(iNoiseInstances,1);
D4 = cell(iNoiseInstances,1);
S1 = cell(iNoiseInstances,1);
S2 = cell(iNoiseInstances,1);
S3 = cell(iNoiseInstances,1);
S4 = cell(iNoiseInstances,1);

err = [0.01,0.05,0.98];

%sensor locations
SL = readmatrix('Sensor_locations_norddalsbrua.xlsx');
SL12 = SL(1:12,4);
%add sensor locations to the modes that will be stored as final results.
```

```
mode1 = zeros(12,501);
mode1(:,1) = SL12;
mode2 = zeros(12,501);
mode2(:,1) = SL12;
mode3 = zeros(12,501);
mode3(:,1) = SL12;
mode4 = zeros(12,501);
mode4(:,1) = SL12;

order = 80; %desired maximum model order to identify
s = 2*order; %number of rows in the block hankel matrix
fs = 200; %sampling frequency of acceleration signal
T = 1/fs; %period of acceleration signal

for i = 1:size(strInFiles,2) %Loop to load acc file and

    curFile = append(strInFiles(1,i),".txt");
    Y = readmatrix(curFile);
    Y(1:1600,:)=[]; %Remove forced vibration response from signal
    Y = transpose(Y(1:8401,2:11));

    %Frequency ranges for extracting four modes from the first solution of
    %each ii iteration

% Frequencies for the undamaged structure:
%     f1low = 2.686;
%     f1high = 2.691;
%     f2low = 3.571;
%     f2high = 3.576;
%     f3low = 6.761;
%     f3high = 6.766;
%     f4low = 10.130;
%     f4high = 10.137;

% Frequencies for damage by the abutment:
    if curFile == ("abutment_I30.95.txt")
    f1low = 2.686;
    f1high = 2.691;
    f2low = 3.570;
    f2high = 3.575;
    f3low = 6.746;
    f3high = 6.751;
    f4low = 10.130;
    f4high = 10.135;
    elseif curFile == ("abutment_I30.9.txt")
    f1low = 2.686;
    f1high = 2.691;
    f2low = 3.569;
    f2high = 3.574;
    f3low = 6.730;
    f3high = 6.735;
    f4low = 10.130;
    f4high = 10.135;
    elseif curFile == ("abutment_I30.8.txt")
    f1low = 2.685;
    f1high = 2.690;
    f2low = 3.567;
    f2high = 3.572;
```

```
    f3low = 6.692;
    f3high = 6.696;
    f4low = 10.125;
    f4high = 10.130;
    elseif curFile == ("abutment_I30.5.txt")
    f1low = 2.682;
    f1high = 2.687;
    f2low = 3.557;
    f2high = 3.562;
    f3low = 6.516;
    f3high = 6.521;
    f4low = 10.108;
    f4high = 10.113;
    elseif curFile == ("abutment_I30.2.txt")
    f1low = 2.670;
    f1high = 2.675;
    f2low = 3.513;
    f2high = 3.517;
    f3low = 5.90;
    f3high = 5.93;
    f4low = 10.05;
    f4high = 10.08;
    end

% Frequencies for damage at quarter-span
%     if curFile == ("quarter_I30.95.txt")
%     f1low = 2.684;
%     f1high = 2.689;
%     f2low = 3.569;
%     f2high = 3.574;
%     f3low = 6.757;
%     f3high = 6.762;
%     f4low = 10.125;
%     f4high = 10.130;
%     elseif curFile == ("quarter_I30.9.txt")
%     f1low = 2.682;
%     f1high = 2.687;
%     f2low = 3.567;
%     f2high = 3.572;
%     f3low = 6.753;
%     f3high = 6.758;
%     f4low = 10.119;
%     f4high = 10.123;
%     elseif curFile == ("quarter_I30.8.txt")
%     f1low = 2.676;
%     f1high = 2.681;
%     f2low = 3.561;
%     f2high = 3.566;
%     f3low = 6.742;
%     f3high = 6.747;
%     f4low = 10.103;
%     f4high = 10.108;
%     elseif curFile == ("quarter_I30.5.txt")
%     f1low = 2.646;
%     f1high = 2.651;
%     f2low = 3.535;
%     f2high = 3.540;
%     f3low = 6.690;
```

```
%     f3high = 6.695;
%     f4low = 10.024;
%     f4high = 10.029;
%     elseif curFile == ("quarter_I30.2.txt")
%     f1low = 2.528;
%     f1high = 2.533;
%     f2low = 3.457;
%     f2high = 3.562;
%     f3low = 6.528;
%     f3high = 6.533;
%     f4low = 9.772;
%     f4high = 9.777;
%     end

% Frequencies for damage at mid-span:
%     if curFile == ("middle_I30.95.txt")
%     f1low = 2.683;
%     f1high = 2.688;
%     f2low = 3.570;
%     f2high = 3.575;
%     f3low = 6.758;
%     f3high = 6.763;
%     f4low = 10.130;
%     f4high = 10.135;
%     elseif curFile == ("middle_I30.9.txt")
%     f1low = 2.680;
%     f1high = 2.685;
%     f2low = 3.569;
%     f2high = 3.574;
%     f3low = 6.755;
%     f3high = 6.760;
%     f4low = 10.130;
%     f4high = 10.135;
%     elseif curFile == ("middle_I30.8.txt")
%     f1low = 2.672;
%     f1high = 2.677;
%     f2low = 3.567;
%     f2high = 3.572;
%     f3low = 6.748;
%     f3high = 6.753;
%     f4low = 10.130;
%     f4high = 10.135;
%     elseif curFile == ("middle_I30.5.txt")
%     f1low = 2.630;
%     f1high = 2.635;
%     f2low = 3.555;
%     f2high = 3.560;
%     f3low = 6.713;
%     f3high = 6.718;
%     f4low = 10.129;
%     f4high = 10.134;
%     elseif curFile == ("middle_I30.2.txt")
%     f1low = 2.486;
%     f1high = 2.491;
%     f2low = 3.523;
%     f2high = 3.528;
%     f3low = 6.615;
%     f3high = 6.620;
```

```
%     f4low = 10.125;
%     f4high = 10.130;
%     end

% Frequencies for damage by the column:
%     if curFile == ("column_I30.95.txt")
%     f1low = 2.686;
%     f1high = 2.691;
%     f2low = 3.567;
%     f2high = 3.572;
%     f3low = 6.761;
%     f3high = 6.766;
%     f4low = 10.130;
%     f4high = 10.135;
%     elseif curFile == ("column_I30.9.txt")
%     f1low = 2.685;
%     f1high = 2.690;
%     f2low = 3.562;
%     f2high = 3.567;
%     f3low = 6.760;
%     f3high = 6.765;
%     f4low = 10.129;
%     f4high = 10.135;
%     elseif curFile == ("column_I30.8.txt")
%     f1low = 2.684;
%     f1high = 2.689;
%     f2low = 3.551;
%     f2high = 3.557;
%     f3low = 6.759;
%     f3high = 6.765;
%     f4low = 10.127;
%     f4high = 10.132;
%     elseif curFile == ("column_I30.5.txt")
%     f1low = 2.678;
%     f1high = 2.683;
%     f2low = 3.500;
%     f2high = 3.506;
%     f3low = 6.755;
%     f3high = 6.760;
%     f4low = 10.114;
%     f4high = 10.120;
%     elseif curFile == ("column_I30.2.txt")
%     f1low = 2.654;
%     f1high = 2.659;
%     f2low = 3.357;
%     f2high = 3.363;
%     f3low = 6.743;
%     f3high = 6.748;
%     f4low = 10.078;
%     f4high = 10.083;
%     end

    for j = 1:size(dBeta,2) %Loop to load current noise level (dBeta)
        curBeta = dBeta(1,j);

        for k = 1:iNoiseInstances %Add noise to the acc time histories
            dBetaFileResult{k} = Y + curBeta*randn(10,8401).*Y;
        end %End of noise addition loop
```

```
        for ii = 1:iNoiseInstances %Calc mode shapes and freqs for stable solutions
            modelOrder = 25; %Model order for extraction of solutions
            [A_cov,C_cov,G_cov,R0_cov] = ssicov(dBetaFileResult{ii},order,s);
            A_cov_500{ii} = A_cov;
            C_cov_500{ii} = C_cov;
            [IDs_cov] = plotstab(A_cov_500{ii},C_cov_500{ii},dBetaFileResult{ii},T,[],↙
err);
            IDs_cov_500{ii} = IDs_cov;
            [fn_cov,zeta_cov,Phi_cov] = modalparams(A_cov_500{ii},C_cov_500{ii},T);
            fn_cov_500{ii} = fn_cov;
            Phi_cov_500{ii} = Phi_cov;
            Phi_cov_500_res{ii} = Phi_cov_500{ii}{modelOrder}(:,IDs_cov_500{ii}↙
{modelOrder});
            fn_cov_500_res{ii} = fn_cov_500{ii}{modelOrder}(IDs_cov_500{ii}{modelOrder});

            if (ii == 1) && (j == 1) %Find locations of four mode shapes with frequency↙
range for the first iteration
                mode1_init_pos = find(fn_cov_500_res{ii}>f1low & fn_cov_500_res{ii}↙
<f1high);
                mode2_init_pos = find(fn_cov_500_res{ii}>f2low & fn_cov_500_res{ii}↙
<f2high);
                mode3_init_pos = find(fn_cov_500_res{ii}>f3low & fn_cov_500_res{ii}↙
<f3high);
                mode4_init_pos = find(fn_cov_500_res{ii}>f4low & fn_cov_500_res{ii}↙
<f4high);

                TF1 = isempty(mode1_init_pos);
                TF2 = isempty(mode2_init_pos);
                TF3 = isempty(mode3_init_pos);
                TF4 = isempty(mode4_init_pos);

                itrCount = 0; %Counter for breaking out of while loop

                while ((itrCount < 11) && (TF1==1 || TF2==1 || TF3==1 || TF4==1)) %↙
Increase model order if modes pertaining to the given frequency ranges cannot be found
                    modelOrder = modelOrder + 10;
                    Phi_cov_500_res{ii} = Phi_cov_500{ii}{modelOrder}(:,IDs_cov_500{ii}↙
{modelOrder});
                    fn_cov_500_res{ii} = fn_cov_500{ii}{modelOrder}(IDs_cov_500{ii}↙
{modelOrder});

                    mode1_init_pos = find(fn_cov_500_res{ii}>f1low & fn_cov_500_res{ii}↙
<f1high);
                    mode2_init_pos = find(fn_cov_500_res{ii}>f2low & fn_cov_500_res{ii}↙
<f2high);
                    mode3_init_pos = find(fn_cov_500_res{ii}>f3low & fn_cov_500_res{ii}↙
<f3high);
                    mode4_init_pos = find(fn_cov_500_res{ii}>f4low & fn_cov_500_res{ii}↙
<f4high);

                    TF1 = isempty(mode1_init_pos);
                    TF2 = isempty(mode2_init_pos);
                    TF3 = isempty(mode3_init_pos);
                    TF4 = isempty(mode4_init_pos);

                    if ((modelOrder > 74) && (TF1==1 || TF2==1 || TF3==1 || TF4==1)) %↙
Calculate mode shapes and freqs again if increased model order does not work
```

```
                        modelOrder = 25;
                        itrCount = itrCount + 1;
                        [A_cov,C_cov,G_cov,R0_cov] = ssicov(dBetaFileResult{ii},order,s);
                        A_cov_500{ii} = A_cov;
                        C_cov_500{ii} = C_cov;
                        [IDs_cov] = plotstab(A_cov_500{ii},C_cov_500{ii},dBetaFileResult↙
{ii},T,[],err);
                        IDs_cov_500{ii} = IDs_cov;
                        [fn_cov,zeta_cov,Phi_cov] = modalparams(A_cov_500{ii},C_cov_500↙
{ii},T);
                        fn_cov_500{ii} = fn_cov;
                        Phi_cov_500{ii} = Phi_cov;
                        Phi_cov_500_res{ii} = Phi_cov_500{ii}{modelOrder}(:,IDs_cov_500↙
{ii}{modelOrder});
                        fn_cov_500_res{ii} = fn_cov_500{ii}{modelOrder}(IDs_cov_500{ii}↙
{modelOrder});

                        mode1_init_pos = find(fn_cov_500_res{ii}>f1low & fn_cov_500_res↙
{ii}<f1high);
                        mode2_init_pos = find(fn_cov_500_res{ii}>f2low & fn_cov_500_res↙
{ii}<f2high);
                        mode3_init_pos = find(fn_cov_500_res{ii}>f3low & fn_cov_500_res↙
{ii}<f3high);
                        mode4_init_pos = find(fn_cov_500_res{ii}>f4low & fn_cov_500_res↙
{ii}<f4high);

                        TF1 = isempty(mode1_init_pos);
                        TF2 = isempty(mode2_init_pos);
                        TF3 = isempty(mode3_init_pos);
                        TF4 = isempty(mode4_init_pos);
                    end
                end

                Ref_Phi{ii} = Phi_cov_500_res{ii};
                Max1 = max(Ref_Phi{1}(:,mode1_init_pos));
                Max2 = max(Ref_Phi{1}(:,mode2_init_pos));
                Max3 = max(Ref_Phi{1}(:,mode3_init_pos));
                Max4 = max(Ref_Phi{1}(:,mode4_init_pos));
                Ref_Phi_norm{1}(:,mode1_init_pos) = Ref_Phi{1}(:,mode1_init_pos)/Max1;
                Ref_Phi_norm{1}(:,mode2_init_pos) = Ref_Phi{1}(:,mode2_init_pos)/Max2;
                Ref_Phi_norm{1}(:,mode3_init_pos) = Ref_Phi{1}(:,mode3_init_pos)/Max3;
                Ref_Phi_norm{1}(:,mode4_init_pos) = Ref_Phi{1}(:,mode4_init_pos)/Max4;

                mode1(2:11,ii+1) = plotBuildingModes_data(Ref_Phi_norm{ii}(:,↙
mode1_init_pos));
                mode2(2:11,ii+1) = plotBuildingModes_data(Ref_Phi_norm{ii}(:,↙
mode2_init_pos));
                mode3(2:11,ii+1) = plotBuildingModes_data(Ref_Phi_norm{ii}(:,↙
mode3_init_pos));
                mode4(2:11,ii+1) = plotBuildingModes_data(Ref_Phi_norm{ii}(:,↙
mode4_init_pos));

            else %Find the same modes for the remaining iterations by comparing mode↙
shapes

                for jj = 1:size(Phi_cov_500_res{ii},2)
                    modelOrder = 25; %Model order for extraction of solutions
                    Max{ii}(1,jj) = max(Phi_cov_500_res{ii}(:,jj));
```

```
                    Phi_cov_500_norm{ii}(:,jj) = Phi_cov_500_res{ii}(:,jj)/Max{ii}(1,jj);

                    D1{ii}(:,jj) = abs(abs(Phi_cov_500_norm{ii}(:,jj)) - abs(Ref_Phi_norm↙
{1}(:,mode1_init_pos)));
                    D2{ii}(:,jj) = abs(abs(Phi_cov_500_norm{ii}(:,jj)) - abs(Ref_Phi_norm↙
{1}(:,mode2_init_pos)));
                    D3{ii}(:,jj) = abs(abs(Phi_cov_500_norm{ii}(:,jj)) - abs(Ref_Phi_norm↙
{1}(:,mode3_init_pos)));
                    D4{ii}(:,jj) = abs(abs(Phi_cov_500_norm{ii}(:,jj)) - abs(Ref_Phi_norm↙
{1}(:,mode4_init_pos)));
                    S1{ii}(:,jj) = sum(D1{ii}(:,jj));
                    S2{ii}(:,jj) = sum(D2{ii}(:,jj));
                    S3{ii}(:,jj) = sum(D3{ii}(:,jj));
                    S4{ii}(:,jj) = sum(D4{ii}(:,jj));
                end

                while (modelOrder < 74) && ((min(S1{ii}) > 0.5) || (min(S2{ii}) > 0.5) ||↙
(min(S3{ii}) > 0.5) || (min(S4{ii}) > 0.5))
                    modelOrder = modelOrder + 10;
                    Phi_cov_500_res{ii} = Phi_cov_500{ii}{modelOrder}(:,IDs_cov_500{ii}↙
{modelOrder});
                    fn_cov_500_res{ii} = fn_cov_500{ii}{modelOrder}(IDs_cov_500{ii}↙
{modelOrder});

                    for jj = 1:size(Phi_cov_500_res{ii},2)
                        Max{ii}(1,jj) = max(Phi_cov_500_res{ii}(:,jj));
                        Phi_cov_500_norm{ii}(:,jj) = Phi_cov_500_res{ii}(:,jj)/Max{ii}(1,↙
jj);

                        D1{ii}(:,jj) = abs(abs(Phi_cov_500_norm{ii}(:,jj)) - abs↙
(Ref_Phi_norm{1}(:,mode1_init_pos)));
                        D2{ii}(:,jj) = abs(abs(Phi_cov_500_norm{ii}(:,jj)) - abs↙
(Ref_Phi_norm{1}(:,mode2_init_pos)));
                        D3{ii}(:,jj) = abs(abs(Phi_cov_500_norm{ii}(:,jj)) - abs↙
(Ref_Phi_norm{1}(:,mode3_init_pos)));
                        D4{ii}(:,jj) = abs(abs(Phi_cov_500_norm{ii}(:,jj)) - abs↙
(Ref_Phi_norm{1}(:,mode4_init_pos)));
                        S1{ii}(:,jj) = sum(D1{ii}(:,jj));
                        S2{ii}(:,jj) = sum(D2{ii}(:,jj));
                        S3{ii}(:,jj) = sum(D3{ii}(:,jj));
                        S4{ii}(:,jj) = sum(D4{ii}(:,jj));
                    end

                    if modelOrder == 75
                        disp('SX > 0.5')
                        disp(curFile)
                        disp(curBeta)
                        disp(ii)
                    end
                end

                mode1_position = find(S1{ii} == min(S1{ii}));
                mode2_position = find(S2{ii} == min(S2{ii}));
                mode3_position = find(S3{ii} == min(S3{ii}));
                mode4_position = find(S4{ii} == min(S4{ii}));

                mode1(2:11,ii+1) = plotBuildingModes_data(Phi_cov_500_norm{ii}(:,↙
mode1_position));
```

```
                mode2(2:11,ii+1) = plotBuildingModes_data(Phi_cov_500_norm{ii}(:,↙
mode2_position));
                mode3(2:11,ii+1) = plotBuildingModes_data(Phi_cov_500_norm{ii}(:,↙
mode3_position));
                mode4(2:11,ii+1) = plotBuildingModes_data(Phi_cov_500_norm{ii}(:,↙
mode4_position));
            end %loop to find modes

            %Represent the mode shapes at the same side of equilibrium
            if mode1(2,ii+1) < 0
                mode1(:,ii+1) = mode1(:,ii+1)*(-1);
            end
            if mode2(2,ii+1) < 0
                mode2(:,ii+1) = mode2(:,ii+1)*(-1);
            end
            if mode3(2,ii+1) < 0
                mode3(:,ii+1) = mode3(:,ii+1)*(-1);
            end
            if mode4(2,ii+1) < 0
                mode4(:,ii+1) = mode4(:,ii+1)*(-1);
            end

            fn = fn_cov_500_res;

        end %END stable solution

        %save natural frequencies and first four modes
        fileSaveName = append(strInFiles(1,i),"_Beta_", num2str(curBeta,'%d'),".mat");
        save(fileSaveName,'fn','mode1','mode2','mode3','mode4');

    end %End of beta loop

end %End of files loop
```

Appendix B

```
clear all
close all
clc

%strings for infiles; uncomment to run
%strInFiles = ["UD_Ref_Beta_5.000000e-03","UD_Ref_Beta_1.000000e-02","UD_Ref_Beta_5.↙
000000e-02","UD_Ref_Beta_1.000000e-01","UD_Ref_Beta_2.000000e-01","UD_Beta_5.000000e-↙
03","UD_Beta_1.000000e-02","UD_Beta_5.000000e-02","UD_Beta_1.000000e-01","UD_Beta_2.↙
000000e-01"];
%strInFiles = ["column_I30.95_Beta_5.000000e-03","column_I30.95_Beta_1.000000e-02","↙
column_I30.95_Beta_5.000000e-02","column_I30.95_Beta_1.000000e-01","column_I30.95_Beta_2.↙
000000e-01","column_I30.9_Beta_5.000000e-03","column_I30.9_Beta_1.000000e-02","↙
column_I30.9_Beta_5.000000e-02","column_I30.9_Beta_1.000000e-01","column_I30.9_Beta_2.↙
000000e-01","column_I30.8_Beta_5.000000e-03","column_I30.8_Beta_1.000000e-02","↙
column_I30.8_Beta_5.000000e-02","column_I30.8_Beta_1.000000e-01","column_I30.8_Beta_2.↙
000000e-01","column_I30.5_Beta_5.000000e-03","column_I30.5_Beta_1.000000e-02","↙
column_I30.5_Beta_5.000000e-02","column_I30.5_Beta_1.000000e-01","column_I30.5_Beta_2.↙
000000e-01","column_I30.2_Beta_5.000000e-03","column_I30.2_Beta_1.000000e-02","↙
column_I30.2_Beta_5.000000e-02","column_I30.2_Beta_1.000000e-01","column_I30.2_Beta_2.↙
000000e-01"];
%strInFiles = ["middle_I30.95_Beta_5.000000e-03","middle_I30.95_Beta_1.000000e-02","↙
middle_I30.95_Beta_5.000000e-02","middle_I30.95_Beta_1.000000e-01","middle_I30.95_Beta_2.↙
000000e-01","middle_I30.9_Beta_5.000000e-03","middle_I30.9_Beta_1.000000e-02","↙
middle_I30.9_Beta_5.000000e-02","middle_I30.9_Beta_1.000000e-01","middle_I30.9_Beta_2.↙
000000e-01","middle_I30.8_Beta_5.000000e-03","middle_I30.8_Beta_1.000000e-02","↙
middle_I30.8_Beta_5.000000e-02","middle_I30.8_Beta_1.000000e-01","middle_I30.8_Beta_2.↙
000000e-01","middle_I30.5_Beta_5.000000e-03","middle_I30.5_Beta_1.000000e-02","↙
middle_I30.5_Beta_5.000000e-02","middle_I30.5_Beta_1.000000e-01","middle_I30.5_Beta_2.↙
000000e-01","middle_I30.2_Beta_5.000000e-03","middle_I30.2_Beta_1.000000e-02","↙
middle_I30.2_Beta_5.000000e-02","middle_I30.2_Beta_1.000000e-01","middle_I30.2_Beta_2.↙
000000e-01"];
%strInFiles = ["quarter_I30.95_Beta_5.000000e-03","quarter_I30.95_Beta_1.000000e-02","↙
quarter_I30.95_Beta_5.000000e-02","quarter_I30.95_Beta_1.000000e-01","quarter_I30.↙
95_Beta_2.000000e-01","quarter_I30.9_Beta_5.000000e-03","quarter_I30.9_Beta_1.000000e-↙
02","quarter_I30.9_Beta_5.000000e-02","quarter_I30.9_Beta_1.000000e-01","quarter_I30.↙
9_Beta_2.000000e-01","quarter_I30.8_Beta_5.000000e-03","quarter_I30.8_Beta_1.000000e-↙
02","quarter_I30.8_Beta_5.000000e-02","quarter_I30.8_Beta_1.000000e-01","quarter_I30.↙
8_Beta_2.000000e-01","quarter_I30.5_Beta_5.000000e-03","quarter_I30.5_Beta_1.000000e-↙
02","quarter_I30.5_Beta_5.000000e-02","quarter_I30.5_Beta_1.000000e-01","quarter_I30.↙
5_Beta_2.000000e-01","quarter_I30.2_Beta_5.000000e-03","quarter_I30.2_Beta_1.000000e-↙
02","quarter_I30.2_Beta_5.000000e-02","quarter_I30.2_Beta_1.000000e-01","quarter_I30.↙
2_Beta_2.000000e-01"];
%strInFiles = ["abutment_I30.95_Beta_5.000000e-03","abutment_I30.95_Beta_1.000000e-02","↙
abutment_I30.95_Beta_5.000000e-02","abutment_I30.95_Beta_1.000000e-01","abutment_I30.↙
95_Beta_2.000000e-01","abutment_I30.9_Beta_5.000000e-03","abutment_I30.9_Beta_1.000000e-↙
02","abutment_I30.9_Beta_5.000000e-02","abutment_I30.9_Beta_1.000000e-01","abutment_I30.↙
9_Beta_2.000000e-01","abutment_I30.8_Beta_5.000000e-03","abutment_I30.8_Beta_1.000000e-↙
02","abutment_I30.8_Beta_5.000000e-02","abutment_I30.8_Beta_1.000000e-01","abutment_I30.↙
8_Beta_2.000000e-01","abutment_I30.5_Beta_5.000000e-03","abutment_I30.5_Beta_1.000000e-↙
02","abutment_I30.5_Beta_5.000000e-02","abutment_I30.5_Beta_1.000000e-01","abutment_I30.↙
5_Beta_2.000000e-01","abutment_I30.2_Beta_5.000000e-03","abutment_I30.2_Beta_1.000000e-↙
02","abutment_I30.2_Beta_5.000000e-02","abutment_I30.2_Beta_1.000000e-01","abutment_I30.↙
2_Beta_2.000000e-01"];


SL_highres = readmatrix('Sensor_locations_norddalsbrua.xlsx');
SL_highres = SL_highres(:,2); %load high resloution sensor locations for interpolation
SL = readmatrix('Sensor_locations_norddalsbrua.xlsx');
```

```
SL = SL(1:12,4);

%add highres sensor locations to modeshape matrix
modeshape1(:,1) = SL_highres;
modeshape2(:,1) = SL_highres;
modeshape3(:,1) = SL_highres;
modeshape4(:,1) = SL_highres;

%add highres sensor locations to curvature matrix
curvature1(:,1) = SL_highres;
curvature2(:,1) = SL_highres;
curvature3(:,1) = SL_highres;
curvature4(:,1) = SL_highres;

iNoiseInstances = 500;  %number of cases with noise

for i = 1:size(strInFiles,2) %loop to load modeshape files for all noise levels and↙
damages

    curFile = append(strInFiles(1,i),".mat");
    load(curFile);

    for j=2:iNoiseInstances+1 %loop to interpolate modeshapes and make curvature by CD

        modeshape1(:,j)=spline(SL(:,1), mode1(:,j), SL_highres(:,1));
        modeshape2(:,j)=spline(SL(:,1), mode2(:,j), SL_highres(:,1));
        modeshape3(:,j)=spline(SL(:,1), mode3(:,j), SL_highres(:,1));
        modeshape4(:,j)=spline(SL(:,1), mode4(:,j), SL_highres(:,1));

        h(1) = curvature1(2,1) - curvature1(1,1);
        curvature1(1,j) = (modeshape1(3,j) - 2*modeshape1(2,j) + modeshape1(1,j))/(h(1)↙
^2);
        h(43) = curvature1(43,1) - curvature1(42,1);
        curvature1(43,j) = (modeshape1(43,j) - 2*modeshape1(42,j) + modeshape1(41,j))/(h↙
(43)^2);
        for k = 2:42
            h(k) = curvature1(k,1) - curvature1(k-1,1);
            curvature1(k,j) = (modeshape1(k+1,j) - 2*modeshape1(k,j) + modeshape1(k-1,j))↙
/(h(k)^2);
        end

        h(1) = curvature2(2,1) - curvature2(1,1);
        curvature2(1,j) = (modeshape2(3,j) - 2*modeshape2(2,j) + modeshape2(1,j))/(h(1)↙
^2);
        h(43) = curvature2(43,1) - curvature2(42,1);
        curvature2(43,j) = (modeshape2(43,j) - 2*modeshape2(42,j) + modeshape2(41,j))/(h↙
(43)^2);
        for k = 2:42
            h(k) = curvature2(k,1) - curvature2(k-1,1);
            curvature2(k,j) = (modeshape2(k+1,j) - 2*modeshape2(k,j) + modeshape2(k-1,j))↙
/(h(k)^2);
        end

        h(1) = curvature3(2,1) - curvature3(1,1);
        curvature3(1,j) = (modeshape3(3,j) - 2*modeshape3(2,j) + modeshape3(1,j))/(h(1)↙
^2);
        h(43) = curvature3(43,1) - curvature3(42,1);
        curvature3(43,j) = (modeshape3(43,j) - 2*modeshape3(42,j) + modeshape3(41,j))/(h↙
```

```
(43)^2);
        for k = 2:42
            h(k) = curvature3(k,1) - curvature3(k-1,1);
            curvature3(k,j) = (modeshape3(k+1,j) - 2*modeshape3(k,j) + modeshape3(k-1,j))↙
/(h(k)^2);
        end

        h(1) = curvature4(2,1) - curvature4(1,1);
        curvature4(1,j) = (modeshape4(3,j) - 2*modeshape4(2,j) + modeshape4(1,j))/(h(1)↙
^2);
        h(43) = curvature4(43,1) - curvature4(42,1);
        curvature4(43,j) = (modeshape4(43,j) - 2*modeshape4(42,j) + modeshape4(41,j))/(h↙
(43)^2);
        for k = 2:42
            h(k) = curvature4(k,1) - curvature4(k-1,1);
            curvature4(k,j) = (modeshape4(k+1,j) - 2*modeshape4(k,j) + modeshape4(k-1,j))↙
/(h(k)^2);
        end

       fileSaveName = append("modeshapes_",curFile);
              save(fileSaveName,'modeshape1','modeshape2','modeshape3','modeshape4');

      fileSaveName = append("curvatures_",curFile);
             save(fileSaveName,'curvature1','curvature2','curvature3','curvature4');

    end %END interpolation and CD loop

end %END loop to load data
```

Appendix C

```
clc
clear all
close all

strInFiles = ["UD_Ref_Beta_5.000000e-03","UD_Ref_Beta_1.000000e-02","UD_Ref_Beta_5.↙
000000e-02","UD_Ref_Beta_1.000000e-01","UD_Ref_Beta_2.000000e-01","UD_Beta_5.000000e-↙
03","UD_Beta_1.000000e-02","UD_Beta_5.000000e-02","UD_Beta_1.000000e-01","UD_Beta_2.↙
000000e-01","column_I30.95_Beta_5.000000e-03","column_I30.95_Beta_1.000000e-02","↙
column_I30.95_Beta_5.000000e-02","column_I30.95_Beta_1.000000e-01","column_I30.95_Beta_2.↙
000000e-01","column_I30.9_Beta_5.000000e-03","column_I30.9_Beta_1.000000e-02","↙
column_I30.9_Beta_5.000000e-02","column_I30.9_Beta_1.000000e-01","column_I30.9_Beta_2.↙
000000e-01","column_I30.8_Beta_5.000000e-03","column_I30.8_Beta_1.000000e-02","↙
column_I30.8_Beta_5.000000e-02","column_I30.8_Beta_1.000000e-01","column_I30.8_Beta_2.↙
000000e-01","column_I30.5_Beta_5.000000e-03","column_I30.5_Beta_1.000000e-02","↙
column_I30.5_Beta_5.000000e-02","column_I30.5_Beta_1.000000e-01","column_I30.5_Beta_2.↙
000000e-01","column_I30.2_Beta_5.000000e-03","column_I30.2_Beta_1.000000e-02","↙
column_I30.2_Beta_5.000000e-02","column_I30.2_Beta_1.000000e-01","column_I30.2_Beta_2.↙
000000e-01"];
strInFiles = append('curvatures_',strInFiles);

Location = ['column']; %use the find and replace function to sort the curvatures for↙
damage occuring at the remaining locations; abutment, middle, quarter

dBeta = [0.005,0.01,0.05,0.1,0.2]; %noise levels

Curv = cell(5,1); %cell for storage of curvatures

betaCount = 1;
rowstart = 1;
rowend = 501;
deltarow = 500;
deltacol = 43;

for i = 1:size(strInFiles,2) %loop to save all curvatures in one cell for each noise↙
level
    curFile = append(strInFiles(1,i),".mat");
    load(curFile);

    curvature1 = transpose(curvature1);
    curvature2 = transpose(curvature2);
    curvature3 = transpose(curvature3);
    curvature4 = transpose(curvature4);

    colstart = 1;
    colend  = size(curvature1,2);
    curvatures(:,colstart:colend) = curvature1(:,:);
    colstart = colend+1;
    colend= colend + deltacol;
    curvatures(:,colstart:colend) = curvature2(:,:);
    colstart = colend+1;
    colend= colend + deltacol;
    curvatures(:,colstart:colend) = curvature3(:,:);
    colstart = colend+1;
    colend= colend + deltacol;
    curvatures(:,colstart:colend) = curvature4(:,:);

    if i < 6 %loop to remove sensor locations (SL) from all except the undamaged scenario
        Curv{betaCount} = [curvatures(rowstart:rowend,:)];
```

```
    else
        Curv{betaCount}(rowstart:rowend,:)=[curvatures(2:501,:)];
    end

    betaCount = betaCount+1;

    if betaCount>5;
        betaCount=1;
        rowstart = rowend+1;
        rowend = rowend+deltarow;
    end

end

A = Curv{1}(:,[3, 7, 12, 17, 21, 25, 29, 33, 37, 41, 46, 50, 55, 60, 64, 68, 72, 76, 80,↙
84, 89, 93, 98, 103, 107, 111, 115, 119, 123, 127, 132, 136, 141, 146, 150, 154, 158,↙
162, 166, 170]);
B = Curv{2}(:,[3, 7, 12, 17, 21, 25, 29, 33, 37, 41, 46, 50, 55, 60, 64, 68, 72, 76, 80,↙
84, 89, 93, 98, 103, 107, 111, 115, 119, 123, 127, 132, 136, 141, 146, 150, 154, 158,↙
162, 166, 170]);
C = Curv{3}(:,[3, 7, 12, 17, 21, 25, 29, 33, 37, 41, 46, 50, 55, 60, 64, 68, 72, 76, 80,↙
84, 89, 93, 98, 103, 107, 111, 115, 119, 123, 127, 132, 136, 141, 146, 150, 154, 158,↙
162, 166, 170]);
D = Curv{4}(:,[3, 7, 12, 17, 21, 25, 29, 33, 37, 41, 46, 50, 55, 60, 64, 68, 72, 76, 80,↙
84, 89, 93, 98, 103, 107, 111, 115, 119, 123, 127, 132, 136, 141, 146, 150, 154, 158,↙
162, 166, 170]);
E = Curv{5}(:,[3, 7, 12, 17, 21, 25, 29, 33, 37, 41, 46, 50, 55, 60, 64, 68, 72, 76, 80,↙
84, 89, 93, 98, 103, 107, 111, 115, 119, 123, 127, 132, 136, 141, 146, 150, 154, 158,↙
162, 166, 170]);

fileSaveName = append("curvatures_",Location,"_sorted");
save(fileSaveName,'A','B','C','D','E');
```

Appendix D

```
clc
clear all
close all

strInFiles = ["curvatures_abutment_sorted","curvatures_quarter_sorted","↙
curvatures_middle_sorted","curvatures_column_sorted"];
dBeta = [0.005,0.01,0.05,0.1,0.2]; %noise levels
dLoc = ["abutment","quarter","middle","column"]; %damage location
dThresholds = [10,25,50]; %threshold values
iDays = 3499; %num days of readings
iSensors = 10; %num sensors

%Matrices and cells for preallocation
curvSort = cell(1,5);
Ic_1 = zeros(3499,10);
Ic_2 = zeros(3499,10);
Ic_3 = zeros(3499,10);
Ic_4 = zeros(3499,10);
Ic_1mode = zeros(3499,10);
Ic_2modes = zeros(3499,10);
Ic_3modes = zeros(3499,10);
Ic_4modes = zeros(3499,10);
sorted_1mode = zeros(499,10);
sorted_2modes = zeros(499,10);
sorted_3modes = zeros(499,10);
sorted_4modes = zeros(499,10);
Detection_1mode = zeros(3499,10);
Detection_2modes = zeros(3499,10);
Detection_3modes = zeros(3499,10);
Detection_4modes = zeros(3499,10);
Thresholds_1mode = cell(3,1);
Thresholds_2modes = cell(3,1);
Thresholds_3modes = cell(3,1);
Thresholds_4modes = cell(3,1);
Ic_1mode_minusThresh = cell(3,1);
Ic_2modes_minusThresh = cell(3,1);
Ic_3modes_minusThresh = cell(3,1);
Ic_4modes_minusThresh = cell(3,1);
Freq_1mode = cell(3,1);
Freq_2modes = cell(3,1);
Freq_3modes = cell(3,1);
Freq_4modes = cell(3,1);

for i = 1:size(strInFiles,2)  %load file, pertaining to each damage location

    curLoc = dLoc(1,i);
    curFile = append(strInFiles(1,i),'.mat');
    load(curFile);

    curvSort{1} = A; %curvatures with 0.5% noise
    curvSort{2} = B; %curvatures with 1% noise
    curvSort{3} = C; %curvatures with 5% noise
    curvSort{4} = D; %curvatures with 10% noise
    curvSort{5} = E; %curvatures with 20% noise

    for j = 1:size(curvSort,2) %load noise level

        curNoise = curvSort(1,j);
```

```
        curBeta = dBeta(1,j);

        for k = 3:iDays+2 %calculate damage indicator

            Ic_1(k-2,1:10) = abs(curNoise{1}(k,1:10) - curNoise{1}(2,1:10));
            Ic_2(k-2,1:10) = abs(curNoise{1}(k,11:20) - curNoise{1}(2,11:20));
            Ic_3(k-2,1:10) = abs(curNoise{1}(k,21:30) - curNoise{1}(2,21:30));
            Ic_4(k-2,1:10) = abs(curNoise{1}(k,31:40) - curNoise{1}(2,31:40));
        end

        %damage indicators for different sums of modes
        Ic_1mode = Ic_1;
        Ic_2modes = Ic_1 + Ic_2;
        Ic_3modes = Ic_1 + Ic_2 + Ic_3;
        Ic_4modes = Ic_1 + Ic_2 + Ic_3 + Ic_4;

        for ii = 1:size(dThresholds,2) %calculate threshold values

            curThresh = dThresholds(1,ii);

            for jj = 1:iSensors

                sorted_1mode(:,jj) = sort(Ic_1mode(1:499,jj));
                sorted_2modes(:,jj) = sort(Ic_2modes(1:499,jj));
                sorted_3modes(:,jj) = sort(Ic_3modes(1:499,jj));
                sorted_4modes(:,jj) = sort(Ic_4modes(1:499,jj));

                Thresholds_1mode{ii}(1,jj) = sorted_1mode(end-curThresh,jj);
                Thresholds_2modes{ii}(1,jj) = sorted_2modes(end-curThresh,jj);
                Thresholds_3modes{ii}(1,jj) = sorted_3modes(end-curThresh,jj);
                Thresholds_4modes{ii}(1,jj) = sorted_4modes(end-curThresh,jj);
            end

            for kk = 1:iDays

                Ic_1mode_minusThresh{ii}(kk,:) = Ic_1mode(kk,:) - Thresholds_1mode{ii}↙
(1,:);
                Ic_2modes_minusThresh{ii}(kk,:) = Ic_2modes(kk,:) - Thresholds_2modes{ii}↙
(1,:);
                Ic_3modes_minusThresh{ii}(kk,:) = Ic_3modes(kk,:) - Thresholds_3modes{ii}↙
(1,:);
                Ic_4modes_minusThresh{ii}(kk,:) = Ic_4modes(kk,:) - Thresholds_4modes{ii}↙
(1,:);


                for jj = 1:iSensors

                    if (Ic_1mode_minusThresh{ii}(kk,jj) > 0)
                        Detection_1mode(kk,jj) = 1;
                    else
                        Detection_1mode(kk,jj) = 0;
                    end
                    if (Ic_2modes_minusThresh{ii}(kk,jj) > 0)
                        Detection_2modes(kk,jj) = 1;
                    else
                        Detection_2modes(kk,jj) = 0;
                    end
                    if (Ic_3modes_minusThresh{ii}(kk,jj) > 0)
                        Detection_3modes(kk,jj) = 1;
```

```
                    else
                        Detection_3modes(kk,jj) = 0;
                    end
                    if (Ic_4modes_minusThresh{ii}(kk,jj) > 0)
                        Detection_4modes(kk,jj) = 1;
                    else
                        Detection_4modes(kk,jj) = 0;
                    end
                end
            end

            for kk = 500:(iDays-99) %frequency of detection
                for ll = 1:iSensors
                    Freq_1mode{ii}(kk-499,ll) = sum(Detection_1mode(kk:kk+99,ll))/100;
                    Freq_2modes{ii}(kk-499,ll) = sum(Detection_2modes(kk:kk+99,ll))/100;
                    Freq_3modes{ii}(kk-499,ll) = sum(Detection_3modes(kk:kk+99,ll))/100;
                    Freq_4modes{ii}(kk-499,ll) = sum(Detection_4modes(kk:kk+99,ll))/100;
                end
            end
        end

        fileSaveName = append("curvature_Ic_",curLoc,"_Beta_", num2str(curBeta,'%d'),".↙
mat");
                save↙
(fileSaveName,'Ic_1mode','Ic_2modes','Ic_3modes','Ic_4modes','Freq_1mode','Freq_2modes','↙
Freq_3modes','Freq_4modes','Thresholds_1mode','Thresholds_2modes','Thresholds_3modes','Th↙
resholds_4modes')
    end
end
```

Appendix E

```
clc
clear all
close all

strInFiles = ["curvatures_highres_abutment_sorted","curvatures_highres_quarter_sorted","↙
curvatures_highres_middle_sorted","curvatures_highres_column_sorted"];
dLoc = ["abutment","quarter","middle","column"]; %damage locations
dBeta = [0.005,0.01,0.05,0.1,0.2]; %noise levels
dThresholds = [10,25,50]; %threshold values

nSensors = 43;
nRows = 172;
nCols = 3500;
nModes = 4;

SL_highres = readmatrix('Sensor_locations_norddalsbrua.xlsx');
SL_highres = SL_highres(:,2);

%cells for variable storage
curvSort = cell(5,1);
curvSquare = zeros(nRows,nCols);
sensorLoc = zeros(1,nSensors);
Modes_squared = cell(4,1);
Partial = cell(4,1);
Length = cell(4,1);
Is = cell(4,1);
I_1mode = zeros(nSensors,nCols-1);
I_2modes = zeros(nSensors,nCols-1);
I_3modes = zeros(nSensors,nCols-1);
I_4modes = zeros(nSensors,nCols-1);
Is_1mode = zeros(10,nCols-1);
Is_2modes = zeros(10,nCols-1);
Is_3modes = zeros(10,nCols-1);
Is_4modes = zeros(10,nCols-1);
sorted_1mode = zeros(nSensors,499);
sorted_2modes = zeros(nSensors,499);
sorted_3modes = zeros(nSensors,499);
sorted_4modes = zeros(nSensors,499);
Detection_1mode = zeros(nSensors,nCols-1);
Detection_2modes = zeros(nSensors,nCols-1);
Detection_3modes = zeros(nSensors,nCols-1);
Detection_4modes = zeros(nSensors,nCols-1);
Thresholds_1mode = cell(3,1);
Thresholds_2modes = cell(3,1);
Thresholds_3modes = cell(3,1);
Thresholds_4modes = cell(3,1);
Is_1mode_minusThresh = cell(3,1);
Is_2modes_minusThresh = cell(3,1);
Is_3modes_minusThresh = cell(3,1);
Is_4modes_minusThresh = cell(3,1);
Freq_1mode = cell(3,1);
Freq_2modes = cell(3,1);
Freq_3modes = cell(3,1);
Freq_4modes = cell(3,1);
F_1mode = cell(3,1);
F_2modes = cell(3,1);
F_3modes = cell(3,1);
F_4modes = cell(3,1);
```

```
toptop1 = zeros(nSensors, nCols-1);
topbot1 = zeros(1, nCols-1);
toptop2 = zeros(nSensors, nCols-1);
topbot2 = zeros(1, nCols-1);
toptop3 = zeros(nSensors, nCols-1);
topbot3 = zeros(1, nCols-1);
toptop4 = zeros(nSensors, nCols-1);
topbot4 = zeros(1, nCols-1);

for i = 1:size(strInFiles,2) %Load file

    curFile = append(strInFiles(1,i),'.mat');
    load(curFile);
    curLoc = dLoc(1,i);

    curvSort{1} = transpose(A);
    curvSort{2} = transpose(B);
    curvSort{3} = transpose(C);
    curvSort{4} = transpose(D);
    curvSort{5} = transpose(E);

    for j = 1:size(curvSort, 1) %Load noise level

        clearvars Is_1mode Is_2modes Is_3modes Is_4modes Thresholds_1mode↙
Thresholds_2modes Thresholds_3modes Thresholds_4modes Freq_1mode Freq_2modes Freq_3modes↙
Freq_4modes
        curNoise = curvSort(j,1);
        curBeta = dBeta(1,j);

        for k = 1:nCols %Calculate integrals for strain energy computation

            curvSquare(1:nRows,k) = curNoise{1}(1:nRows,k+1).*curNoise{1}(1:nRows,k+1);

            Modes_squared{1}(1:nSensors,k) = curvSquare(1:43,k);
            Modes_squared{2}(1:nSensors,k) = curvSquare(44:86,k);
            Modes_squared{3}(1:nSensors,k) = curvSquare(87:129,k);
            Modes_squared{4}(1:nSensors,k) = curvSquare(130:172,k);

            for ii = 1:nModes

                curMode = Modes_squared{ii};

                for jj = 2:(nSensors-1)

                    x = [SL_highres(jj-1,1) SL_highres(jj,1)];
                    y = [curMode(jj-1,k) curMode(jj,k)];
                    Partial{ii}(jj,k) = trapz(x,y);
                end

                Partial{ii}(1,k) = 0.85*Partial{ii}(2,k);
                Partial{ii}(nSensors,k) = 0.85*Partial{ii}(nSensors-1,k);
                Length{ii}(1,k) = trapz(SL_highres(:,1),curMode(:,k));
            end
        end

        for k = 1:(nCols-1) %Calculate strain energy damage indicator Is

            toptop1(:,k) = Partial{1}(:,k+1);
```

```
            topbot1(1,k) = Length{1}(1,k+1)+1;
            bottop1 = Partial{1}(:,1);
            botbot1 = Length{1}(1,1)+1;
            I_1mode(:,k) = ((toptop1(:,k))./(topbot1(:,k)))./((bottop1)./(botbot1));

            toptop2(:,k) = Partial{1}(:,k+1) + Partial{2}(:,k+1);
            topbot2(1,k) = (Length{1}(1,k+1)+1) + (Length{2}(1,k+1)+1);
            bottop2 = Partial{1}(:,1) + Partial{2}(:,1);
            botbot2 = (Length{1}(1,1)+1) + (Length{2}(1,1)+1);
            I_2modes(:,k) = ((toptop2(:,k))./(topbot2(:,k)))./((bottop2)./(botbot2));

            toptop3(:,k) = Partial{1}(:,k+1) + Partial{2}(:,k+1) + Partial{3}(:,k+1);
            topbot3(1,k) = (Length{1}(1,k+1)+1) + (Length{2}(1,k+1)+1) + (Length{3}(1,↙
k+1)+1);
            bottop3 = Partial{1}(:,1) + Partial{2}(:,1) + Partial{3}(:,1);
            botbot3 = (Length{1}(1,1)+1) + (Length{2}(1,1)+1) + (Length{3}(1,1)+1);
            I_3modes(:,k) = ((toptop3(:,k))./(topbot3(:,k)))./((bottop3)./(botbot3));

            toptop4(:,k) = Partial{1}(:,k+1) + Partial{2}(:,k+1) + Partial{3}(:,k+1) +↙
Partial{4}(:,k+1);
            topbot4(1,k) = (Length{1}(1,k+1)+1) + (Length{2}(1,k+1)+1) + (Length{3}(1,↙
k+1)+1) + (Length{4}(1,k+1)+1);
            bottop4 = Partial{1}(:,1) + Partial{2}(:,1) + Partial{3}(:,1) + Partial{4}(:,↙
1);
            botbot4 = (Length{1}(1,1)+1) + (Length{2}(1,1)+1) + (Length{3}(1,1)+1) +↙
(Length{4}(1,1)+1);
            I_4modes(:,k) = ((toptop4(:,k))./(topbot4(:,k)))./((bottop4)./(botbot4));
        end

        Is_1mode(:,:) = I_1mode([3, 7, 12, 17, 21, 25, 29, 33, 37, 41],:);
        Is_2modes(:,:) = I_2modes([3, 7, 12, 17, 21, 25, 29, 33, 37, 41],:);
        Is_3modes(:,:) = I_3modes([3, 7, 12, 17, 21, 25, 29, 33, 37, 41],:);
        Is_4modes(:,:) = I_4modes([3, 7, 12, 17, 21, 25, 29, 33, 37, 41],:);

        for ii = 1:size(dThresholds,2) %calculate threshold values

            curThresh = dThresholds(1,ii);

            for jj = 1:nSensors

                sorted_1mode(jj,:) = sort(I_1mode(jj,1:499));
                sorted_2modes(jj,:) = sort(I_2modes(jj,1:499));
                sorted_3modes(jj,:) = sort(I_3modes(jj,1:499));
                sorted_4modes(jj,:) = sort(I_4modes(jj,1:499));

                Thresholds_1mode{ii}(jj,1) = sorted_1mode(jj,end-curThresh);
                Thresholds_2modes{ii}(jj,1) = sorted_2modes(jj,end-curThresh);
                Thresholds_3modes{ii}(jj,1) = sorted_3modes(jj,end-curThresh);
                Thresholds_4modes{ii}(jj,1) = sorted_4modes(jj,end-curThresh);
            end

            for kk = 1:(nCols-1)

                Is_1mode_minusThresh{ii}(:,kk) = I_1mode(:,kk) - Thresholds_1mode{ii}(:,↙
1);
                Is_2modes_minusThresh{ii}(:,kk) = I_2modes(:,kk) - Thresholds_2modes{ii}↙
(:,1);
                Is_3modes_minusThresh{ii}(:,kk) = I_3modes(:,kk) - Thresholds_3modes{ii}↙
```

```
(:,1);
                Is_4modes_minusThresh{ii}(:,kk) = I_4modes(:,kk) - Thresholds_4modes{ii}↙
(:,1);

                for jj = 1:nSensors

                    if (Is_1mode_minusThresh{ii}(jj,kk) > 0)
                        Detection_1mode(jj,kk) = 1;
                    else
                        Detection_1mode(jj,kk) = 0;
                    end
                    if (Is_2modes_minusThresh{ii}(jj,kk) > 0)
                        Detection_2modes(jj,kk) = 1;
                    else
                        Detection_2modes(jj,kk) = 0;
                    end
                    if (Is_3modes_minusThresh{ii}(jj,kk) > 0)
                        Detection_3modes(jj,kk) = 1;
                    else
                        Detection_3modes(jj,kk) = 0;
                    end
                    if (Is_4modes_minusThresh{ii}(jj,kk) > 0)
                        Detection_4modes(jj,kk) = 1;
                    else
                        Detection_4modes(jj,kk) = 0;
                    end
                end
            end

            for kk = 500:(nCols-100) %frequency of detection
                for ll = 1:nSensors
                    F_1mode{ii}(ll,kk-499) = sum(Detection_1mode(ll,kk:kk+99))/100;
                    F_2modes{ii}(ll,kk-499) = sum(Detection_2modes(ll,kk:kk+99))/100;
                    F_3modes{ii}(ll,kk-499) = sum(Detection_3modes(ll,kk:kk+99))/100;
                    F_4modes{ii}(ll,kk-499) = sum(Detection_4modes(ll,kk:kk+99))/100;
                end
            end

            Freq_1mode{ii} = F_1mode{ii}([3, 7, 12, 17, 21, 25, 29, 33, 37, 41],:);
            Freq_2modes{ii} = F_2modes{ii}([3, 7, 12, 17, 21, 25, 29, 33, 37, 41],:);
            Freq_3modes{ii} = F_3modes{ii}([3, 7, 12, 17, 21, 25, 29, 33, 37, 41],:);
            Freq_4modes{ii} = F_4modes{ii}([3, 7, 12, 17, 21, 25, 29, 33, 37, 41],:);
        end

        fileSaveName = append("IsEnergy_",curLoc,"_Beta_", num2str(curBeta,'%d'),".mat");
                save↙
(fileSaveName,'Is_1mode','Is_2modes','Is_3modes','Is_4modes','Freq_1mode','Freq_2modes','↙
Freq_3modes','Freq_4modes','Thresholds_1mode','Thresholds_2modes','Thresholds_3modes','Th↙
resholds_4modes');
    end
end
```

Appendix F

```
clear all
close all
clc


%Files for damage by the abutment:
strInFiles = ["UD_Ref_Beta_5.000000e-03","UD_Ref_Beta_1.000000e-02","UD_Ref_Beta_5.↙
000000e-02","UD_Beta_1.000000e-01","UD_Ref_Beta_2.000000e-01","UD_Beta_5.000000e-03","↙
UD_Beta_1.000000e-02","UD_Beta_5.000000e-02","UD_Beta_1.000000e-01","UD_Beta_2.000000e-↙
01","abutment_I30.95_Beta_5.000000e-03","abutment_I30.95_Beta_1.000000e-02","↙
abutment_I30.95_Beta_5.000000e-02","abutment_I30.95_Beta_1.000000e-01","abutment_I30.↙
95_Beta_2.000000e-01","abutment_I30.9_Beta_5.000000e-03","abutment_I30.9_Beta_1.000000e-↙
02","abutment_I30.9_Beta_5.000000e-02","abutment_I30.9_Beta_1.000000e-01","abutment_I30.↙
9_Beta_2.000000e-01","abutment_I30.8_Beta_5.000000e-03","abutment_I30.8_Beta_1.000000e-↙
02","abutment_I30.8_Beta_5.000000e-02","abutment_I30.8_Beta_1.000000e-01","abutment_I30.↙
8_Beta_2.000000e-01","abutment_I30.5_Beta_5.000000e-03","abutment_I30.5_Beta_1.000000e-↙
02","abutment_I30.5_Beta_5.000000e-02","abutment_I30.5_Beta_1.000000e-01","abutment_I30.↙
5_Beta_2.000000e-01","abutment_I30.2_Beta_5.000000e-03","abutment_I30.2_Beta_1.000000e-↙
02","abutment_I30.2_Beta_5.000000e-02","abutment_I30.2_Beta_1.000000e-01","abutment_I30.↙
2_Beta_2.000000e-01"];

%Files for damage at quarter-span:
%strInFiles = ["UD_Ref_Beta_5.000000e-03","UD_Ref_Beta_1.000000e-02","UD_Ref_Beta_5.↙
000000e-02","UD_Beta_1.000000e-01","UD_Ref_Beta_2.000000e-01","UD_Beta_5.000000e-03","↙
UD_Beta_1.000000e-02","UD_Beta_5.000000e-02","UD_Beta_1.000000e-01","UD_Beta_2.000000e-↙
01","quarter_I30.95_Beta_5.000000e-03","quarter_I30.95_Beta_1.000000e-02","quarter_I30.↙
95_Beta_5.000000e-02","quarter_I30.95_Beta_1.000000e-01","quarter_I30.95_Beta_2.000000e-↙
01","quarter_I30.9_Beta_5.000000e-03","quarter_I30.9_Beta_1.000000e-02","quarter_I30.↙
9_Beta_5.000000e-02","quarter_I30.9_Beta_1.000000e-01","quarter_I30.9_Beta_2.000000e-↙
01","quarter_I30.8_Beta_5.000000e-03","quarter_I30.8_Beta_1.000000e-02","quarter_I30.↙
8_Beta_5.000000e-02","quarter_I30.8_Beta_1.000000e-01","quarter_I30.8_Beta_2.000000e-↙
01","quarter_I30.5_Beta_5.000000e-03","quarter_I30.5_Beta_1.000000e-02","quarter_I30.↙
5_Beta_5.000000e-02","quarter_I30.5_Beta_1.000000e-01","quarter_I30.5_Beta_2.000000e-↙
01","quarter_I30.2_Beta_5.000000e-03","quarter_I30.2_Beta_1.000000e-02","quarter_I30.↙
2_Beta_5.000000e-02","quarter_I30.2_Beta_1.000000e-01","quarter_I30.2_Beta_2.000000e-↙
01"];

%Files for damage at mid-span:
%strInFiles = ["UD_Ref_Beta_5.000000e-03","UD_Ref_Beta_1.000000e-02","UD_Ref_Beta_5.↙
000000e-02","UD_Beta_1.000000e-01","UD_Ref_Beta_2.000000e-01","UD_Beta_5.000000e-03","↙
UD_Beta_1.000000e-02","UD_Beta_5.000000e-02","UD_Beta_1.000000e-01","UD_Beta_2.000000e-↙
01","middle_I30.95_Beta_5.000000e-03","middle_I30.95_Beta_1.000000e-02","middle_I30.↙
95_Beta_5.000000e-02","middle_I30.95_Beta_1.000000e-01","middle_I30.95_Beta_2.000000e-↙
01","middle_I30.9_Beta_5.000000e-03","middle_I30.9_Beta_1.000000e-02","middle_I30.↙
9_Beta_5.000000e-02","middle_I30.9_Beta_1.000000e-01","middle_I30.9_Beta_2.000000e-01","↙
middle_I30.8_Beta_5.000000e-03","middle_I30.8_Beta_1.000000e-02","middle_I30.8_Beta_5.↙
000000e-02","middle_I30.8_Beta_1.000000e-01","middle_I30.8_Beta_2.000000e-01","↙
middle_I30.5_Beta_5.000000e-03","middle_I30.5_Beta_1.000000e-02","middle_I30.5_Beta_5.↙
000000e-02","middle_I30.5_Beta_1.000000e-01","middle_I30.5_Beta_2.000000e-01","↙
middle_I30.2_Beta_5.000000e-03","middle_I30.2_Beta_1.000000e-02","middle_I30.2_Beta_5.↙
000000e-02","middle_I30.2_Beta_1.000000e-01","middle_I30.2_Beta_2.000000e-01"];

%Files for damage by the column:
%strInFiles = ["UD_Ref_Beta_5.000000e-03","UD_Ref_Beta_1.000000e-02","UD_Ref_Beta_5.↙
000000e-02","UD_Beta_1.000000e-01","UD_Ref_Beta_2.000000e-01","UD_Beta_5.000000e-03","↙
UD_Beta_1.000000e-02","UD_Beta_5.000000e-02","UD_Beta_1.000000e-01","UD_Beta_2.000000e-↙
01","column_I30.95_Beta_5.000000e-03","column_I30.95_Beta_1.000000e-02","column_I30.↙
95_Beta_5.000000e-02","column_I30.95_Beta_1.000000e-01","column_I30.95_Beta_2.000000e-↙
```

```
01","column_I30.9_Beta_5.000000e-03","column_I30.9_Beta_1.000000e-02","column_I30.↙
9_Beta_5.000000e-02","column_I30.9_Beta_1.000000e-01","column_I30.9_Beta_2.000000e-01","↙
column_I30.8_Beta_5.000000e-03","column_I30.8_Beta_1.000000e-02","column_I30.8_Beta_5.↙
000000e-02","column_I30.8_Beta_1.000000e-01","column_I30.8_Beta_2.000000e-01","↙
column_I30.5_Beta_5.000000e-03","column_I30.5_Beta_1.000000e-02","column_I30.5_Beta_5.↙
000000e-02","column_I30.5_Beta_1.000000e-01","column_I30.5_Beta_2.000000e-01","↙
column_I30.2_Beta_5.000000e-03","column_I30.2_Beta_1.000000e-02","column_I30.2_Beta_5.↙
000000e-02","column_I30.2_Beta_1.000000e-01","column_I30.2_Beta_2.000000e-01"];

iNoiseInstances = 500;
rowstart = 1;
rowend = 501;
deltarow = 500;
n = 1;
i = 1;
Days = (1:3500);
dBeta = [0.005,0.01,0.05, 0.1, 0.2];

%Cells and matrices to store results
Max4_highres = zeros(3500, 43);
Max3_highres = zeros(3500, 43);
Max2_highres = zeros(3500, 43);
Max1_highres = zeros(3500, 43);
Max4 = zeros(3500,10);
Max3 = zeros(3500,10);
Max2 = zeros(3500,10);
Max1 = zeros(3500,10);



while i < 35
for i = n:5:size(strInFiles,2) %loop to load modeshape files for nth noise level and all↙
damages


    curFile = append("modeshapes_",strInFiles(1,i),".mat");
  load(curFile);
  curBeta = dBeta(1,n);

% choose natural frequency (assumed same for all noise levels)

% Frequencies for damage by abutment
   if i <= 10 %abutment_UD
   f1 = 2.6886;
   f2 = 3.5734;
   f3 = 6.7636;
   f4 = 10.1341;
   elseif i >= 11 && i <= 15 %abutment_I30.95
   f1 = 2.6884;
   f2 = 3.5727;
   f3 = 6.7486;
   f4 = 10.1323;
   elseif i >= 16 && i<= 20 %abutment_I30.9
   f1 = 2.6882;
   f2 = 3.5719;
   f3 = 6.7322;
   f4 = 10.1305;
   elseif i >= 21 && i <= 25 %abutment_I30.8
```

```
    f1 = 2.6877;
    f2 = 3.5699;
    f3 = 6.6939;
    f4 = 10.1270;
    elseif i >= 26 && i <= 30 %abutment_I30.5
    f1 = 2.6848;
    f2 = 3.5594;
    f3 = 6.5186;
    f4 = 10.1104;
    elseif i >= 31 && i >= 35 %abutment_I30.2
    f1 = 2.6727;
    f2 = 3.5151;
    f3 = 5.9253;
    f4 = 10.0637;
    end % choose frequency

% Frequencies for damage at quarter-span
%     if i <= 10 %quarter_UD
%     f1 = 2.6886;
%     f2 = 3.5734;
%     f3 = 6.7636;
%     f4 = 10.1341;
%     elseif i >= 11 && i <= 15 %quarter_I30.95
%     f1 = 2.6865;
%     f2 = 3.5714;
%     f3 = 6.7596;
%     f4 = 10.1278;
%     elseif i >= 16 && i<= 20 %quarter_I30.9
%     f1 = 2.6842;
%     f2 = 3.5691;
%     f3 = 6.7553;
%     f4 = 10.1213;
%     elseif i >= 21 && i <= 25 %quarter_I30.8
%     f1 = 2.6786;
%     f2 = 3.5639;
%     f3 = 6.7450;
%     f4 = 10.1054;
%     elseif i >= 26 && i <= 30 %quarter_I30.5
%     f1 = 2.6488;
%     f2 = 3.5371;
%     f3 = 6.6927;
%     f4 = 10.0271;
%     elseif i >= 31 && i >= 35 %quarter_I30.2
%     f1 = 2.5309;
%     f2 = 3.4597;
%     f3 = 6.5306;
%     f4 = 9.7726;
%     end % choose frequency

% Frequencies for damage at mid-span
%     if i <= 10 %middle_UD
%     f1 = 2.6886;
%     f2 = 3.5734;
%     f3 = 6.7636;
%     f4 = 10.1341;
%     elseif i >= 11 && i <= 15 %middle_I30.95
%     f1 = 2.6855;
%     f2 = 3.5725;
```

```
%    f3 = 6.7607;
%    f4 = 10.1339;
%    elseif i >= 16 && i<= 20 %middle_I30.9
%    f1 = 2.6821;
%    f2 = 3.5715;
%    f3 = 6.7578;
%    f4 = 10.1338;
%    elseif i >= 21 && i <= 25 %middle_I30.8
%    f1 = 2.6741;
%    f2 = 3.5691;
%    f3 = 6.7501;
%    f4 = 10.1335;
%    elseif i >= 26 && i <= 30 %middle_I30.5
%    f1 = 2.6319;
%    f2 = 3.5578;
%    f3 = 6.7157;
%    f4 = 10.1323;
%    elseif i >= 31 && i >= 35 %middle_I30.2
%    f1 = 2.4893;
%    f2 = 3.5276;
%    f3 = 6.6158;
%    f4 = 10.1270;
%    end % choose frequency

%   Frequencies for damage by column
%    if i <= 10 %column_UD
%    f1 = 2.6886;
%    f2 = 3.5734;
%    f3 = 6.7636;
%    f4 = 10.1341;
%    elseif i >= 11 && i <= 15 %column_I30.95
%    f1 = 2.6881;
%    f2 = 3.5692;
%    f3 = 6.7632;
%    f4 = 10.1328;
%    elseif i >= 16 && i<= 20 %column_I30.9
%    f1 = 2.6876;
%    f2 = 3.5646;
%    f3 = 6.7628;
%    f4 = 10.1319;
%    elseif i >= 21 && i <= 25 %column_I30.8
%    f1 = 2.6864;
%    f2 = 3.5540;
%    f3 = 6.7621;
%    f4 = 10.1297;
%    elseif i >= 26 && i <= 30 %column_I30.5
%    f1 = 2.6801;
%    f2 = 3.5032;
%    f3 = 6.7575;
%    f4 = 10.1169;
%    elseif i >= 31 && i >= 35 %column_I30.2
%    f1 = 2.6565;
%    f2 = 3.3601;
%    f3 = 6.7451;
%    f4 = 10.0803;
%    end % choose frequency

for j = 2:iNoiseInstances + 1 % 500 days
```

```
    if (i==n) && (j==2) % Flexibility matrix for reference day only
    Fref4 = (modeshape1(:,j)*transpose(modeshape1(:,j)))/f1^2 + (modeshape2(:,j)↙
*transpose(modeshape2(:,j)))/f2^2 + (modeshape3(:,j)*transpose(modeshape3(:,j)))/f3^2 +↙
(modeshape4(:,j)*transpose(modeshape4(:,j)))/f4^2;
    Fref3 = (modeshape1(:,j)*transpose(modeshape1(:,j)))/f1^2 + (modeshape2(:,j)↙
*transpose(modeshape2(:,j)))/f2^2 + (modeshape3(:,j)*transpose(modeshape3(:,j)))/f3^2;
    Fref2 = (modeshape1(:,j)*transpose(modeshape1(:,j)))/f1^2 + (modeshape2(:,j)↙
*transpose(modeshape2(:,j)))/f2^2 ;
    Fref1 = (modeshape1(:,j)*transpose(modeshape1(:,j)))/f1^2 ;

    else %Flexxibility matrix and max delta
    F4 = (modeshape1(:,j)*transpose(modeshape1(:,j)))/f1^2 + (modeshape2(:,j)*transpose↙
(modeshape2(:,j)))/f2^2 + (modeshape3(:,j)*transpose(modeshape3(:,j)))/f3^2 + (modeshape4↙
(:,j)*transpose(modeshape4(:,j)))/f4^2;
    F3 = (modeshape1(:,j)*transpose(modeshape1(:,j)))/f1^2 + (modeshape2(:,j)*transpose↙
(modeshape2(:,j)))/f2^2 + (modeshape3(:,j)*transpose(modeshape3(:,j)))/f3^2;
    F2 = (modeshape1(:,j)*transpose(modeshape1(:,j)))/f1^2 + (modeshape2(:,j)*transpose↙
(modeshape2(:,j)))/f2^2;
    F1 = (modeshape1(:,j)*transpose(modeshape1(:,j)))/f1^2;

    Delta4 = abs(F4-Fref4);
    Delta3 = abs(F3-Fref3);
    Delta2 = abs(F2-Fref2);
    Delta1 = abs(F1-Fref1);



    for k = 1:43 %Find max loaction and value of Delta

        Max4_highres(rowstart+j-2,k) = max(Delta4(:,k));
        Max3_highres(rowstart+j-2,k) = max(Delta3(:,k));
        Max2_highres(rowstart+j-2,k) = max(Delta2(:,k));
        Max1_highres(rowstart+j-2,k) = max(Delta1(:,k));

    end

     l = [3, 7, 12, 17, 21, 26, 30, 34, 38, 42]; %10 sensor locations
        Max4(rowstart+j-2,:) = Max4_highres(rowstart+j-2,l);
        Max3(rowstart+j-2,:) = Max3_highres(rowstart+j-2,l);
        Max2(rowstart+j-2,:) = Max2_highres(rowstart+j-2,l);
        Max1(rowstart+j-2,:) = Max1_highres(rowstart+j-2,l);

            if j == 501 % Loop to get all 3500 days of the noise level
                rowstart = rowstart + deltarow;
            end

    end
end
    if i > 30 && i <  35 %Save results from the nth nosie level

             fileSaveName = append("flexibility_abutment","_Beta_", num2str(curBeta,'%↙
d'), ".mat"); % change name depending on damage location
             save(fileSaveName,'Max4','Max3','Max2','Max1');

        % Load next noise level and restart loop
        n = n+1;
        i = n;
```

```
        rowstart = 1;
        break

    elseif i == 35 %Save results from the last noise level and finish

         fileSaveName = append("flexibility_abutment","_Beta_", num2str(curBeta,'%d'), ".↙
mat");  % change name depending on damage location
         save(fileSaveName,'Max4','Max3','Max2','Max1');

        break
    end
  end
end
```

Appendix G

```
clear all
close all
clc

strInFiles = ["flexibility_abutment_Beta_5.000000e-03", "flexibility_abutment_Beta_1.↙
000000e-02", "flexibility_abutment_Beta_5.000000e-02", "flexibility_abutment_Beta_1.↙
000000e-01", "flexibility_abutment_Beta_2.000000e-01", "flexibility_quarter_Beta_5.↙
000000e-03", "flexibility_quarter_Beta_1.000000e-02", "flexibility_quarter_Beta_5.↙
000000e-02", "flexibility_quarter_Beta_1.000000e-01", "flexibility_quarter_Beta_2.↙
000000e-01", "flexibility_middle_Beta_5.000000e-03", "flexibility_middle_Beta_1.000000e-↙
02", "flexibility_middle_Beta_5.000000e-02", "flexibility_middle_Beta_1.000000e-01",↙
"flexibility_middle_Beta_2.000000e-01", "flexibility_column_Beta_5.000000e-03",↙
"flexibility_column_Beta_1.000000e-02", "flexibility_column_Beta_5.000000e-02",↙
"flexibility_column_Beta_1.000000e-01", "flexibility_column_Beta_2.000000e-01"];

dThresholds = [10,25,50]; %threshold values
nSensors = 10;
nDays = 3499;

%Cells and matrices to store results
sorted1 = zeros(499,10);
sorted2 = zeros(499,10);
sorted3 = zeros(499,10);
sorted4 = zeros(499,10);
Thresholds1 = cell(3,1);
Thresholds2 = cell(3,1);
Thresholds3 = cell(3,1);
Thresholds4 = cell(3,1);
Max1_minusThresh = cell(3,1);
Max2_minusThresh = cell(3,1);
Max3_minusThresh = cell(3,1);
Max4_minusThresh = cell(3,1);
Detection1 = zeros(nDays,nSensors);
Detection2 = zeros(nDays,nSensors);
Detection3 = zeros(nDays,nSensors);
Detection4 = zeros(nDays,nSensors);
Freq_1mode = cell(3,1);
Freq_2modes = cell(3,1);
Freq_3modes = cell(3,1);
Freq_4modes = cell(3,1);


for i = 1:size(strInFiles,2)

    curFile = append(strInFiles(1,i),'.mat');
    load(curFile);

   for j = 1:size(dThresholds,2) %calculate threshold values

        curThresh = dThresholds(1,j);

       for k = 1:nSensors
            %Calculate thresold values from first 500 days
            sorted1(1:499,k) = sort(Max1(2:500,k));
            sorted2(1:499,k) = sort(Max2(2:500,k));
            sorted3(1:499,k) = sort(Max3(2:500,k));
            sorted4(1:499,k) = sort(Max4(2:500,k));
```

```
            Thresholds1{j}(1,k) = sorted1(end-curThresh,k);
            Thresholds2{j}(1,k) = sorted2(end-curThresh,k);
            Thresholds3{j}(1,k) = sorted3(end-curThresh,k);
            Thresholds4{j}(1,k) = sorted4(end-curThresh,k);
        end  % Reference days for threshold calculation


          Max1_minusThresh{j}(:,:) = Max1(2:3500,:) - Thresholds1{j}(1,:);
          Max2_minusThresh{j}(:,:) = Max2(2:3500,:) - Thresholds2{j}(1,:);
          Max3_minusThresh{j}(:,:) = Max3(2:3500,:) - Thresholds3{j}(1,:);
          Max4_minusThresh{j}(:,:) = Max4(2:3500,:) - Thresholds4{j}(1,:);


   %Frequency calculations

        for l = 1:nDays
            for k = 1:nSensors

                if (Max1_minusThresh{j}(l,k) > 0)

                    Detection1(l,k) = 1;
                else
                    Detection1(l,k) = 0;
                end
                if (Max2_minusThresh{j}(l,k) > 0)

                    Detection2(l,k) = 1;
                else
                    Detection2(l,k) = 0;
                end
                if (Max3_minusThresh{j}(l,k) > 0)

                    Detection3(l,k) = 1;
                else
                    Detection3(l,k) = 0;
                end
                if (Max4_minusThresh{j}(l,k) > 0)

                    Detection4(l,k) = 1;
                else
                    Detection4(l,k) = 0;
                end
            end
        end

        for kk = 500:(nDays-99) %frequency of detection
            for ll = 1:nSensors
                Freq_1mode{j}(kk-499,ll) = sum(Detection1(kk:kk+99,ll))/100;
                Freq_2modes{j}(kk-499,ll) = sum(Detection2(kk:kk+99,ll))/100;
                Freq_3modes{j}(kk-499,ll) = sum(Detection3(kk:kk+99,ll))/100;
                Freq_4modes{j}(kk-499,ll) = sum(Detection4(kk:kk+99,ll))/100;
            end
        end

    end % threshold calculations
     fileSaveName = append("Freq_",curFile);
                save(fileSaveName,'Max1', 'Max2', 'Max3', 'Max4',↙
'Freq_1mode','Freq_2modes','Freq_3modes','Freq_4modes','Thresholds1','Thresholds2','Thres↙
```

```
holds3','Thresholds4');

end
```